Concentration Dependent Ion–Protein Interaction Patterns Underlying Protein Oligomerization Behaviours

Dissertation

zur

Erlangung des Doktorgrades (Dr. rer. nat.)

der

Mathematisch-Naturwissenschaftlichen Fakultät

der

Rheinischen Friedrich-Wilhelms-Universität Bonn

vorgelegt von

Helena Batoulis

aus

Mainz

Bonn 2016

Angefertigt mit Genehmigung der Mathematisch-Naturwissenschaftlichen
Fakultät der Rheinischen Friedrich-Wilhelms-Universität Bonn

1. Gutachter **Herr Prof. Dr. Thorsten Lang**

2. Gutachter **Herr Prof. Dr. Ulrich Kubitscheck**

Tag der Promotion: 03.05.2017

Erscheinungsjahr: 2017

Eidesstattliche Erklärung

Ich versichere, dass ich die vorgelegte Dissertation selbstständig und ohne unerlaubte Hilfe angefertigt habe. Diese Arbeit hat in gleicher oder ähnlicher Form noch keiner Prüfungsbehörde vorgelegen.

Bonn, den 26.11.2016

Vorname: **Helena** Nachname: **Batoulis**

Unterschrift:

Declaration / Erklärung

Parts of this work were previously published in advance in /

Teile dieser Arbeit wurden bereits vorab veröffentlicht in

Batoulis H, Schmidt TH, Weber P, Schloetel JG, Kandt C, Lang T. Concentration Dependent Ion-Protein Interaction Patterns Underlying Protein Oligomerization Behaviours. Sci Rep. 6, 24131 (2016).

Table of Contents

List of Figures

List of Tables

List of Abbreviations

BSA	bovine serum albumin
CD	circular dichroism
CN	coordination number
ddH_2O	double distilled water
DLS	dynamic light scattering
DLVO theory	Derjaguin-Landau-Verwey-Overbeek theory
DMEM	Dulbecco's modified eagle's medium
DMSO	dimethyl sulfoxide
DNA	deoxyribonucleic acid
DTT	dithiothreitol
EDTA	ethylenediaminetetraacetic acid
EGFP	enhanced green fluorescent protein
EGTA	ethylene-bis(oxyethylenenitrilo)tetraacetic acid
FCS	fluorescence correlation spectroscopy
FITC	fluorescein isothiocyanate
F_{norm}	normalized fluorescence
FRAP	fluorescence recovery after photobleaching
GABA	γ-aminobutyric acid
GST	glutathione-S-transferase
IgG	immunoglobulin G
IPTG	isopropyl-thiogalactoside
IR	infrared
MD	molecular dynamics
min	minutes
MST	microscale thermophoresis
NA	numerical aperture

NHS ester	N-hydroxysuccinimidyl ester
OD	optical density
PBS	phosphate buffered saline
PC12	phaeochromocytoma 12
PCC	Pearson's correlation coefficient
PCR	polymerase chain reaction
PDB-ID	protein data bank identifier
PFA	paraformaldehyde
PIP_2	phosphatidylinositol bisphosphate
PLL	poly-L-lysine
PMSF	phenylmethylsulfonylfluoride
px	pixel
rel. SD	relative standard deviation
RNA	ribonucleic acid
ROI	region of interest
RT	room temeprature
s.d.	standard deviation
SDS-PAGE	sodium dodecyl sulfate polyacrylamide gel electrophoresis
s.e.m.	standard error of the mean
SNAP25	Synaptosomal-associated protein of 25 kDa
SNARE	Soluble N-ethylmaleimide Sensitive Factor (NSF) Attachment Protein Receptor
STED	stimulated emission depletion
TAMRA	tetramethylrhodamine
TBS	tris buffered saline
TRITC	tetramethylrhodamine
UV	ultra violet
Vis	visible

1 Summary

Most proteins do not exist as monomers. Instead, proteins assemble into oligomeric structures, which range from small dimers to intermediately sized clusters to large polymers. Oligomerization is driven by protein–protein interactions between charged residues, (induced) dipoles, aromatic residues and hydrophobic patches.

Ionic protein–protein interactions, and thus the oligomeric state of a protein, can be influenced by metal ions. There are several theories that strive to explain interactions between metal ions and charged proteins. Continuum electrostatic theories assume a decaying electrostatic potential from a charged protein surface which attracts oppositely charged ions to the point of charge neutralization, while the water solvent is treated as passive medium characterized only by its permittivity. More recent concepts, however, recognize the importance of water coordination. The hydration enthalpy of metal ions and ionic protein groups is envisaged as the driving force for ion pairing.

Research and theory have so far focussed on single protein species in simple aqueous solutions. This work comparatively analyses Ca^{2+}-induced oligomerization of the negatively charged SNAP25 protein in solution and in the crowded multi-component environment of the plasma membrane. It proves ion-induced protein oligomerization to be a fundamental chemico-physical principle that is conserved in both environments. The restricted protein movement and the manifold interactions with other proteins and lipids in the membrane appear to mainly influence the number of monomers comprised in an oligomer, but not the phenomenon of oligomerization itself.

Comparison of Ca^{2+} to other positively charged metal ions indicates that ions need to convey a certain charge density and to possess a certain water affinity to induce membrane protein clustering. The results suggest a direct interaction

between calcium ions and negatively charged protein residues. It appears that the stoichiometry of calcium–carboxylate group interactions determines the degree of oligomerization. At low calcium concentrations which induce protein clustering, the ions function as bridges between the carboxylate groups, and attenuate the negative protein charge and thus repulsive protein–protein interactions. At high calcium concentrations, binding of one or more calcium ions to a single negatively charged residue is frequently encountered. The calcium ions thus no longer function as bridges between several carboxylate groups. In addition, the local overcharging entails repulsive forces between proteins which again favour protein dispersion. The study provides a conceptual framework for the influence of ions on electrostatically driven protein–protein interactions and protein aggregation with implications for biological and industrial settings.

2 Introduction

2.1 Molecules of Life

Living matter is made up of a few basic components. In essence, there are four classes of biological macromolecules – polysaccharides, lipids, proteins and nucleic acids – which are immersed in salty water (Table 1)[1].

The structure and function of biomolecules depend on three important water properties: its ability to form an elaborate hydrogen bond network (with four bonds formed on average per water molecule), to solvate biomolecules, and its weak tendency to dissociate into H^+ and OH^- ions[2]. Besides the large organic molecules, there are a few types of inorganic ions immersed in the cytosol and the extracellular fluids, which regulate the cells' osmotic pressure, i.e. lastly the movement of water.

Each of the biological macromolecules fulfils a certain function. Lipids are hydrocarbon derivatives which serve as energy stores and as building elements of membranes – hydrophobic barriers that allow living organisms to build structural and functional compartments. The elementary compartment is the cell, the smallest unit of life which can independently reproduce itself. Organisms may consist of merely one cell, such as bacteria, or several trillion cells which then serve specialized functions, such as in mammals[3].

Polysaccharides also serve as an energy storage system for cells. These sugar polymers additionally function as ligands for proteins.

Nucleic acids, of which there are two basic types, are linear polymers composed of nucleotides (nitrogen-containing ring compounds linked to a ribose sugar). Deoxyribonucleic acid (DNA) serves as storage for genetic information, i.e. the building plans for the organism's proteins. Ribonucleic acids (RNAs) are transcribed from DNA templates, and are crucial for protein synthesis and perform regulatory functions, mainly on DNA or other RNAs.

The largest (weight) fraction[1,4] of biologic macromolecules are proteins, polymeric molecules composed of amino acids. All amino acids comprise a carboxylic acid and an amine group attached to a central carbon atom. Formation of peptide bonds (-CO–NH-) between these groups (concomitantly releasing water) links amino acids to each other during protein synthesis. Proteins are the class of biomolecules which are at the heart of any cellular function.

Table 1 Molecules of Life

molecule	total number per cell	% of total weight	number of different kinds	average MW
H_2O	4×10^{10}	75	1	18
Inorganic Ions (Na^+, K^+, Mg^{2+}, Ca^{2+}, Fe^{3+}, Cl^-, PO_4^{3-}, SO_4^{2-}, etc.)	2.5×10^8	1	20	40
Carbohydrates and precursors	10^8	3	300	150
Lipids and precursors	4×10^7	2	200	500
Amino acids and precursors	3×10^7	0.4	150	120
other small molecules	1.5×10^7	0.2	200	150
Nucleotides and precursors	1.2×10^7	0.4	200	300
Proteins	3×10^6	12	1,000-3,000	40,000
RNA	6×10^4	5	1,000-2,000	750
DNA	1	1	1	2×10^9

The table lists the different chemical molecules present in an *E. coli* cell, and gives their approximate total number, percent of cell weight, number of different molecular sub-species, and average molecular weight (MW). The table is adapted from ref. 1.

2.2 Proteins

2.2.1 Proteins as "nature's robots"

Almost every task in living organisms is carried out by proteins. Proteins located in the cell membrane work as transporters and channels which actively or passively transfer molecules or ions in- and outside of the cell. They govern movement of single cells or of large muscle fibres. Proteins work as enzymes – biological catalysts

for chemical reactions – which for example metabolize dietary polysaccharides and lipids. Proteins function as receptors for external stimuli of cells, e.g. during visual perception and olfaction. The "weapons" of the immune system are composed of proteins, which opsonize and destroy microbes. Proteins are also used as a mean of cell–cell communication by immune cells and many other cell types.

In short, proteins can be regarded as the main workforce of cells, or "nature's robots", automatons that perform the functions of the genetic program[5]. Function is of course intimately connected to protein structure. The individual properties of a protein, its fold and interaction with other biomolecules, are conveyed by the chemical nature of the amino acid side chains; each protein being unique in its amino acid composition and sequence.

Protein properties are typically assayed in a test tube and therefore in a diluted form and isolated from other biomolecules. In biological systems however, whether in the cytosol, in membranes or extracellular fluids, a protein encounters crowded environments – densely populated by lipids, polysaccharides, ions and also by other proteins. In this environment, further protein packing is observed. In the plasma membrane, an electron microscopy analysis indicated that proteins are not randomly scattered, but rather assemble into large supramolecular structures, designated as protein islands by the authors[6] (see Fig. 1)[7]. This finding indicates that proteins, rather than residing as isolated molecules, interact with one another to substantial degrees.

2.2.2 Protein Oligomerization

2.2.2.1 Protein oligomerization, aggregation and precipitation

A survey of *E. coli* proteins suggests that merely ~20 % of the proteins annotated in the SWISS-PROT protein sequence databank are monomeric[8]. The majority of proteins, whether soluble or membrane bound, instead assemble into higher-

order structures which are composed of several individual polypeptide chains. In polymer science, a process in which dispersed molecules or particles assemble rather than remain isolated is generally referred to as aggregation[9,10].

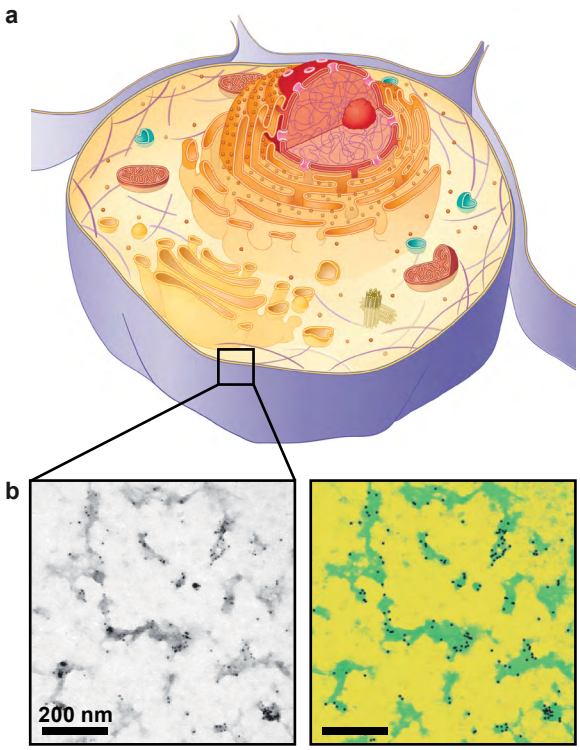

Fig. 1 Membrane proteins are assembled in protein islands. (**a**) Sketch of a eukaryotic cell (adapted from ref. 7) (**b**) Plasma membrane of a resting T cell imaged with transmission electron microscopy. Electron-dense membrane regions appear grey in unprocessed images (left) and were pseudocoloured in green (right). Proteins were non-specifically biotinylated at SH-groups, and detected with streptavidin-conjugated gold beads (small electron-dense, black dots). Any other specific and non-specific protein-labelling procedure invariably showed that proteins are located in the electron-dense (green) regions, which were thus designated as protein islands (micrographs adapted from ref. 6).

The term "aggregate" is here applied to proteins, and thus used to define any structure which contains more than one polypeptide chain. The aggregate may be classified as an oligomer or polymer, depending on the number of its building blocks (individual polypeptides). Homo-oligomers are composed of several

identical polypeptide chains, while hetero-oligomers contain at least one copy of a different polypeptide chain[11]. Since proteins are diverse in their structure, one encounters a variety of interactions and accordingly different types of aggregation phenomena. Protein aggregates differ in their number of monomers, variety of conformational arrangements, reversibility of their association, and bond type between the monomers[12]. While there is no canonical oligomer classification, they are often divided based on their symmetry and shape into globular and fibrous oligomers[11].

Depending on their size, concentration, hydrophilicity and charge, protein aggregates may precipitate from solution[13-15]. Precipitation or phase separation may involve misfolding, such as in amyloid fibrils, but can also occur with natively folded proteins e.g. during protein crystallization (which is in fact the most widely used technique to elucidate protein structure[16]). Precipitation means that the molecule or aggregate is no longer fully solvated, i.e. enclosed by hydrating water molecules, and therefore separates from the water phase[13]. Through centrifugation or mere gravitation the aggregate can be sedimented[17]. The nature of this phase separation can be liquid–solid (e.g. in the case of protein crystals), liquid–gel, or liquid–liquid in protein rich and poor phase[13]. In short, aggregation refers to the molecular associative state, while precipitation indicates the physical phase separation due to insolubility. Different protein aggregates, the functional consequences of aggregation and aggregation mechanisms will be explored in the following sections.

2.2.2.2 Implications of protein aggregation in different contexts

Protein aggregates can be found in every protein environment: in extracellular spaces, in the cytosol and in membranes. These aggregation phenomena are important in (patho)physiological and industrial contexts.

Functional protein aggregates

Prominent examples of extracellular oligomeric proteins are bacterial toxins, such as α-hemolysin. *Staphylococcus aureus* secrets the water-soluble hemolysin monomers. These monomers bind to cell membranes, and then self-assemble into globular heptamers forming a transmembrane pore[18] (see Fig. 2 a). These pores entail leakage of ions and low molecular weight molecules, and ultimately cell lysis. Thus, membrane-dependent α-hemolysin oligomerization is crucial for its function.

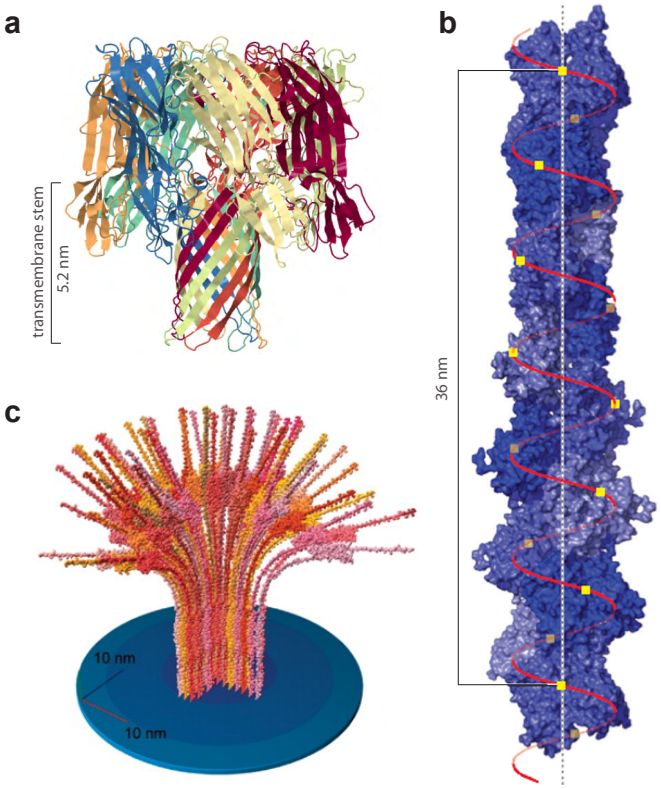

Fig. 2 Different kinds of protein aggregates. (**a**) Crystal structure of the heptameric α-hemolysin (the individual subunits are represented by different colours). The stem domain forms the transmembrane channel (figure adapted from ref. 18, PDB-ID: 7AHL). (**b**) Cryoelectron microscopy-derived structure of an actin filament consisting of helically arranged actin monomers (depicted in different shades of blue with a central yellow square) (adapted from ref. 19). (**c**) In silico reconstruction of a syntaxin cluster in the plasma membrane oligomerized via the proteins' SNARE domains (adapted from ref. 25).

Higher-order protein oligomers, or polymers, are found in the extracellular matrix. Collagen, one of the most abundant proteins in animals, is composed of a homo- or hetero-trimeric helix, so-called tropocollagen, which assembles into

large collagen fibrils or networks. The resulting insoluble polymer endows tensile strength to tissues such as tendons and ligaments. Large *intra*cellular fibrous polymers are cytoskeleton components such as actin[19] (Fig. 2 b), microtubules and intermediate filaments. Dynamic polymerization and de-polymerization of these components both maintains cell shape and drives cell movement. When considering polymeric protein structures, three major advantages of protein aggregates over synthesis of a large single-chain protein become particularly obvious: the economy with respect to genetic material, the reduced likelihood of transcription errors in short sequences[8,20], and the great structural plasticity that follows from individually assembling monomers into constructs with diverse sizes and shapes.

Intracellular higher-order oligomers also include molecular scaffolds such as gephyrin lattices which stabilize and organize the neuronal GABA and glycine receptors at the postsynaptic membrane[21]. These receptors and ion channels are composed of several subunits and are thus of oligomeric nature themselves. Most plasma membrane proteins, and also protein complexes like ion channels or receptors[22-24], further associate into so-called protein clusters. Syntaxin, a member of the SNARE protein family involved in neuronal exocytosis, is known to self-assemble into oligomers (or clusters) comprising on average 75 individual syntaxin molecules (Fig. 2 c). The nature of this association is comparably loose; the clustered proteins are in a dynamic equilibrium with "freely diffusing", non-clustered proteins[25]. Several functional consequences of membrane protein clustering have been discussed. On the one hand, it may increase receptor signalling efficiency in order to generally accelerate reaction kinetics[26] or to a exceed a conceivable threshold[27]. On the other hand, clustering could serve the exact opposite function, i.e. storage and biochemical inactivation of e.g. SNARE proteins thus controlling the number of reactive (non-clustered) molecules[28,29]. Finally, oligomerization is considered advantageous because the reduction in surface area provides stability against denaturation and degradation[8,20].

Protein aggregates in pathophysiology

Several diseases are characterized by extra- or intracellular deposition of amyloid fibrils – insoluble filamentous protein aggregates of several nanometres in diameter and microns in length[11] – which are also called amyloid plaques. A prominent example is the aggregation of Aβ and tau proteins in Alzheimer's disease[30]. Interestingly, not the amyloid plaques but the lower-order aggregates like the protofilaments are believed to drive disease pathology. These smaller aggregates have a higher surface-to-volume ratio than mature fibrils, and can therefore engage in more pathological interactions with cellular components[30].

Protein aggregates in industrial settings

Unwanted aggregation during recombinant protein production can arise from freeze-thaw cycles, shaking, drying, and heterologous expression[14]. Aggregation may entail phase separation, and the turbid solution decreases the aesthetic appeal and possibly patient compliance[31]. It may also indicate that the protein lost its native structure and on that account shows reduced biological activity[31]. Therefore, the intentional induction of solvated protein nanoclusters via crowding agents in pharmaceutical protein formulations can stabilize protein conformation in highly concentrated solutions[32].

In the food industry, heat-induced aggregation and gelation of milk whey proteins such as β-lactoglobulin and albumins are used for texture control, for example in reduced fat yoghurts and ice creams[33].

2.2.2.3 The nature of protein aggregation

Proteins typically assemble into homo-oligomers giving rise to symmetrical structures, most frequently with cyclic, dihedral or cubic anatomy, because this provides more stability and fine control of assembly [8,20]. Aggregates differ in their

number of monomers, protein conformation, reversibility of their association, and bond type linking the monomers to each other. These differences indicate that there are multiple aggregation mechanisms[34].

Thermodynamics of protein–protein interactions

The aggregation process is driven by the chemical properties of the protein building blocks, the amino acids. There are twenty canonical amino acids, whose side chains can be classified as hydrophobic, aromatic, polar, and negatively or positively charged. Accordingly, proteins can engage in hydrophobic interactions[35], in aromatic-aromatic and cation–π interactions[36-41], in van-der-Waals interactions between permanent or induced dipoles, in hydrogen bonding involving a donor hydrogen atom of a polar or charged group and an electronegative acceptor atom of a polar or charged group[42,43], electrostatic repulsion or attraction between charged residues[42], and less often covalent bonds such as disulphide bridges between cysteine residues[44] (see Table 2).

The individual enthalpic contributions of all involved interaction types determine the total strength of a protein–protein interaction. In this regard, the magnitude of the enthalpic contributions depends on the distance between the interaction partners (cf. Table 2), and thus ultimately on shape complementarity between proteins or protein domains[45]. *Intra*molecular protein–protein interactions lead to protein folding into its secondary structure, which comprises α-helices and β-sheets mainly stabilized by hydrogen bonds of the protein backbone[4], and further folding into the protein's three-dimensional tertiary structure which typically encompasses a hydrophobic core[4] that is stabilized by all the aforementioned forces. *Inter*molecular protein–protein interactions drive protein aggregation. Both intra- and intermolecular protein–protein interactions are accompanied by an entropic penalty. In case of protein folding, there is a loss of configurational entropy, while protein aggregation entails a loss

of translational/rotational entropy, and entropy loss at the interfacial side chains[46]. On the other hand, both processes increase the entropy of solvent molecules such as water (or lipids) so that the net entropy of the entire system may actually increase[42,4,47]. In summary, enthalpic and entropic contributions of both protein and solvent determine the total free energy of folding and complex formation.

Table 2 Protein–Protein Interactions

type of interaction	interacting partners	typical potential energy [kJ/mol]	distance (r) dependence of potential energy	ref.
covalent bonds	two cysteines forming a disulfide bridge	290*	none / bond length ~2 Å	44
ion-ion	between charged amino acids	250	1/r	42
hydrogen bond (X-H...Y)	X/Y = N/O atoms of charged or polar side chains or the backbone	20	none / bond length ~2 Å	42, 43
ion-dipole	between ions and polar molecules	15	$1/r^2$	42
cation-pi	aromatic and positively charged amino acids	13	~ 1/r	38, 39, 41
hydrophobic	hydrophobic amino acids and hydrophobic protein core	13**		35
aromatic-aromatic (π-π)	two aromatic residues	6	$1/r^6$	36, 40
dipole-dipole	between stationary polar molecules	2	$1/r^3$	42
dispersion	all types of molecules	2	$1/r^6$	42
dipole-dipole	between rotating polar molecules	0.6	$1/r^6$	42

The table lists different types of protein–protein interactions, as well as their typical energy and distance dependence. * The exact binding energy of disulfide bridges depends on the orientation and also on the presence of reducing agents. ** Hydrophobic interactions, unlike all the other interactions types listed here, do not rely on intrinsic attraction between two non-polar amino acids. Instead, they are the results of minimizing the number of ordered water molecules which cannot bond with the hydrophobic amino acid rests. As a model for hydrophobic interaction energies, the average free energy of transferring an apolar amino acid from water into cyclohexane (which resembles the hydrophobic protein core) is used.

Common types of interaction patterns in protein aggregates

Many fibrillar aggregates, including amyloid depositions[30] and heat-induced protein gels in foods[48] are rich in β-sheets running perpendicular to the fibril longitudinal axis which are stabilized by hydrophobic and polar interactions[30]. Beta-sheet formation often precedes amyloid formation, but can also occur as a secondary process[49]. Hydrogen bonding leading to an increase in β-sheet content is a frequent type of interaction in non-physiological settings. However, hydrogen bonds in other fibrous proteins such as collagens are likewise crucial for assembly, but are not accompanied by β-sheet formation.

Hydrophobic interactions are found in large aggregates that arise after protein denaturation and thus exposure of usually buried hydrophobic groups[48,50], but also in physiological contexts such as elastin assembly[51]. In addition, coiled-coil oligomers – such as the neuronal SNARE complex which is formed of twisted α-helices of syntaxin (Fig. 2 c), SNAP25 and synaptobrevin – are mainly stabilized by hydrophobic interactions[52]. In coiled-coils but also in other types of aggregates, polar and electrostatic residues are believed to mediate not the strength but the specificity of an interaction[52,46]. In fact, the net effect of electrostatic interactions is actually destabilizing[46].

The accounts on frequent interaction types given above are reflective of a study by Chiti[53], which found aggregation proceeds faster when proteins are more hydrophobic and have a higher propensity to form β-sheets, but slower when the net charge of the protein is increased. These parameters (hydrophobicity, propensity to form β-sheets, and net charge) can be used to accurately predict aggregation-prone protein regions or peptides[53,54,55].

Interaction dynamics

Aggregates and the underlying protein–protein interactions differ in their temporal stability. To account for protein–protein interactions that are transient or optional in nature, the term protein quinary structure was coined[56]. This fifth organisational level includes e.g. interactions between ribosomes and initiation, elongation and termination factors, or interactions between enzymes and their protein substrates[56]. This level is different from the quaternary structure, which refers to an obligatory polypeptide assembly, e.g. in the case of ion channels[4]. Quinary interactions are often overlooked since protein stability and function are usually assessed in dilute solutions of a single protein species. In these systems, quinary interactions may either not occur, or become apparent in the form of "oligomeric bands" which do often not receive further attention. However, in crowded environments such as the cytoplasm, quinary interactions may play a crucial role for protein stability and function[57]. Quinary interactions are assumed to rely mainly on charged residues, which can explain why charged protein residues or the isoelectric point of proteins in general are evolutionary conserved[56].

The concept of quinary and quaternary structure is also helpful for the classification of oligomers according to their temporal stability. Aggregation, and even subsequent precipitation, may be reversible and monomer functionality can be restored[58,59]. Weakly associating homo-oligomers can be envisaged as a variant of a quinary protein structure. In accordance with this view, transient oligomers rely on polar interaction surfaces, which is reminiscent of the electrostatically driven quinary interactions. Conversely, stable obligatory complexes, which can be classified as protein quaternary structure, have intertwined, larger and more hydrophobic interfaces[60,61].

2.3 Ion–protein interactions

As outlined above, protein aggregation and quinary interactions rely – amongst other forces – on electrostatic attraction and repulsions. It is interesting to note that charged amino acids can engage in particularly strong interactions (with an interaction energy in the range of 250 kJ/mol[42], cf. Table 2). In biological systems, electrostatic interactions also involve another, very different class of biomolecules, namely inorganic ions. These actually present the most abundant charged particles in cells (cf. Table 1).

2.3.1 Ions control fundamental physiological processes

Most biologically relevant ions belong to the third and fourth period. Prominent members include Na^+, K^+, Cl^-, Mg^{2+}, Ca^{2+}, and several transition metal ions (e.g. Mn^{2+}, $Fe^{2+/3+}$, Ni^{2+}, $Cu^{+/2+}$, Zn^{2+} Mo^{2+}). Besides defining the osmotic pressure and the cell potential[62], ions engage in specific, electrostatically driven interactions with biological macromolecules. Interactions with the cell's protein machineries trigger fundamental physiological events.

In the presynaptic nerve terminal, for example, inflowing calcium ions bind to the vesicular protein synaptotagmin and ultimately trigger SNARE protein zippering and synaptic vesicle fusion, and thus signal propagation to a second neuron or a muscle cell[63]. The calcium ions are thought to trigger an electrostatic switch[64]: they neutralize the negative charge at synaptotagmin's calcium binding pocket, and thus allow for an interaction between synaptotagmin and the negatively charged plasma membrane, which is supposed to pull the vesicle towards the presynaptic membrane[64].

Calcium also plays a crucial role as a second messenger in cell signalling pathways, for example via activation of enzymes such as protein kinase C or calmodulin, and in apoptosis, during which it targets multiple proteins[65].

Finally, ions are important as protein co-factors. Superoxide dismutases for example, which are proteins that protect cells from oxidative stress, bind to several transition metal ions (copper, zinc, manganese, iron, nickel) which actively participate in the catalytic process[66].

2.3.2 Ions influence protein aggregation

Considering the accounts given above, it seems inevitable that metal ions likewise affect the process of protein aggregation. In fact, metal ions are involved in all kinds of protein aggregates, ranging from small oligomers to large aggregates or precipitates, in aggregates formed by intracellular, membrane or extracellular proteins, and in aggregates which occur in physiological, pathological or technical settings. Metal ions can promote protein aggregation via three mechanisms: protein bridging, reducing protein net charge, and via inducing an aggregation-prone conformation[67]. Conversely, ions may also reduce protein aggregation by increasing protein net charge and preventing an aggregation-prone conformation.

2.3.2.1 Ions and physiological protein aggregates

An example of a small, intracellular protein oligomer whose assembly is driven by ions is the *E. coli* RNA polymerase. One polypeptide subunit of this enzyme requires binding of a Zn^{2+} ion via a zinc-finger motif to secure a conformation that allows subunit assembly into a functional enzyme[68]. There are in fact several accounts of protein–protein interactions that rely on zinc-finger domains[69].

Electrostatically driven protein aggregation is observed for several negatively charged rod-like biopolymers, including actin filaments, microtubules

and the filamentous viruses, in the presence of oppositely charged metal ions (such as Co^{2+}, Mn^{2+}, Ca^{2+} and Mg^{2+})[70]. This process is reversible upon addition of either co-ions (i.e. like-charged ions) which compete with the proteins for counterion binding, or upon addition of monovalent salts which increase the ionic strength of the solution and thus the electrostatic screening length.

At the plasma membrane of neuroendocrine cells, calcium ions lead to increased clustering of SNARE proteins such as SNAP25, SNAP23 and syntaxin[29]. The extent of calcium-induced clustering correlates with the net percentage of negatively charged amino acid residues of the protein, likewise arguing for an electrostatic mechanism. Calcium was also described to induce aggregation of spectrin and other proteins in erythrocyte membranes[71]. In case of SNARE protein clustering, calcium removal restored the initial (lower) degree of clustering. In case of spectrin, the aggregates were irreversible and could neither be dissolved via calcium chelation nor by treatment with sodium dodecyl sulfate buffer. Calcium appeared to merely trigger spectrin aggregation, but was apparently not an integral part of the aggregate structure. For SNARE protein clustering, in contrast, calcium proved to be crucial for aggregate stabilization and maintenance.

2.3.2.2 Ions and aggregation in pathophysiological and industrial contexts

Metal ions are also comprised in large, extracellular protein aggregates, such as amyloidogenic fibrils (Table 3)[72-78]. Transition metal ions, which are implicated in the aggregation of almost all amyloidogenic proteins, typically interact with the side chains of histidine and cysteine or the N-terminal amine group[67].

Table 3 Metal ions implicated in the aggregation of amyloidogenic proteins

disease	aggregating protein	metals involved in aggregation	references
Alzheimer's disease	Aβ	Al^{3+}, Cu^{2+}, Fe^{3+}, Zn^{2+}	72
	tau	Al^{3+}, Fe^{3+}, Ca^{2+}, Mg^{2+}, Hg^{2+}, Zn^{2+}	72
Parkinson's disease	α-synuclein	Al^{3+}, Ca^{2+}, Mg^{2+}, Cu^{2+}, Fe^{3+}, Pb^{2+}, Hg^{2+}, Zn^{2+}	72, 163, 164
Spongiform encephalopathies	Prion Protein	Cu^{2+}, Zn^{2+}, Mn^{2+}	72
Amyotrophic lateral sclerosis (ALS)	superoxide dismutase (SOD) 1	Ca^{2+}, Cu^{2+}, Zn^{2+}	73, 74
Huntington's disease	Huntingtin	Cu^{2+}	72
Cataract	crystallins	Cu^{2+}, Zn^{2+}	75
Type II diabetes	amylin	Cu^{2+}, Zn^{2+}	76, 77
	insulin	Zn^{2+}	78

The table lists the most prominent diseases characterized by amyloidogenic protein aggregates, and the metal ions that were found to affect protein aggregation. Metals highlighted in green appear to have protective effects.

In some amyloidogenic peptides this promotes aggregation because binding of e.g. Zn^{2+} and Cu^{2+} favours β-sheet conversion[79]. In the case of Aβ peptides, aggregation is facilitated because Zn^{2+} and Al^{3+} lead to surface exposure of hydrophobic patches[80].

In laboratory settings, metal ions are deliberately employed to induce protein aggregation. Ammonium ions are used to precipitate proteins (for subsequent change of buffer type or volume) in laboratory routines[81]. Ions are likewise crucial to initiate protein crystallization[75,84]. Finally, protein self-assembly is also

beginning to be used for the synthesis of novel synthetic materials. In the field of bionanomaterials, the assembly process and the functional properties of protein-based nanomaterials can be controlled via addition of ions[85,86].

2.3.2.3 Concentration-dependent biphasic oligomerization

Perhaps the most intriguing phenomenon is ion-induced biphasic protein oligomerization. Addition of counterions to charged proteins initially induces protein aggregation and in some cases even phase separation. However, further increasing the ion concentration leads to a reversal in the aggregation trend, and promotes protein dispersal. Biphasic oligomerization and re-entrant phase transitions were described for a variety of (bio)polymers, first and foremost in the context of DNA[87,88]. Only within the last decade the phenomenon has been investigated for proteins, which in comparison to DNA have a more complex charge pattern and an irregular surface geometry. Albumins such as bovine serum albumin (BSA) and ovalbumin were found to experience biphasic (or re-entrant) phase separation in response to La^{3+} and Y^{3+} ions[89] (see Fig. 3 a,b). This phase behaviour is governed by the balance of long-range repulsions and short-range attractions. Albumins are negatively charged and therefore repulse each other electrostatically. Monte Carlo simulations suggest that addition of Y^{3+} gradually attenuates the negative protein surface charge (see Fig. 3 c). Around the point of neutralization, short-range attractive interactions originating from hydrophobic interactions and dispersion forces predominate, leading to aggregation and finally phase transition. If the Y^{3+} concentration is further increased, the protein surface charge is inverted. The albumin–ion complexes now carry a positive net charge (i.e. the opposite net charge than the albumins alone). This causes again electrostatic repulsions between the proteins which exceed their short-range attractions and therefore impede protein aggregation[89].

This counter-intuitive phenomenon of BSA charge inversion or overcharging with Y^{3+} was experimentally confirmed with electrophoretic mobility measurements[90,91]. Biphasic BSA aggregation can also be induced with Al^{3+} and Fe^{3+}, but the regime of phase separation is much narrower, probably because of metal ion hydrolysis leading to a shift in the pH value of the (unbuffered) solution and thus a change in the amino acid side chain protonation state[91].

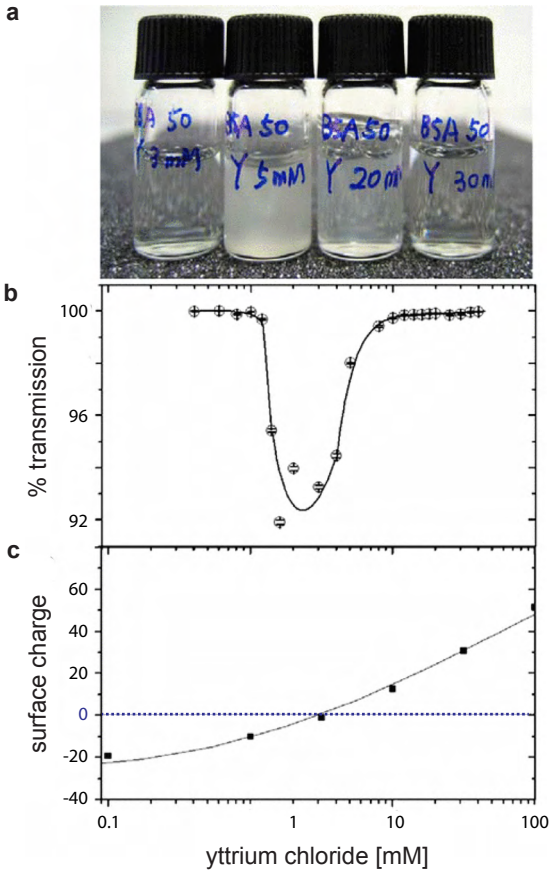

Fig. 3 Biphasic aggregation of BSA in response to Y^{3+} ions.(**a**) Photograph of samples with 50 mg/ml BSA incubated with increasing concentrations of YCl_3. (**b**) The extent of aggregation (phase separation) was evaluated with optical transmission measurement. (**c**) Monte Carlo simulations suggest that the surface charge of the BSA proteins becomes constantly more positive with increasing Y^{3+} concentration. Note that aggregation occurs around the point of surface charge neutralization. This figure is adapted from ref. 89.

Similar to BSA, electrophoretic mobility measurements proved charge inversion of polyaspartate peptides incubated with La^{3+} [92]. Atomistic MD simulations show that multivalent ions associate with the peptide and also suggested charge

inversion with Ca^{2+} and Mg^{2+} [92]. Monovalent ions, on the other hand, are not capable of inducing biphasic aggregation, neither in the case of BSA[90] nor polyaspartate[92]. Conversely to biphasic aggregation of negatively charged proteins with multivalent cations, the positively charged protein lysozyme experiences biphasic aggregation in the presence of anions such as I^-, Br^-, SCN^-, and ClO_4^- [93].

There are also accounts of weakening protein–protein interactions at high counterion concentrations which are not accompanied by overcharging. The filamentous bacteriophage fd (which can be conceived as a rod-shaped, negatively charged capsid protein polymer) undergoes biphasic oligomerization into virus bundles upon continuous addition of Mg^{2+} [94]. However, both electrophoretic mobility measurements as well as Monte Carlo simulations unveiled that the Mg^{2+} ions do not inverse the proteins' charge, but merely attenuate it. The authors speculate that virus bundle re-dispersion at high Mg^{2+} concentrations is rather the result of the increased ionic strength, leading to a greater screening of the counterion-induced attractive forces than the electrostatic repulsive forces between the virus particles[94].

2.4 Concepts for understanding ion–protein interactions

2.4.1 Continuum electrostatics theories

There are several theories that consider the interface between a charged object – such as a protein – and ions. The classical Poisson-Boltzmann theory treats ions as point charges which are electrostatically attracted to and associate with a macroion, thus screening its charge. The electrical potential and the counterion concentration decay exponentially with increasing distance from the interface, the slope depending in the macroion's surface charge density and the medium's electric permittivity[95].

Later theories accommodate for spatial extension of ions and the existence of quantum mechanical forces. The DLVO (Derjaguin-Landau-Verwey-Overbeek)

theory states that like-charged macroions in solution (e.g. two identical proteins) experience a screened long-range electrostatic repulsion, and a short-range van-der-Waals attraction[96–98]. The balance of these forces at each distance determines whether two particles are separated (at large distances) or aggregate (at shorter distances). This balance can be tuned by changing the ionic strength, since the Coulomb force becomes increasingly screened at high ionic strength, whereas the van-der-Waals attraction is hardly affected[98]. Particles are thus more likely to aggregate if the ionic strength is increased or the repulsive barrier can be overcome otherwise, e.g. via activation of thermal motion[99]. Balancing weakly screened electrostatic repulsion and short-range attraction was indeed reported to result in equilibrium cluster formation of the positively charged protein lysozyme[100,101].

While these classical theories have been successful in describing the relationships between charged particles in solution in many cases, they all rely on a similar simplification. The solvent, in biological systems water, is treated as a passive continuum with a certain permittivity for the Coulomb force between ions and charged proteins. In addition, the theories neglect the discreteness of charges both in proteins (picturing them instead as particles with a uniform or smeared charge), as well as for ions (thus ignoring ion-ion correlations)[102,95]. As we shall see below, there are several cases for which these classical theories of colloid and physical chemistry are therefore not applicable.

2.4.2 Water ordering and the law of matching water affinities

As early as in 1888, Hofmeister[103] described that ions differ in their capacity to precipitate – in this context also referred to as salt out – egg white proteins from solution. Since then many cases of ion-mediated protein–protein interactions which resemble the so-called Hofmeister or lyotropic series[102,104,105] of ions (Fig. 4) have been described. Examples include aggregation of pharmaceutical antibody preparations[106], amyloid formation of the prion protein[107], but also ion channel permeability[108] and enzyme activity[109].

These observations suggest a common underlying molecular mechanism, which is still not completely understood. Hofmeister effects cannot be explained simply by the amount of ion charge and thus continuum electrostatic theories. It has become evident that the solvent – the water network that is necessary to hydrate proteins thus keeping them in solution – cannot be treated as an electrostatic continuum, but must be accounted for as individual water molecules which specifically interact with the ions.

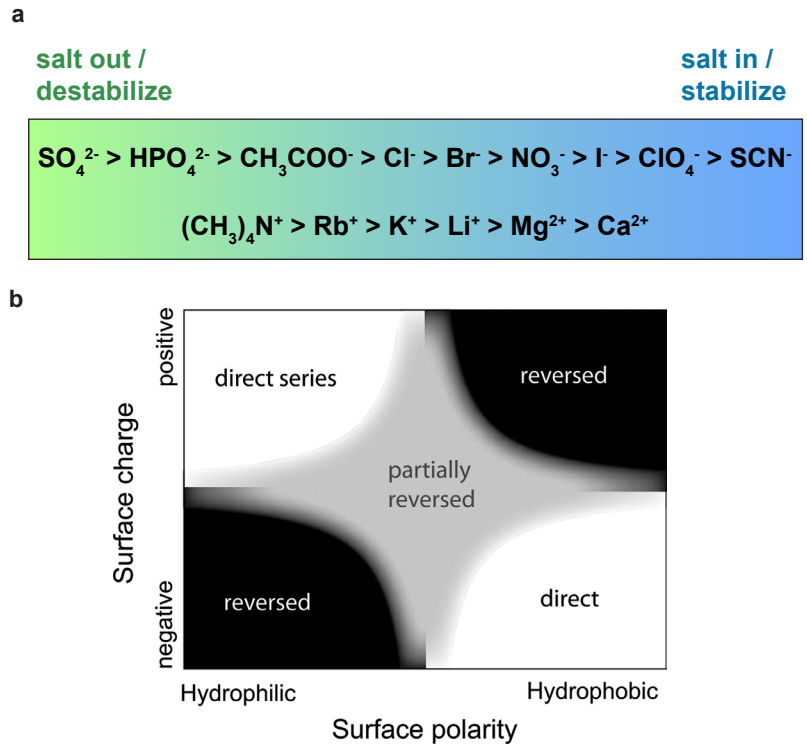

Fig. 4 Anionic and cationic Hofmeister series. (**a**) Ions are ordered according to their efficiency to salt proteins out of solution (based on the concentration that is necessary to achieve protein precipitation) (adapted from ref. 102). Ions on the left hand side thus destabilize proteins in solution, while ions on the right hand side stabilize proteins in solution (also referred to as salting in). (**b**) Depending on protein surface charge and polarity, the Hofmeister series can be (partially) inversed. Panel **b** is adapted from ref. 104.

It was indeed proposed that long-range electrostatic interactions between charged particles are insignificant compared to the effects on interfacial water molecules[110]. To explain protein precipitation and stabilization in the light of solvent granularity, i.e. individually interacting water molecules, the concept of

chaotropic and kosmotropic ions was put forward. Initially it was assumed that kosmotropes induce a long-ranged order in the hydrogen-bonded water network, while chaotropes were conceived as water structure breakers. Several well-known macroscopic observations such as ion-induced alterations of the water viscosity appeared to support this hypothesis. However, modern technologies finally proved that ions do not induce a long-range enhancement or breakdown of water's hydrogen bond system[111]. In fact, the orientation of water molecules is only affected in the first hydration layer (Fig. 5). Nonetheless, the strength of ion–water interactions appears to be one key parameter for understanding ion–protein interactions, but interactions between ions, proteins and water molecules are dominated by short-range interfacial effects[110].

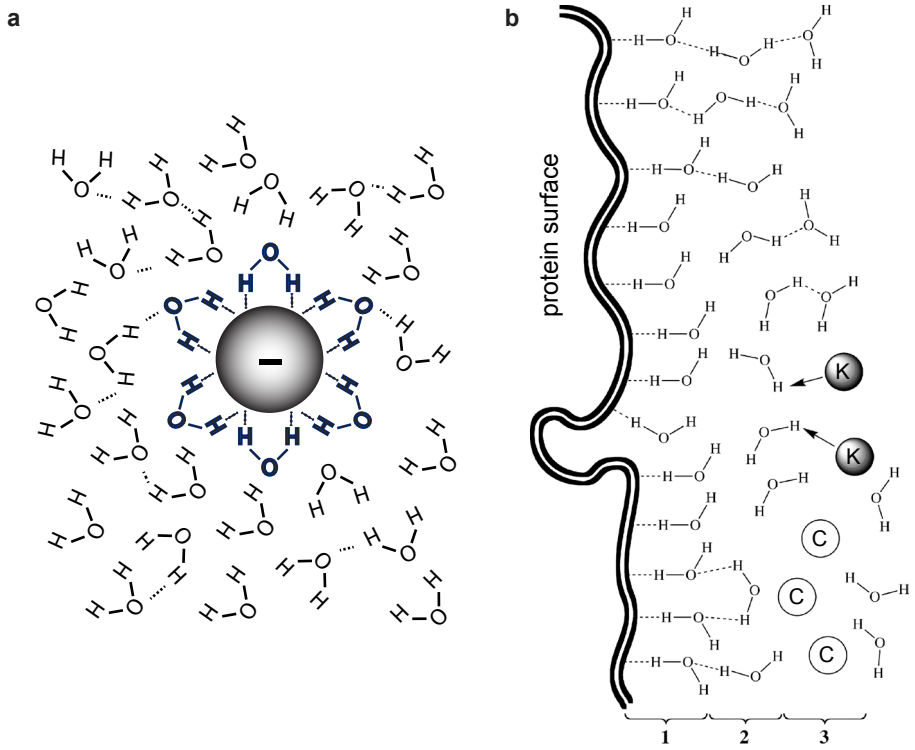

Fig. 5 Hydration of ions and proteins. (**a**) Anion in aqueous solution. The hydration shell of the anion is printed in bold. While the hydrating water molecules also interact with the bulk layer, there is no long-range water ordering. (**b**) Hydrated protein surface in aqueous solution. There are three layers of interfacial water near the negatively charged protein surface: the solvation layer (1), which is the only highly ordered water layer, the transition layer (2), and the bulk layer (3). The circles present kosmotropic ions (K, dark) which interact more strongly with water molecules (indicated by the arrow) than chaotropic ions (C, white). Panel **b** is adapted from ref. 105.

In this regard, an interesting observation that was proposed as a phenomenological rule is the so-called law of matching water affinities. Oppositely charged particles – e.g. ions or charged ion-like atom groups of protein residues – preferentially associate with each other when they have similar water affinities[112] (see Fig. 6 a). According to this concept, chaotropes are reckoned to weakly bind their hydration shell, while kosmotropes are strongly hydrated ions. The terms weak and strong refer to a comparison between the strength of ion–water interactions and water–water interactions. Water molecules thus interact with chaotropes weaker and with kosmotropes stronger than they interact with each other. Hence, oppositely charged kosmotropes bind to each other because of electrostatic attraction. In contrast, the interaction between two chaotropes is not driven by the ions themselves, but rather by the hydrating water molecules which are released upon ion pairing. These water molecules then interact with water molecules from the bulk solution, which is energetically more favourable than interacting with the chaotropic ions. Water affinity is inherently related to ion size, so that small, charge dense ions are typically kosmotropes, and large ions of low charge density are chaotropes (see Fig. 6 b)[112,110].

While the law of matching water affinities readily accounts for a wide range of Hofmeister phenomena, such as ion-induced (de)stabilization of enzyme dimers[113], or the extent of solubility of different salts (e.g. the low solubility of $CaCO_3$), it does not explicitly take into account quantum mechanical effects such as dispersion interactions. Dispersion interactions, however, drive ionic adsorption to uncharged or even like-charged surfaces, and are also involved in several Hofmeister phenomena for which the sequence of ions is not predicted correctly by the law of matching water affinities[102]. Lastly, the interplay of electrostatic and dispersion forces at surfaces with discretely charged sites probably provides a (yet to be established) theoretical framework for the law of matching water affinities and will refine the correct prediction of ion sequences in protein aggregation and related phenomena[102].

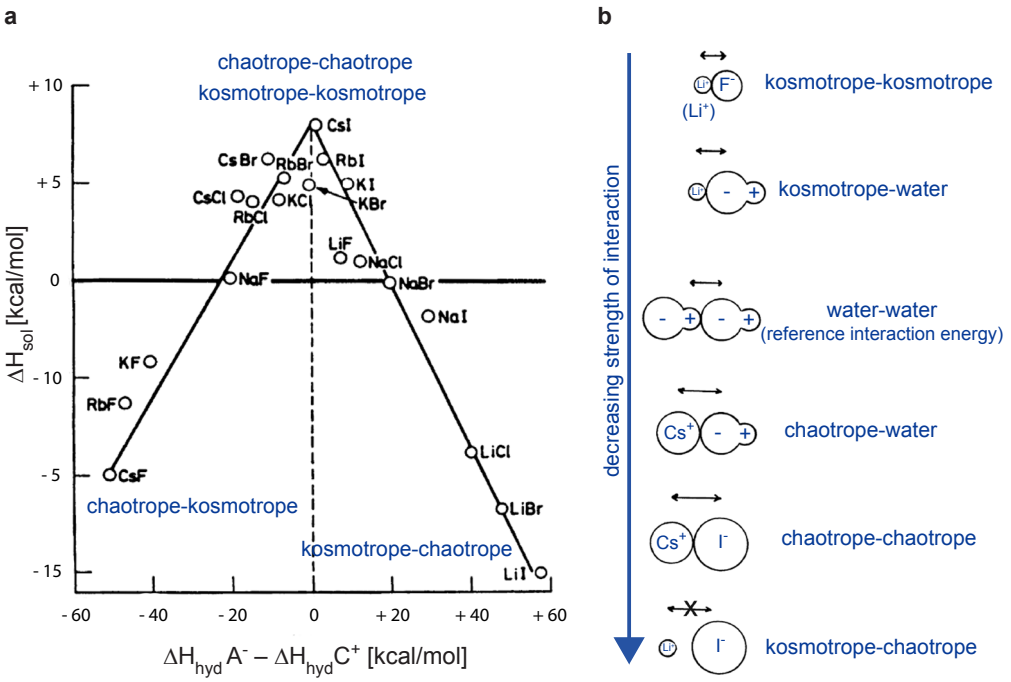

Fig. 6 Ions with similar water affinities preferentially interact with each other. (**a**) Volcano plot of the relationship between the measured heat of solution upon salt solvation (ΔH_{sol}) and the difference in absolute hydration enthalpy of the corresponding gaseous anion and cation of each salt ($\Delta H_{hyd}\,A^- - \Delta H_{hyd}\,C^+$). Note that dissolution of ion pairs with similar water affinities ($\Delta H_{hyd}\,A^- - \Delta H_{hyd}\,C^+ \sim 0$) takes up heat ($\Delta H_{sol} > 0$) indicating the breaking of strong bonds. These endothermic reactions are observed for salts composed of two chaotropic ions or two kosmotropic ions. In contrast, the dissociation of ion pairs composed of a kosmotrope and a chaotrope is an exothermic process, because the kosmotropic ion now experiences stronger interactions with water molecules than with its former chaotropic crystal partner. (**b**) Interaction strengths between kosmotropes, chaotropes and water molecules (depicted as spheres with a point charge in the centre). Kosmotropic ions (here Li^+ and F^-) have comparably small, and chaotropic ions (here Cs^+ and I^-) have comparably large sizes. Water molecules are depicted as dipoles. Ion pairing between a kosmotrope and an oppositely charged chaotrope does not occur spontaneously. The figure is modified from ref. 112.

2.4.3 Explanations for counterion association beyond charge neutralization

There are different hypotheses regarding the driving force for further counterion binding after protein charge neutralization. One explanation is Wigner crystal-like ion correlations: a multivalent ion approaching an already neutralized macroion (charged protein) surface repels other multivalent ions to a certain degree. This is supposed to create a negative correlation hole (or image charge)

on the protein surface which then attracts the approaching ion[114]. Theoretical consideration show that correlations between counterions may even result in a giant charge reversal, i.e. the net charge of the complex (macroion + counterions) after counterion association is greater than without ion association (only charged macroion)[115].

Another hypothesis states that association of additional counterions beyond charge neutrality is entropy-driven, because it minimizes the excluded volume for the solvent (water) molecules[116,117]. Continuum model simulations (without explicit water molecules) predict that the counterion concentration decays exponentially from the polyelectrolyte surface and the polyelectrolyte charge is merely attenuated. Explicitly modelling water molecules instead reveals oscillating density profiles of both counterions and water molecules at the polyelectrolyte surface. This shows that the presence of small water molecules pushes ions to the macromolecule surface because of water excluded volume effects[117].

Finally, dispersion interactions can lead to non-specific ion adsorption to neutralized surfaces. The positively charged lysozyme protein experiences biphasic ion-induced oligomerization, i.e. clustering at low and dispersion at high anion concentrations. At high ion concentrations, highly polarizable anions are more effective at inducing oligomer dissolution than anions with a lower polarizability[93]. The authors speculate that the proceeding ion association is due to dispersion forces and reduces the surface tension at the protein–water interface which in turn inhibits aggregation.

In summary, several theories have been proposed to explain ionic interactions between metal ions and proteins and the resulting protein aggregation phenomena. So far, however, research on this topic has been mostly focused on soluble proteins.

3 Aims of the study

This study was set out to investigate the influence of metal cations on the aggregation behaviour of a negatively charged plasma membrane protein. The experimental set-up comprises the SNARE protein SNAP25 as a biological anion chain, and calcium ions as a biologically relevant cation species. The study specifically addresses the following two points:

3.1 Comparison of ion-induced oligomerization in solution and in the cell membrane

The calcium-induced aggregation behaviour of recombinant, soluble SNAP25 is compared to the behaviour of the endogenous, membrane-anchored protein. It is particularly investigated whether the phenomenon of biphasic ion-induced aggregation, which has been described in simple (bio)polymer solutions, also applies to a cellular multi-component environment.

3.2 Determination of the physico-chemical properties of the ion required to induce membrane protein oligomerization

Hofmeister phenomena have been described for the aggregation propensities of a wide variety of soluble proteins. Here, I comparatively studied the effect of mono-, di- and trivalent ions on the clustering propensity of SNAP25 anchored to the native plasma membrane. The effect strength of the different ions is related to the physico-chemical ion properties to shed light on the underlying mechanism of protein clustering. The results of these experiments are compared to atomistic molecular dynamics simulations of a collaborator to unravel the atomistic details of ion–protein interaction patterns.

4 Materials and Methods

4.1 Materials

4.1.1 Hardware

4.1.1.1 Microscopes

Table 4 Microscopes and equipment details.

Equipment	specifications	manufacturer/source
Axio Observer D1 Epifluorescence microscope		Zeiss, Jena, Germany
objective	Plan-Apochromat 100x/NA 1.4 oil immersion	Zeiss
lamp	N XBO 75 (75 Watt Xenon arc lamp)	Zeiss
filter sets	UV filter set F11-000 EGFP HC filter set F36-525 TRITC HC filter set F36-525 Cy5 HC filter set F36-523	all from AHF Analysetechnik, Tübingen, Germany
detector	cooled digital CCD camera “Seniscam QE”, 12 bit 1376 × 1040 pixels, 6.45 µm × 6.45 µm pixel size	PCO, Kelheim, Germany
software	CamWare version 3.01	PCO

easy3D stimulated emission depletion (STED) microscope		Abberior Instruments, Göttingen, Germany
objective	UPlanSApo 100x/NA 1.4 oil immersion	Olympus, Hamburg, Germany
lasers	pulsed 488 nm excitation laser pulsed 640 nm excitation laser pulsed 775 nm STED laser	Abberior Instruments Abberior Instruments MPBC, Montreal, Canada
filter sets	500–520 nm filter set 650–720 nm filter set	Abberior Instruments Abberior Instruments
detector	single photon counting modules	Excelitas, Waltham, MA
software	Imspector version 0.10	Abberior Instruments

Confocor 1 fluorescence correlation spectroscopy (FCS) microscope		Zeiss
objective	C-Apochromat 63x/NA 1.2 water immersion	Zeiss
laser	argon ion laser	Lasos, Jena, Germany
filter sets	excitation: 515 FS 10-25 dichroic mirror: FT 510 emission: BP515-565	Zeiss Zeiss Zeiss
detector	single photon counting module	PerkinElmer, Waltham, MA
software	FCS access version 1.2.1.1	Zeiss

4.1.1.2 Appliances

Table 5 List of appliances

equipment / purpose	instrument name	manufacturer
gel imager	Odyssey® CLx Imaging System	LI-COR, Lincoln, USA
medium pressure liquid chromatography	BioLogic DuoFlow	BioRad, Hercules, CA, USA
UV-Vis detector for chromatography	BioLogic QuadTec, deuterium lamp	BioRad
microplate reader	Infinite® 200 PRO	Tecan, Maennedorf, Switzerland
dynamic light scattering	DynaPro NanoStar	Wyatt, Santa Barbara, CA
MST (label-free)	NT.LabelFree	Nanotemper, Munich, Germany
MST (with dye-coupled proteins)	Monolith NT.115	Nanotemper, Munich, Germany
Sonicator	Sonopuls HD 2070	Bandelin, Berlin, Germany

4.1.1.3 Size exclusion chromatography columns

Table 6 Size exclusion chromatography columns used for dye removal and buffer exchange

name	matrix	fractionation range	format	supplier
HR 10/30	Superdex 75	3–70 kDa	high performance	GE Healthcare, Little Chalfont, UK
illustra NAP-5	Sephadex G-25	1–5 kDa	gravity flow	GE Healthcare
Zeba desalting	proprietary	7 kDa cut-off	spin	ThermoFisher

4.1.1.4 Glass and plastic ware

Table 7 List of glass and plastic ware

item	specifications	manufacturer
Amicon Ultra-15 centrifuge filter	10 kDa cut-off	Merck Millipore, Darmstadt, Germany
384-well plate	flat bottom, non-binding, clear, polystyrol	Greiner Bio-One, Frickenhausen, Germany
6-well plate	for culturing adherent cells, polystyrol	Sarstedt, Nürnbrecht, Germany
75 cm^2 flask	for culturing adherent cells, polystyrol	Sarstedt
multiwell plate sealer	EASYseal, transparent, standard adhesive foil	Greiner Bio-One
cuvettes for DLS	4 µL, cyclic olefin copolymer (disposable)	Wyatt
chambered coverglass	borosilicate	Nunc/ThermoFisher, Waltham, MA
glass capillaries for MST	NT.115 standard treated NT.LabelFree Zero Background standard treated	Nanotemper
coverslips for epifluorescence	25 mm in diameter, No. 1	Marienfeld, Lauda-Königshofen, Germany
coverslips for STED	22x22 mm, No. 1.5	Marienfeld
Neubauer counting chamber	improved	Marienfeld
freezing container	Nalgene "Mr. Frosty"	Thermo Scientific, Rockford, USA

4.1.2 Chemicals

Table 8 List of chemicals

chemical	distributor
2-mercaptoethanol	Sigma, St. Louis, MO
acrylamide/bisacrylamide	Carl Roth, Karslruhe, Germany
$Al_2(SO_4)_3$	Carl Roth
$BaCl_2$	Carl Roth
bromophenol blue	Carl Roth
$CaCl_2$	Carl Roth

chemical	distributor
carbenicillin	Carl Roth
chloramphenicol	Carl Roth
cOmplete (protease inhibitor cocktail)	Roche, Basel, Switzerland
Coomassie Brilliant Blue G-250	ThermoScientific , Waltham, MA
cyanine5-NHS (N-succinimidylester)	Lumiprobe, Hannover, Germany
DMSO (dimethyl sulfoxide)	Carl Roth
DTT (dithiothreitol)	Sigma
EDTA (ethylenediaminetetraacetic acid)	Carl Roth
EGTA (Ethylene-bis(oxyethylenenitrilo)tetraacetic acid)	Carl Roth
ethanol	Schmittmann, Düsseldorf, Germany
fast DiO (3,3'-dilinoleyloxacarbocyanine perchlorate)	Thermo Fisher Scientific
glycerol	Carl Roth
Hepes	Carl Roth
IPTG (isopropyl-β-D-thiogalactoside)	Fisher Scientific
kanamycin	Carl Roth
KCl	Carl Roth
KH_2PO_4	Carl Roth
$LaCl_3$	Sigma
$MgCl_2$	Carl Roth
Na_2HPO_4	Carl Roth
NaCl	Carl Roth
$NaHCO_3$	Carl Roth
nail polish (transparent)	p2 cosmetics, Vienna, Austria
NH_4Cl	Carl Roth
NP-40 (nonylphenylpolyethylene glycol)	Sigma
ortho-phosphoric acid	Carl Roth
PFA (paraformaldehyde)	Carl Roth
pluronic-F127	Sigma
PMSF (phenylmethylsulfonyl fluoride)	Carl Roth
poly-L-lysine (PLL)	Sigma
ProLong Gold Antifade Mountant	Thermo Fisher Scientific
SDS (sodium dodecyl sulfate)	Carl Roth
TAMRA-NHS (5-carboxy-tetramethylrhodamine N-succinimidylester)	Sigma
TMA-DPH (1-(4-tri-methyl-ammonium-phenyl)-6-phenyl-1,3,5-hexatriene-p-toluenesulfonate)	ThermoFisher
trehalose	Carl Roth
Tris-HCl	Carl Roth
YCl_3	Sigma
$ZnCl_2$	Sigma

4.1.3 Buffers and solutions

Table 9 Composition of buffers and solutions

buffer/solution	composition	pH
PBS (phosphate buffered saline)	137 mM NaCl 2.7 mM KCl 10 mM Na_2HPO_4 1.76 mM KH_2PO_4	7.4
TBS (Tris buffered saline)	50 mM Tris-HCl 150 mM NaCl	7.4
Hepes/KCl	140 mM KCl 20 mM Hepes-KOH	7.2
Hepes/KCl/EGTA	Hepes/KCl + 10 mM EGTA	7.2
cleavage buffer	50 mM Tris-HCl 150 mM NaCl 1 mM EDTA 1 mM DTT	7.4
binding buffer	50 mM Tris-HCl 150 mM NaCl 1 mM EDTA 1x cOmplete 1 mM PMSF 1 mM DTT	7.4
bicarbonate buffer	100 mM $NaHCO_3$	8.4
4x Laemmli	8 % SDS 10% 2-mercaptoethanol 40% glycerol 0.0008 % bromphenol blue 250 mM Tris-HCl	6.8
Coomassie solution	5 % $Al_2(SO_4)_3$ 10% ethanol 2 % phosphoric acid 0.02 % Coomassie	–
PLL stock solution	2 mg/ml in ddH_2O	–
metal ion solution	$CaCl_2$, $SrCl_2$, $BaCl_2$, $MgCl_2$, NaCl, $ZnCl_2$, YCl_3, or $LaCl_3$ in Hepes/KCl	7.2

The presumably unimportant anion of the background salt was shown to play a crucial role in the activity of a restriction enzyme by inducing cavitation in a hydrophobic pocket of the enzyme[118]. In order to exclude hydrophobic or other effects originating from different anion background salts, all cations including buffer cations were used in the form of chloride salts in the Hepes/KCl buffer

and the metal ion solution. The metal ions used in this study are all available as chloride salts, but not all can be commercially obtained as acetate or glutamate salts. The Hepes/KCl/EGTA buffer used for sheeting cells in this study is therefore different from the standard buffer for this procedure[119], in that the glutamate and acetate anions were replaced by chloride. This was done in in order to keep the number of anions during incubation with the metal ion solution down to one species (chloride).

4.1.4 Biological materials

4.1.4.1 Antibodies

Table 10 Primary and secondary antibodies

antigen	clone	host species	fluorophore	dilution	catalog no.	manufacturer
SNAP25	71.1	mouse	–	1/200 (Epi) 1/100 (STED)	111 011	Synaptic Systems, Göttingen, Germany
SNAP25	polyclonal	rabbit	–	1/200	111 002	Synaptic Systems
Syntaxin-1	HPC-1	mouse	–	1/200	S0664	Sigma
mouse IgG	polyclonal	donkey	Alexa Fluor 594	1/200	A-21203	ThermoFisher
mouse IgG	polyclonal	goat	Star 635p	1/500	2-0002-007-5	Abberior
rabbit IgG	polyclonal	goat	Alexa Fluor 488	1/500	A-11034	ThermoFisher
mouse IgG	polyclonal	goat	Alexa Fluor 647	1/500	A-21235	ThermoFisher

4.1.4.2 Enzymes

Table 11 List of enzymes

enzyme	catalog no.	manufacturer
DNAse I	M0303	NEB, Ipswich, MA
GoTaq	M0480S	NEB, Ipswich, MA
lysozyme	8259.1	Carl Roth
trypsin/EDTA for cell culture	P10-0231SP	PAN Biotech, Aidenbach, Germany
trypsin for partial proteolysis	T4799	Sigma
PreScission Protease	27-0843-01	GE Healthcare

4.1.4.3 Plasmids

Table 12 Plasmids used for cloning and SNAP25 expression

plasmid	antibiotic resistance	source
pEGFP-C1	kanamycin	Clontech
pGEX-6P1	ampicillin	GE Healthcare
pGEM-T easy	ampicillin	Promega, Mannheim, Germany

4.1.4.4 Organisms

Table 13 List of organisms

organism	source
E. coli XL-10 Gold® Ultracompetent Cells	Stratagene, La Jolla, CA
E. coli Rosetta(DE3)pLysS	Merck
rat PC12 cell line	kind gift from Rolf Heumann, Bochum University

4.1.4.5 Culture media

Table 14 Culture media and supplements

culture medium	composition	supplier
LB medium	2 % [w/v] LB powder according to Lennox in ddH_2O in case of plates: + 2 % [w/v] agar-agar	AppliChem, Darmstadt, Germany Carl Roth
PC12 growth medium	DMEM with 4.5 g/l glucose and L-glutamine 10% [v/v] horse serum 5% [v/v] fetal calf serum 1% [v/v] penicillin/streptomycin	PAN biotech Biochrom AG, Berlin, Germany Biochrom AG PAN biotech

Table 15 Other biological materials

material	catalog no.	supplier
Bovine serum albumin (BSA)	8076.4	Carl Roth
Glutathione sepharose beads	17075601	GE Healthcare
FITC-labelled lactadherin	BLAC-FITC	HaemTech, Essex Junction, VT

4.1.5 Software

Table 16 Software used for data analysis

software	version	supplier	use
ApE	2.0.45	by M.W. Davis (open source)	sequence alignment development of cloning strategies
ImageJ	1.50c	W. Rasband, National Institute of Health, USA (open source)	image analysis
MS Excel	2010	Microsoft Corporation, Redmond, WA	calculations and data organization
OriginPro	8.0951	OriginLab Corporation, Northampton, MA	curve fitting
Sigma Plot	11.0	Systat Software, San Jose, CA	plotting data

Appliances listed in Table 5 were operated with the accompanying equipment software of the manufacturer.

4.2 Methods

If not specified otherwise, experiments were carried out at room temperature (RT).

4.2.1 Cloning

For recombinant production of soluble SNAP25, its DNA sequence was subcloned into a bacterial expression vector as follows. Rat SNAP25b DNA was amplified from a previously generated pEGFP-C1-SNAP25 construct[120]. This amplification was done via polymerase chain reaction (PCR) using primers which contained restriction sites for BamHI (forward primer) and EcoRI (reverse primer) at their 5' ends. Subsequently, an adenine was added to the PCR product using GoTaq polymerase, and it was ligated into the pGEM-T easy vector. Using the inserted BamHI and EcoRI restriction sites, the sequence was then subcloned into the bacterial expression vector pGEX-6P1. SNAP25 is thus N-terminally fused to a glutathione S-transferase (GST) tag, under the control of an IPTG-sensitive promotor. Plasmids were transformed into *E. coli* XL-10 Gold for construct amplification. Bacteria were grown in LB medium containing either 50 µg/ml carbenicillin (which is a less toxic and more stable analogue of ampicillin) or 50 µg/ml kanamycin, depending on the plasmid antibiotic resistance. Successful cloning was verified by sequencing and comparison to the rat SNAP25b sequence (AB003992).

4.2.2 SNAP25 purification

The GST-SNAP25 construct was transformed into *E. coli* Rosetta(DE3)pLysS. This strain is optimized for eukaryotic protein expression since it contains an extra plasmid which encodes rare codon tRNAs (and a chloramphenicol resistance for selection). A small volume of LB medium containing 50 µg/ml carbenicillin and 34 µg/ml chloramphenicol was inoculated overnight. This pre-culture was used

to inoculate several litres of LB medium not containing antibiotics (to maximize protein production). Bacteria were grown until they reached the exponential growth phase, and then protein expression was induced with 1 mM IPTG at 18 °C overnight. Bacteria were then harvested by centrifugation, washed once with PBS, and then frozen at -80 °C. The pellet was thawed in a water bath at 37 °C, and carefully resuspended in ice-cold binding buffer additionally containing 100 µg/ml lysozyme and 2 units/ml DNAse I. The bacteria were mildly sonicated and then centrifuged at 4 °C. The supernatant was incubated with glutathione sepharose beads pre-equilibrated with binding buffer rolling in a gravity flow column overnight at 4 °C.

The column was washed several times with ice-cold cleavage buffer, and the GST tag was cleaved with PreScission protease (incubated rolling slowly for 5 h at 4 °C). The purified non-tagged protein was then eluted from the column. The protein was concentrated and the buffer was exchanged to TBS containing 1 mM DTT using Amicon centrifuge filters. The protein concentration was determined photometrically, and adjusted to 400–600 µM. The sample was supplemented with 10 % [v/v] glycerol, aliquoted, snap-frozen in liquid nitrogen and stored at -80 °C. Samples from all steps of the purification procedure were analysed with sodium dodecyl sulfate polyacrylamid gel electrophoresis (SDS-PAGE).

4.2.3 SDS-PAGE

Protein samples were mixed with Laemmli buffer, boiled for 10 min at 95 °C, and loaded onto SDS-PA gels. The separation gel contained 15 % acrylamide/0.32 % bisacrylamide and the stacking gel 4 % acrylamide/0.11 % bisacrylamide. Gels were run for 1.5 h at 100 V and stained with Coomassie solution. The fluorescence was recorded with an Odyssey Clx imaging system at 700 nm.

4.2.4 SNAP25 labelling

SNAP25 was dialyzed against bicarbonate buffer, and then incubated with the amine-reactive cyanine5- or TAMRA-NHS esters for 2 h at RT. The reaction was stopped by addition of TBS (neutralizing the pH), and non-bound dye was removed via gel filtration in a TBS-equilibrated column. In case of cyanine5, a gravity flow Sephadex G-25 column was used, the separation was monitored by eye and the labelled protein was collected manually. Non-bound TAMRA was removed with a Superdex column coupled to a medium pressure liquid chromatography system. Elution of the dye and labelled protein was monitored with the attached UV-Vis detector and fractions containing SNAP25-TAMRA were automatically collected with a fractionator. Fractions were pooled, and stored at a concentration of 10–25 µM in TBS containing 10 % [v/v] glycerol at -80 °C.

4.2.5 Partial proteolysis

SNAP25 at a concentration of 200 µM was incubated in TBS containing 1 mM DTT and 250 mg/ml trehalose with 0, 1, 10, 100 or 1000 mM calcium, and partially digested with varying concentrations of trypsin at 37 °C. The digest was monitored by taking a sample from each reaction vessel after 5, 10, 15, 20, and 30 min, and comparing it to a sample before addition of trypsin (-1 min). The samples were mixed with PMSF (1 mM final concentration) to inhibit the protease, and then calcium ions were removed using desalting spin columns to avoid precipitation of calcium dodecyl sulfate during subsequent mixing with Laemmli buffer. The products were analysed via SDS-PAGE.

4.2.6 Optical density (OD) measurements

SNAP25 at a concentration of 70 µM was incubated in TBS with calcium concentrations between 0 and 1000 mM in a 384-well plate. The plate was sealed with a transparent plate sealer to avoid evaporation. The OD for 595 nm

light was measured every 5 minutes at a 180° angle with a Tecan microplate reader. One min before each measurement, the plate was briefly shaken to avoid sedimentation of potentially forming precipitates. All measurements were performed at least as duplicates, and the OD was corrected for control solutions which did not contain SNAP25, but the respective calcium concentration. To check for potential degradation, the solutions were recovered from the microtiter plate, the calcium ions were removed via a short gel filtration and subjected to SDS-PAGE as described above.

4.2.7 Dynamic light scattering (DLS)

SNAP25 was incubated for 8–10 minutes with calcium in TBS in the cuvette before starting the measurements at 37 °C. Scattered light was detected at a 90° angle; laser wavelength was 663 nm, and laser intensity was auto-attenuated by the software to keep the intensity of the scattered light within the linear detection limit. All solutions were sterile-filtered and all plastic ware was rinsed three times with ddH_2O to avoid dust particles in the measurement. Data were recorded and analysed using Wyatt's Dynamics software (version 7.1). The autocorrelation curves were fitted using the DYNALS algorithm. According to Wyatt, DYNALS is more suitable than the standard CONTIN algorithm to determine semi-quantitative distributions for broadly (i.e. over several orders of magnitude) polydisperse samples. This was verified for the measurements presented here by comparing the fit quality of both algorithms. The autocorrelation curves were used to calculate the mass-weighted particle size distributions.

4.2.8 Fluorescence correlation spectroscopy (FCS)

TAMRA-labelled SNAP25 at a concentration of 500 nM in TBS was incubated with 0–1000 mM calcium for 10 min at RT in a chambered coverglass before imaging each sample with a ConfoCor 1 microscope. SNAP25-TAMRA was

excited with an argon ion laser. Ten 60 s fluorescence intensity fluctuation time courses were recorded and the signal was time correlated with the built-in hardware correlator to generate autocorrelation curves.

4.2.9 Microscale thermophoresis (MST)

MST measurements were performed in TBS with two-fold serial dilutions of calcium or magnesium chloride at fixed protein concentrations. The Nanotemper Analysis software (version 1.5.41) was used for data acquisition and analysis. Recordings involved a 5 s fluorescent baseline scan, followed by 30 s of infrared (IR) laser illumination, and 5 s of recording after turning off the IR laser. The normalized protein fluorescence (F_{norm}) was calculated by normalizing the fluorescence time trace to the initial fluorescence (before turning on the IR laser), and expressing the fluorescence after thermophoresis and temperature jump (during the last second before turning off the IR laser) in per mille.

Experiments with cyanine5-labelled SNAP25 were conducted with the Monolith NT.115 instrument. Cyanine5-labelled SNAP25 was used at a concentration of 500 nM, and 750 nM unlabelled SNAP25 was added to increase the amount of available interaction partners. Control measurements involved no protein, but only 500 nM cyanine5 dye. The TBS buffer contained 0.05 % NP-40 to minimize sticking to the standard glass capillaries used for measurements. The IR laser power was set to 10 %, the power of the LED used for exciting the cyanine5 fluorescence was adjusted to the sample brightness. Brightness varied considerably between runs, probably because cyanine5 is very sticky and adsorbs to the reaction vessel of the protein stock solution. Therefore, the lowest F_{norm} value was set to zero, and the highest to 100 % in each run, before averaging the runs.

Label-free MST was performed with 10 µM unlabelled SNAP25 in the NT.LabelFree instrument using Zero Background capillaries. Control

measurements contained only calcium and buffer (TBS supplemented with 0.1 % Pluronic). Tryptophan fluorescence was excited using 30 % LED power, and thermophoresis was induced with 40 % IR laser power.

4.2.10 Cell culture

All cell culture work was carried out under a sterile hood. Cells were maintained at 37 °C / 5 % CO_2 in 75 cm^2 flasks or six-well plates.

4.2.10.1 Cleaning and coating of coverslips

For cleaning, coverslips were incubated for 1 h with 1 M HCl, rinsed with ddH_2O, incubated for 1 h with 1 M NaOH, rinsed again with ddH_2O, and then incubated overnight in 100 % ethanol. The ethanol was discarded, and the glassware was sterilized in the oven at 180 °C.

A PLL stock solution was diluted to a concentration of 0.1 mg/ml with ddH_2O. Coverslips were placed into six-well cell culture dishes, and incubated with 500 µl PLL each for 30 min. The liquid was then removed, coverslips were dried for at least one hour, and sterilized by a 20 min exposure to UV light. Coated coverslips were stored at 4 °C.

4.2.10.2 Passaging and seeding of cells

Cells were detached from their culturing flasks by a brief wash with pre-warmed PBS, followed by a 5 min incubation with trypsin/EDTA at 37 °C. Enzymatic activity was stopped by adding pre-warmed growth medium, and cells were centrifuged. For passaging, cells were resuspended in a small volume of growth medium and part of the cell suspension was transferred into a new flask.
For seeding, cells were resuspended in PBS, and counted in a Neubauer chamber. An appropriate number of cells was pelleted and resuspended in growth medium

to seed 6×10^5 cells per coverslip. Cells were left to attach and grow for 24 h before use in experiments.

4.2.10.3 Freezing and thawing of cells

Cells were detached and resuspended at a concentration of 10^7 cells/ml in growth medium lacking penicillin/streptomycin but supplemented with 10 % [v/v] DMSO. The cell suspension was transferred to cryovials. Vials were placed in a freezing container containing isopropanol, and frozen at -80 °C. After 24 h, vials were transferred to nitrogen vapour phase for long-term storage.

4.2.10.4 Membrane sheet preparation and incubation with ions

Cells were briefly washed with PBS, and placed into a petri dish filled with ice-cold Hepes/KCl/EGTA. The coverslip with the cells facing up was placed at a distance of 5 mm from the sonicator tip, and the apical membrane was removed with a 0.1 s ultrasound pulse (see also Fig. 7). This leaves behind the native basal membrane with the inner leaflet (to which SNAP25 is attached) now being accessible for treatment and staining. This two-dimensional membrane sheet preparation is also ideal for epifluorescence microscopy, since there is no out-of-focus light in the z-plane.

After sheeting, the coverslips were washed once in Hepes/KCl, and then incubated with 100 µl of a metal ion solution, face-down on parafilm for 10 min at 37 °C. Afterwards, membrane proteins were fixed for 45 min in 4 % PFA.

4.2.10.5 Staining of membrane sheets

The fixative was quenched with NH_4Cl (50 mM in PBS) for 15 min, and coverslips were rinsed with PBS three times for 5 min. Non-specific binding sites were blocked with BSA (3 % [w/v] in PBS) for 1 h. Sheets were then incubated with the primary

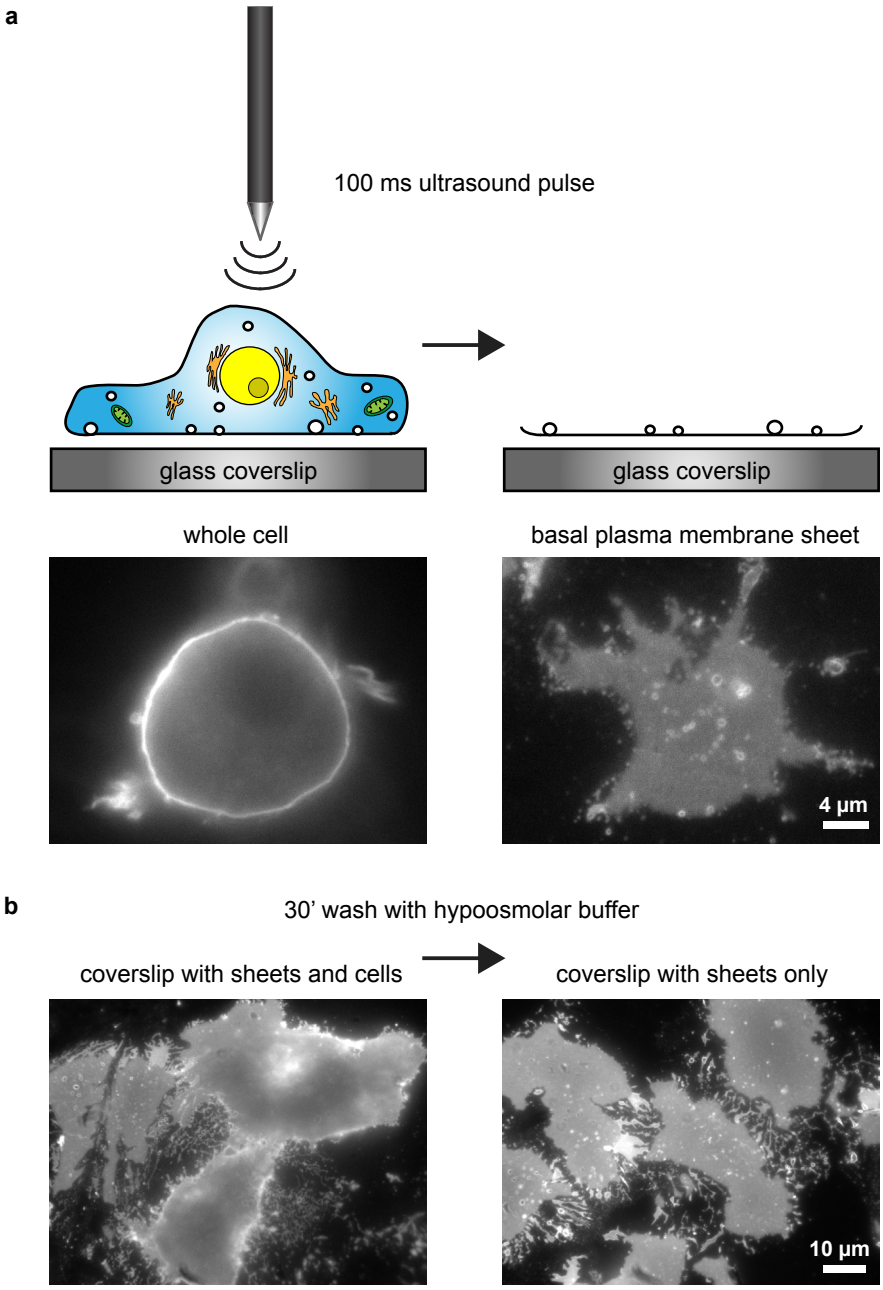

Fig. 7 Preparation of plasma membrane sheets. (**a**) A 100 ms ultrasound pulse is applied to cells adhered on glass coverslips (left). This shearing force removes the apical cell membrane and cytosol, while the intact basal plasma membrane is left behind with the inner membrane leaflet exposed to the buffer solution (right). The epifluorescence images illustrate the z-resolution of the plasma membranes (stained with TMA-DPH) before (left) and after sheeting (right). (**b**) The procedure described above generates plasma membrane sheets predominately in close proximity to the ultrasonic device, while more distant cells remain intact (left). If a pure membrane sheet preparation is desired, a subsequent 30 min washing step in hypoosmolar buffer can be performed (right). The epifluorescence images display TMA-DPH stained HeLa plasma membrane sheets before and after the washing step.

antibody(ies) in blocking solution overnight at 4 °C in a humid chamber. The next day, coverslips were rinsed with PBS, and incubated with the secondary antibody(ies) for 1 h at RT in a humid chamber. Coverslips were rinsed again with PBS. For SNAP25 single stainings, clone 71.1 was used in combination with an Alexa 594-coupled secondary antibody for epifluorescence, and a Star 635p-coupled secondary antibody for STED microscopy. In case of double stainings with syntaxin which was visualized with an Alexa 647-coupled secondary, the polyclonal SNAP25 antibody was used in combination with an Alexa 488-coupled secondary antibody (cf. Table 10 for details on antibody specifications and dilutions). Phosphatidylserine was stained with lactadherin-FITC (diluted 1/20 in PBS) for 15 min at RT. For epifluorescence microscopy, the membrane was counterstained with TMA-DPH (diluted 1/10 from a saturated solution in PBS) and coverslips were immediately used for imaging. For STED microscopy, the membrane was counterstained with fast DiO (0.5 µg/ml in PBS) for 10 min, followed by a PBS rinse. For mounting, excess liquid was blotted onto a paper towel, and a 20 µl drop of mounting medium was added to the coverslip, which was then mounted onto a cover slide. Samples were air-dried overnight, and then sealed with nail polish.

4.2.11 Microscopy

4.2.11.1 Epifluorescence microscopy

Coverslips were placed in a microscopy chamber filled with PBS containing 10 % TMA-DPH solution, and imaged first in the TMA-DPH channel to ensure blind selection of intact membranes. Subsequently, a picture was taken in the immunostaining channel(s). FITC and Alexa 488 fluorescence were imaged with the EGFP filter set, Alexa 594 fluorescence was imaged with the TRITC filter set, and Alexa 647 fluorescence was imaged with the Cy5 filter set. The exposure time was kept constant for each staining throughout all experiments.

4.2.11.2 STED microscopy

Membrane sheets were again selected blindly, based on membrane integrity. The fast DiO membrane stain was excited with a pulsed 488 nm laser set to 20 % and detected with a 500–520 nm filter. SNAP25 immunofluorescence was excited using a 640 nm laser set to 30 %, depleted with a 775 nm STED laser set to 800 mW, and recorded with 1.25 ns gate through a 650–720 nm filter. Images were acquired with a pixel size of 20 nm × 20 nm, and 20 µs dwell time.

4.2.12 Image analysis

All analyses were performed in regions of interest (ROIs) within the images. ROIs were placed in the membrane channel to ensure blind selection of intact membrane stretches. For the quantification of fluorescence in epifluorescence images, each sheet ROI was accompanied by a background ROI placed next to the sheet. The ROI sets were subsequently transferred to the immunofluorescence channel(s). ROI size was 50 px × 50 px for epifluorescence, and 150 px × 150 px for STED images.

For the analyses described in the following subsections, the data for all sheets per condition and day were averaged (corresponding to n = 1). These averaged values were then used to calculate the mean value and the s.e.m. using the averaged data of other days.

4.2.12.1 Average fluorescence intensity

The average fluorescence intensity of a sheet was calculated by subtracting the average fluorescence intensity of the background ROI pixels from the average fluorescence intensity of the sheet ROI pixels.

4.2.12.2 Relative standard deviation (rel. SD)

The rel. SD of the fluorescence intensity of a sheet was calculated by dividing the SD of the sheet ROI's grey values by its background corrected mean fluorescence intensity (cf. 4.2.12.1)

4.2.12.3 Segmentation of the immunofluorescence into uniform and punctuate signal areas

This segmentation seeks to differentiate between clustered and non-clustered proteins. ROIs were segmented using the following algorithm (kindly provided by Dr. Jan-Gero Schloetel). First, a Gaussian blur filter was applied. Then, punctuate areas were defined according to a variable local threshold: The threshold was exceeded if the central pixel intensity was higher than the sum of the average intensity of the surrounding 5 px × 5 px area + 4 % of the average ROI intensity. A mask of the punctuate areas was created, and enlarged by one pixel to include signal flanks. The mask was then transferred to the original, non-processed image. Immunofluorescence within the mask was designated as punctuate signal pool, while fluorescence outside of the mask was designated as uniform signal pool. The average fluorescence intensity was then measured separately in each of these two segments.

The integrated intensity, i.e. the amount of fluorescence, originating from uniform signal pool was calculated by multiplying the total ROI area with the average uniform fluorescence intensity.

integrated uniform signal = total area × average uniform signal intensity

The integrated intensity originating from the punctuate signal pool was calculated by multiplying the punctuate signal area by the difference between the average punctuate intensity and the average uniform intensity.

Integrated punctuate signal
= punctuate area × (average punctuate intensity – average uniform intensity)

4.2.12.4 Cluster diameter

The cluster diameter was analysed in STED images by shifting a ROI pixel-wise to the right, and calculating the Pearson correlation coefficient (PCC) between the original image and each shifted image. The thus generated autocorrelation curves were then averaged for all ROIs from a certain condition and day. Curves were fitted using a polynomial function. The function was used to calculate the distance at which the PCC dropped to 50 % of its original value. This distance corresponds to the average radius of objects in the image.

4.2.12.5 Number of clusters per area

Clusters were identified in STED images using ImageJ's "find maxima" tool with a similar noise level for all ROIs. The number of thus identified clusters was then expressed per area (μm^2).

4.2.12.6 Colocalization

The images of the two immunostaining channels were aligned. Then, the degree of colocalization was determined based on a pixel-wise PCC between the fluorescent intensities in the aligned images.

5 Results

5.1 SNAP25 oligomerization in solution

The first aim of this study is the comparison of ion-induced protein oligomerization between soluble and membrane-bound SNAP25. Oligomerization was first evaluated in solution, to determine whether SNAP25 behaves similarly to other charged proteins (like BSA and lysozyme) in response to oppositely charged ions. Here, primarily calcium ions were used, because these are both highly charged and biologically relevant. Based on the considerations on aggregation mechanisms and ion–protein interactions discussed in the introduction, it is hypothesized that calcium ions influence SNAP25 clustering through an electrostatic mechanism, i.e. through interactions with its negatively charged amino acid residues. A previous study on SNAP25 indeed already pointed in this direction[29]. To exclude that protein charge is not only modulated directly by ion binding, but also indirectly by metal ion hydrolysis and a subsequent change in pH[91], all experiments were performed in buffered solutions at physiological pH.

5.1.1 SNAP25 expression and purification

Analysing oligomerization of soluble SNAP25 required a pure protein preparation, preferably without a tag that might interfere with oligomerization. To this end, the sequence of rat SNAP25b was subcloned into the bacterial expression vector pGEX-6P1. SNAP25 is fused with its N terminus to a GST tag which contains a cleavage site for the PreScission protease. The vector was transformed into *E. coli* and SNAP25-GST was expressed overnight at 18°C.

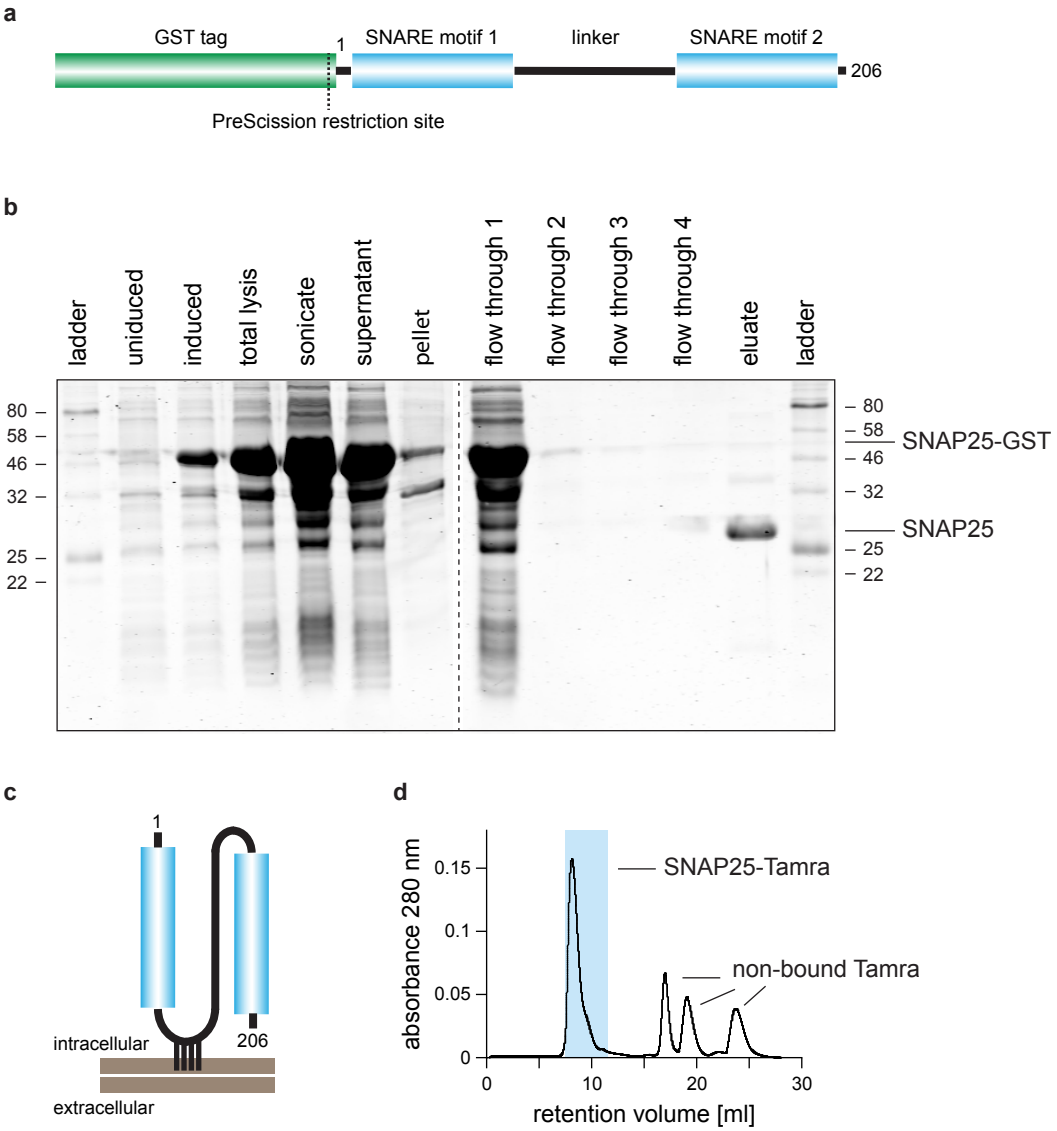

Fig. 8 Purification and labelling of recombinant SNAP25. (**a**) Structure of the expressed protein which consists of the N-terminal GST-tag with a C-terminal PreScission cleavage site, followed by the SNAP25 protein comprising two SNARE motifs connected by a linker. (**b**) Coomassie stained SDS-PA gel loaded with samples from each step of the SNAP25 purification process: SNAP25-GST (~50 kDa) was expressed and purified from *E. coli*. Bacterial pellets were taken up in lysis buffer, sonicated, and insoluble components were removed by centrifugation. The supernatant was bound to a glutathione column, and after several washing steps the GST-tag was cut off using the PreScission protease which then allows for the elution of untagged SNAP25 (~25 kDa). (**c**) In the cell, SNAP25 is attached to the intracellular plasma membrane leaflet at its linker region via palmitoyl anchors. Note that recombinant expression of SNAP25 in *E. coli* leads to a non-palmitoylated protein. (**d**) Elution profile of TAMRA-labelled SNAP25. Recombinant SNAP25 was labelled with TAMRA and then subjected to gel filtration to remove non-bound dye from the labelled protein. Protein and dye were monitored via their absorbance at 280 nm (which is dominated by the dye absorbance). The blue shaded area depicts the elution fractions that were collected and pooled for further experiments.

Bacteria were harvested and lysed, and the protein supernatant was bound to a glutathione sepharose column. Non-binding protein was removed via several washing steps. The GST tag was cleaved using the PreScission protease, which released the non-tagged, fairly pure SNAP25 protein from the column (see Fig. 8 a, b). While in mammalian cells SNAP25 is palmitoylated and thus attached to the inner plasma membrane (Fig. 8 c), expression in *E. coli* yields a soluble, non-palmitoylated protein because this host lacks the necessary palmitoyl transferases.

Several methods were tested to find a suitable approach to probe SNAP25 oligomerization in solution, in some cases requiring labelling with fluorophores such as TAMRA, Alexa 532, or cyanine5. To this end, the NHS-ester-activated fluorophores were coupled to primary amine groups of the protein yielding stable amide bonds. Non-bound fluorophores were removed from the labelled protein preparation via gel filtration (see Fig. 8 d).

5.1.2 Analysing SNAP25 oligomerization with partial proteolysis

In a first attempt to analyse ion-induced oligomerization of SNAP25, the protein was partially digested with low concentrations of protease in the presence of variable calcium concentrations, and its resistance to digestion was evaluated with SDS-PAGE. Partial Proteolysis is a standard biochemical method for determining the structural accessibility of a protein: Proteases preferentially cut those parts which are most exposed to the solvent (and thus the enzyme). Hence, oligomerized and tightly packed SNAP25 should be less efficiently digested than single protein strands. Here, trypsin was chosen as a protease since SNAP25 has many (29) trypsin cleavage sites distributed throughout its entire sequence, and trypsin is active at physiological pH. (Major changes in the pH would affect the protonation state of the protein residues and thus protein charge.) The digestion is stopped after various time points, and the products are separated on an SDS-PA gel.

While partial proteolysis is usually regarded as a simple and straightforward method, several difficulties had to be circumnavigated in this case. First, the activity of trypsin (and of many other proteases) varies with ion concentration. The catalytic activity of trypsin increases with calcium concentration and reaches a plateau at 1 mM calcium[121]. Therefore, SNAP25 samples incubated with concentrations lower than 1 mM calcium were excluded from the analysis. Second, the protein concentration needs to be sufficiently high to detect a band with Coomassie staining, which is why 200 µM SNAP25 were used in this assay. However, it was observed that SNAP25 at high concentrations precipitates with calcium ions. To prevent precipitation, 250 mg/ml trehalose was added to the solution as a stabilizing agent. Trehalose creates a depletion attraction between proteins, which stabilizes protein conformation[32]. Addition of trehalose successfully prevented precipitation, but dramatically increased solution viscosity. Third, calcium ions form insoluble calcium dodecyl sulfate upon mixing with Laemmli buffer. For this reason, the proteolysis was first blocked with PMSF, and calcium ions were subsequently removed via gel filtration of the samples. Only afterwards samples were mixed with Laemmli buffer and subjected to SDS-PAGE. These many experimental steps complicate loading equal amounts of protein to the SDS-PA gel.

Several partial proteolysis experiments were carried out, with varying trypsin-to-SNAP25 ratios (1/5,000 – 1/25,000). The sample incubated with the lowest calcium concentration was generally most efficiently digested, arguing for the lowest degree of oligomerization (see also Fig. 9, right). However, there was no clear trend in SNAP25 digestion efficiency at increasing calcium concentrations. In the experiment shown in Fig. 9 (right) the extent of the proteolysis was comparable at higher calcium concentrations. In other experiments, calcium concentrations between 10 and 100 mM seemed to have the most protective effect (arguing for the highest degree of oligomerization).

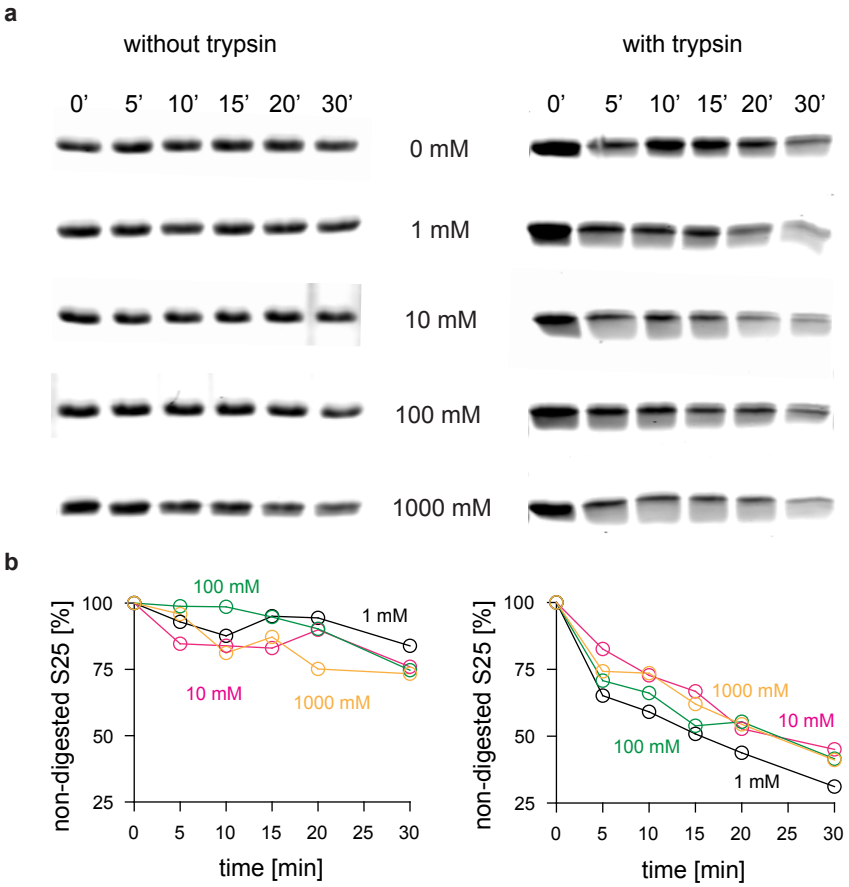

Fig. 9 Partial proteolysis is not suitable for detecting changes in the oligomeric state of SNAP25 because of the high assay variability. The figure shows the SDS-PA gels (**a**) and corresponding analyses (**b**) of one experiment without (left) and with trypsin (right) out of a series of partial proteolysis experiments. (**a**) 200 µM SNAP25 were incubated with the indicated calcium concentrations and partially digested with 0.01 µM trypsin (right) or not incubated with proteases for control purposes (left). The digestion was blocked with PMSF before the addition of protease (0 min) or after 5, 10, 15, 20 or 30 min after protease addition. (**b**) The efficacy of the proteolysis was analysed by quantifying the amount of remaining full-length SNAP25 at each time point after digestion compared to the initial amount of full-length SNAP25 (0 min time point). The quantification of the 0 mM calcium sample is not shown because trypsin activity is reduced in the absence of calcium. The differences in digestion efficiencies observed in the experiment shown on the right could not be reproduced in other experiments. A considerable degree of variability is also observed in the control experiment, which did not contain trypsin (left). Note the fluctuation in the recorded amount of SNAP25 fluorescence within the samples over time, and the loss of protein after 30 min even without proteolytic digest in all the samples.

A control experiment which was performed in the absence of trypsin (Fig. 9, left) underlines the great variability in this assay: there is an approx. 20 % fluctuation in the recorded amount of SNAP25 fluorescence within the samples over time, and about 25 % of the protein is lost after 30 minutes, regardless of the calcium concentration. It appears that the many steps that are involved in the experimental set-up (see above and cf. Methods for details) produce a high experimental variability which in turn masks the (comparably subtle) ion-induced differences in oligomerization.

While detailed information on the calcium dependence of protein accessibility could thus not be obtained, the experiments point to an increase in oligomerization induced with 10–100 mM calcium.

5.1.3 Optical density (OD) measurements

In a next step, oligomerization of SNAP25 was analysed in optical density measurements. The optical density (or turbidity) of a solution depends on the capacity of particles to scatter and absorb light, which is influenced by the presence of non-dissolved (or precipitated) particles, particle concentration, and particle size[12]. The optical density presents a somewhat indirect or crude readout for oligomerization since it is dominated by precipitates which form as a consequence of preceding oligomerization. SNAP25 was incubated with increasing amounts of calcium ions in a 384-well plate at 37°C, and the OD of the solution was monitored for several hours (Fig. 10 a-c). The multi-well plate was shaken for a few seconds one minute before each measurement to resuspend possibly unevenly sedimented precipitates. (Sedimentation was not directly observed between the measurements or after completion of the experiment, but it may have become obvious after a centrifugation step). An increased turbidity indicating multimerization is visible in all conditions. In the absence of calcium, this is probably the result of spontaneous protein precipitation. Initially, the OD increases with increasing calcium concentration.

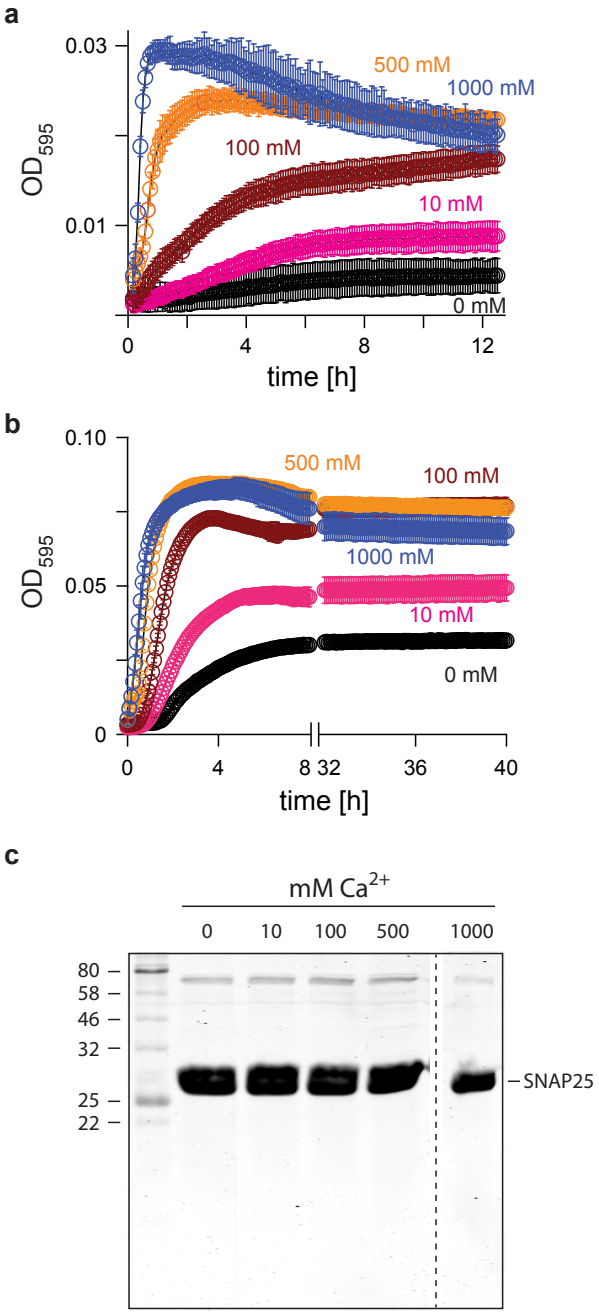

Fig. 10 Optical density measurements suggest biphasic oligomerization of soluble SNAP25 in response to calcium ions. SNAP25 (70 µM) was incubated with the indicated Ca^{2+} concentrations in TBS in a multi-well plate at 37 °C for several hours. The optical density of the solution at a 180° angle with light of 595 nm wavelength was determined every 5 min after briefly shaking the plate. The measurements were blank corrected for the OD of a buffer solution containing the respective Ca^{2+} concentration (but no protein). (**a**) At 1000 and 500 mM Ca^{2+}, the initial precipitation phase is apparently reversible, while protein precipitation at 100 mM Ca^{2+} increases over time (mean ± s.d., n = 4–5 technical replicates prepared in parallel). (**b**) In other experiments, the same trend with a somewhat different kinetic pattern during the first few hours was observed (n = 3 technical replicates). A similar behaviour was also observed in a third set of measurements (not shown). Because of these kinetic differences the experiments were not averaged but are shown individually. (**c**) SDS-PAGE of SNAP25 samples recovered after the experiment shown in **b** to analyse potential protein degradation during the long-term incubation. Samples were run on two SDS-PA gels (separated by the dashed line) and stained with Coomassie. There are no degradation products visible in any of the samples. Panel **a** of this figure was previously published in ref. 122.

After the first approx. two hours, however, the degree of turbidity declines again at high calcium concentrations (500 and 1000 mM), which argues for a reduction in multimer size or re-dissolution of precipitates. Conversely, the turbidity at 100 mM calcium increases further, indicating on-going oligomerization, while at lower calcium concentrations oligomerization apparently stagnates.

In summary, this indirect read-out for oligomerization argues for a biphasic oligomerization behaviour of SNAP25 in response to Ca^{2+} ions[122]. At intermediate calcium concentrations of 100 mM, oligomerization increases – either steadily (Fig. 10 a) or intermittently (Fig. 10 b) – until the end of the experiment.

To exclude that the changes in turbidity after long incubation times at 37 °C are associated with protein degradation, the protein was recovered after the experiment and subjected to SDS-PAGE (Fig. 10 d). There were no bands visible that would argue for SNAP25 degradation.

5.1.4 Dynamic light scattering (DLS) measurements

To gain more detailed information on the distribution of oligomer sizes, the calcium effect on SNAP25 was analysed with DLS. In DLS, the hydrodynamic radius of an object is calculated from the temporal correlations of light that is scattered by diffusing objects. Unlike the relatively crude OD measurements, DLS measurements can detect very small particles (down to ~0.2 nm in case of the instrument used here), and can also resolve mixed populations with particles of different radii. Two sets of DLS measurements each comprising three experiments were conducted. Even in the absence of calcium ions, SNAP25 shows a polydisperse (i.e. broad) size distribution (Fig. 11 a–c, upper row) which argues for the co-existence of monomers and lower order oligomers. With increasing calcium concentration (e.g. at 100 mM), oligomer size increases in all experiments (Fig. 11 a–c). The oligomerization behaviour at higher calcium concentration varies between experiments: While at 500 mM in some experiments the small and large oligomers coexist (Fig. 11 b), only small (Fig. 11 a) or large (Fig. 11 c) oligomers are present in other. Sometimes, co-existing populations of large and a few decades smaller particles are detected at high calcium concentrations (see Fig. 11 c). This argues for a randomly occurring biphasic oligomerization response.

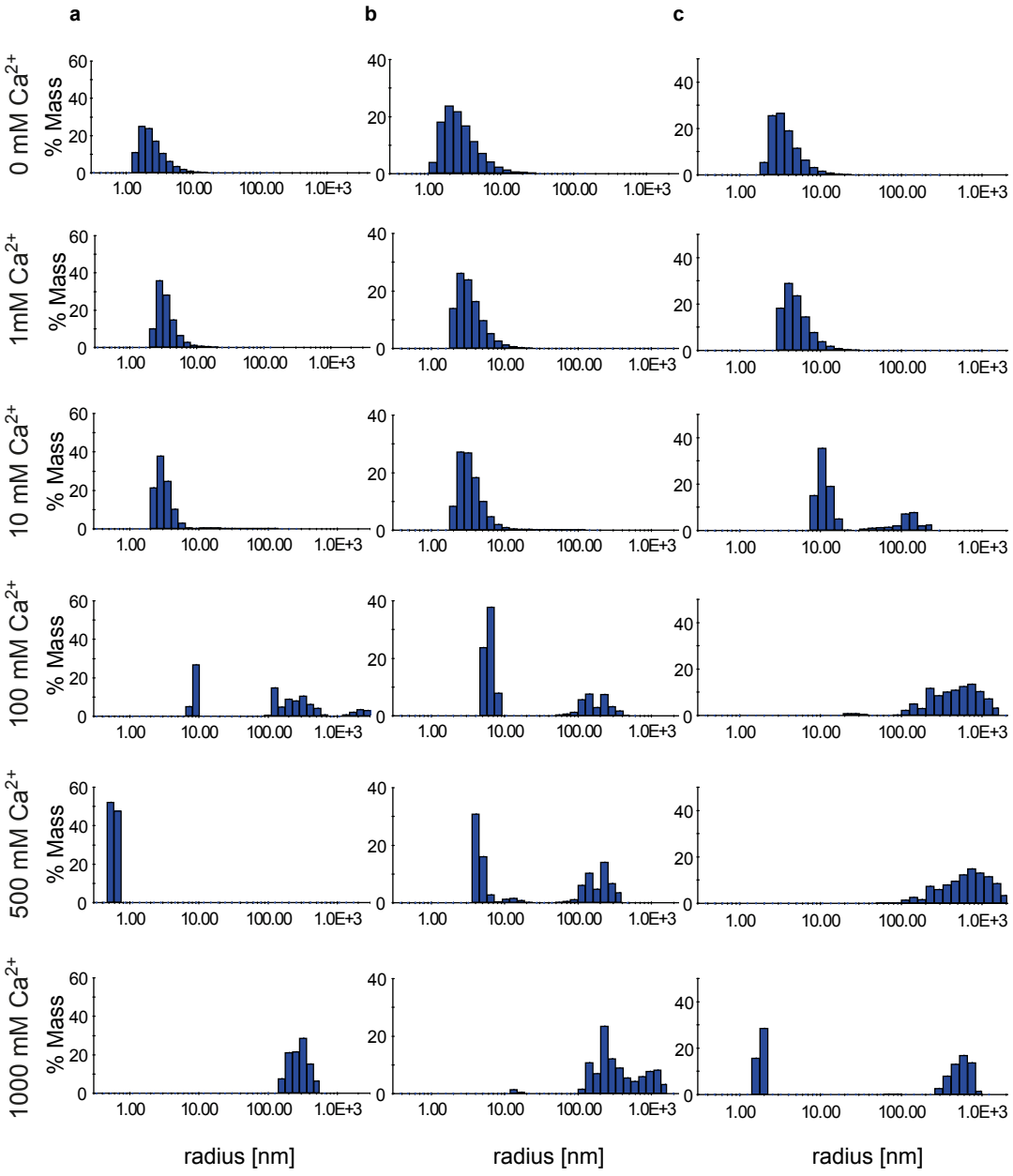

Fig. 11 Reversibility of SNAP25 oligomerization analysed with dynamic light scattering (DLS). SNAP25 at a concentration of 6.4 mg/ml (274.5 μM) (**a**), 1.0 mg/ml (43 μM) (**b**), and 3.2 mg/ml (137 μM) (**c**) was incubated for 8–10 minutes with the indicated Ca^{2+} concentrations in TBS at 37 °C, and 663 nm light scattered at a 90° angle was measured on a DynaPro Nanostar instrument. The temporal correlations of the scattered light intensities were used to calculate the mass-weighted particle size distributions. While a population of small particles appears at 500 mM calcium in **a**, large precipitates form at 1000 mM calcium both in run **a** and **b**. In run **c**, small and large particles co-exist at 1000 mM calcium. The differences in the oligomerization behaviour are not due to protein concentration but to the random nature of the oligomerization/precipitation process; a second set of three experiments all performed with 3.2 mg/ml SNAP25 protein yielded essentially the same results. Note that the calculated hydrodynamic radii assume Brownian motion of spherical particles. Since this does not apply to charged proteins, the hydrodynamic radii shown here cannot be directly translated into actual radii of the protein oligomers. I would like to thank Catherine Tardin and Laurence Salomé (IPBS Toulouse) for help with DLS measurements.

An exact analysis of the oligomer sizes is hampered for two reasons. The calculated hydrodynamic radii assume Brownian motion of spherical, neutral particles. In this measurement, we used proteins which are charged and additionally probably not spherically shaped. Second, the intensity of the scattered light increases with the sixth power of particle radius. If a solution contains a mixture of oligomers that differ in their sizes by a few decades, the autocorrelation curve is dominated by signal contributions of large particles. The size estimation of the small particles is therefore less certain, and very sensitive to minor changes in the fitting parameters of the autocorrelation curve. Despite these drawbacks, the trend that is observed in the size distributions shows that biphasic oligomerization in response to calcium ions can principally take place. Nevertheless, quantification and reproducibility of the behaviour is difficult due to the variable degrees of calcium-induced SNAP25 precipitation. We therefore turned to approaches allowing measurements with more diluted SNAP25 samples.

5.1.5 Fluorescence correlation spectroscopy (FCS)

SNAP25 oligomerization was next assayed with FCS. This technique is similar to DLS in that temporal correlations of signals from diffusing objects are used to analyse object size. In the case of FCS, the recorded signal is the fluorescence of a dye attached to the molecule of interest. FCS measurements were conducted with TAMRA-labelled SNAP25 after 10 min of incubation with calcium concentrations between 1 and 1000 mM or in the absence of calcium. Multimers were visible in the recorded fluorescence time courses as soon as calcium was present (Fig. 12 a). These multimers occurred sporadically and in various sizes, which resulted in autocorrelation curves derived from the time courses that were too diverse to reliably calculate the diffusion time of SNAP25 (Fig. 12 b). Therefore, information about the size cannot be accurately extracted from these FCS measurements. However, judging from the peak intensities in the time courses (Fig. 12 a) and the points of inflection in the autocorrelation curves (Fig. 12 b) it appears that the

brightest and slowest multimers are found at 500 mM calcium. Consistently, the number of SNAP25 particles drops at 500 mM calcium, and increases again at 1000 mM calcium, apparently following a similar biphasic trend (see Fig. 12). This could be due to the individual SNAP25-TAMRA proteins forming fewer (and thus larger and brighter) multimers at 500 mM than at 1000 mM calcium. It should be noted, though, that high calcium concentrations led to an increased noise level in FCS measurements, which may artificially increase particle number.

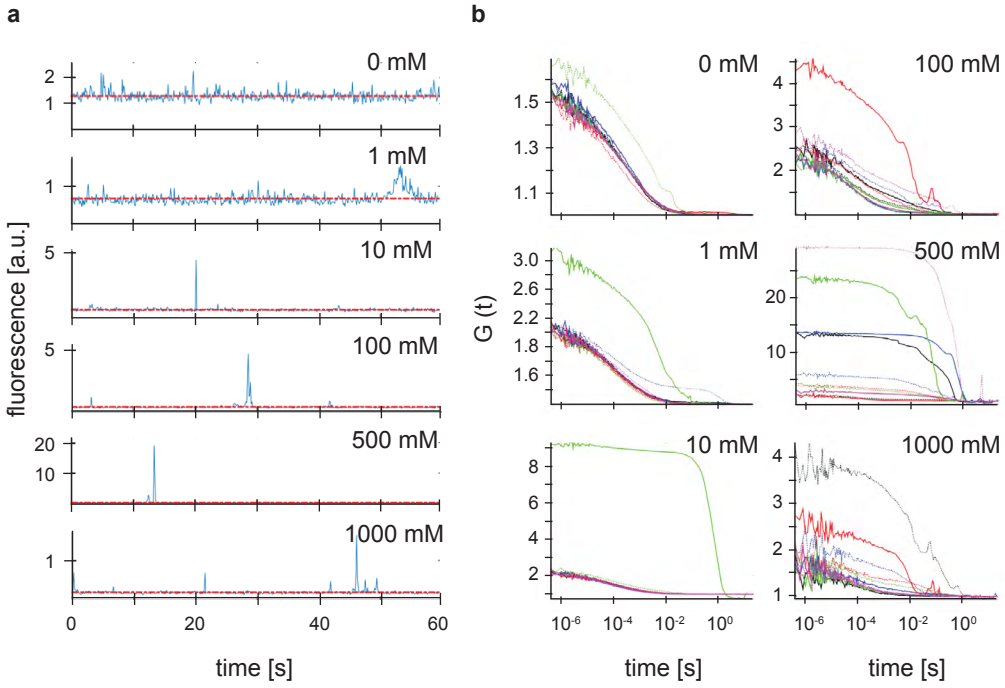

Fig. 12 Reversibility of SNAP25 oligomerization analysed with fluorescence correlation spectroscopy (FCS). TAMRA-labelled SNAP25 at a concentration of 500 nM was incubated with the indicated calcium concentrations for 10 min at RT, and then 60 s fluorescent time courses were recorded. (**a**) Example time courses of the SNAP25-TAMRA fluorescence and (**b**) autocorrelation functions (G(t)) of the fluorescence intensity fluctuation for all ten time courses (represented by different colours). Already at 1mM calcium, large SNAP25-TAMRA aggregates are randomly detected in the focal volume (see peaks in **a**). Because of these aggregates, the variation between the individual autocorrelation functions is too great to reliably calculate the diffusion time of the calcium samples. However, the number of SNAP25 particles apparently follows a biphasic trend with increasing calcium concentration: The reciprocal of the y-intercept of the autocorrelation function is equivalent to the number of particles in the focal volume, which drops at 500 mM calcium, and increases again at 1000 mM calcium. The data correspond to one FCS measurement. A similar observation was made in an FCS measurement with AlexaFluor532-labelled SNAP25. I would like to thank Dr. Thomas Sorkalla (IBMB, Bonn) for supervision and help with FCS measurements and interpretation.

The FCS measurements were flawed with additional technical issues, such as an increased viscosity that resulted in doubled diffusion times at 1000 mM calcium in control measurements. In addition, the fluorescence intensity decreased with increasing calcium concentration. This could be due to SNAP25-TAMRA depletion from the solution; z-scans showed an increased stickiness to the bottom of the experimental vessel. Alternatively, this could be an effect of molecular crowding leading to TAMRA self-quenching.

In summary, the increase in oligomerization at low to intermediate calcium concentrations is clearly observed despite all technical flaws. In contrast, while there are several hints that the degree of oligomerization declines at 1000 mM calcium, the FCS measurements do not unequivocally proof it.

5.1.6 Microscale thermophoresis (MST)

To collect further evidence for SNAP25 dispersal at high calcium concentrations and thus corroborate the results from the OD, DLS, and FCS measurements, SNAP25 oligomerization was analysed with MST. Thermophoresis (or thermodiffusion) is a mass-dependent movement of particles in an induced temperature gradient, and is monitored via recording the local concentration of fluorescence originating from the particles of interest. Initially, cyanine5-labelled SNAP25 was used for MST experiments, because labelling proteins with a fluorophore in the visible range provides a better signal-to-noise ratio than the intrinsic protein fluorescence. SNAP25 thermodiffusion was studied at two-fold serial dilutions of calcium. Thermodiffusion of SNAP25-cyanine5 slowed down with increasing calcium concentrations up to ~63 mM, and gradually sped up again at higher concentrations (see Fig. 13 a, b). The cyanine5 dye on its own also showed a Ca^{2+}-dependent change in its thermophoretic mobility – albeit in the

opposite direction, i.e. it became slower at high calcium (Fig. 13 c, d). These dye dynamics may lead to an underestimation of the increase in SNAP25 thermodiffusion at high calcium concentrations in this approach.

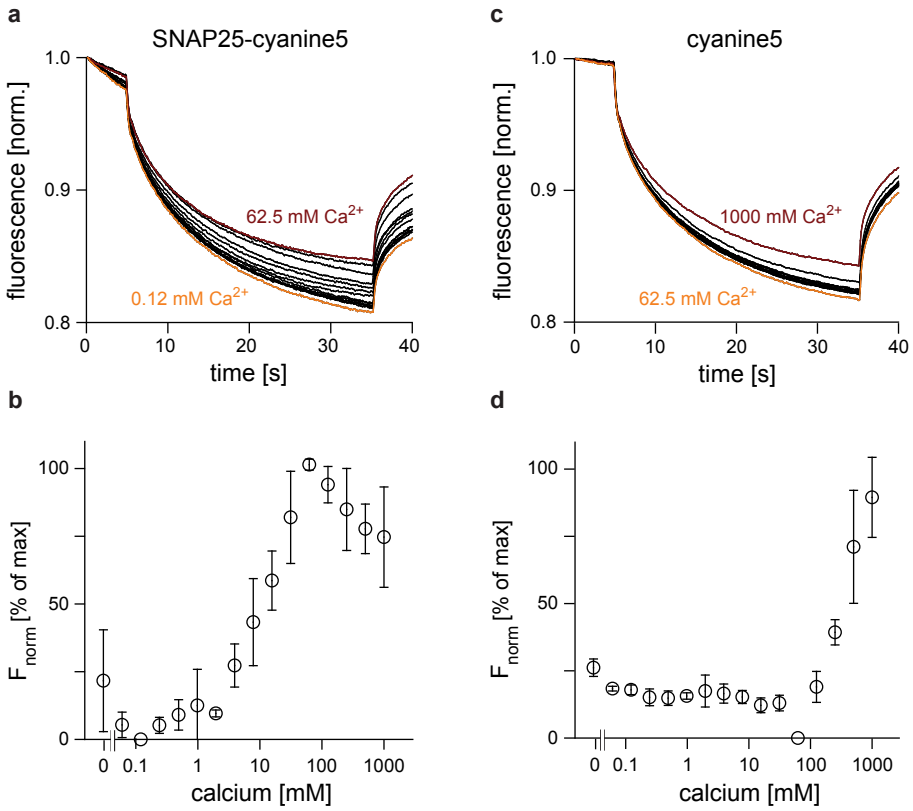

Fig. 13 Microscale thermophoresis (MST) with cyanine5-labelled SNAP25 suggests biphasic SNAP25 oligomerization in response to Ca^{2+} ions. MST measurements with 1.25 µM SNAP25 (from which 500 nM were cyanine5-labelled and 750 nM unlabelled SNAP25) were performed with serial dilutions of $CaCl_2$ in TBS containing 0.05 % NP-40 at 37 °C. (**a**) Normalized fluorescence traces of SNAP25-cyanine5, illustrating its temperature-jump and thermophoresis at different calcium concentrations in one experiment. Traces with the minimum (62.5 mM $CaCl_2$) and maximum (0.12 mM $CaCl_2$) thermophoretic mobility are coloured in purple and orange, respectively. (**b**) Normalized SNAP25-cyanine5 fluorescence after thermophoresis and temperature jump (F_{norm}, expressed in % of the maximum), averaged and plotted versus the calcium concentration. The increase in F_{norm} at intermediate calcium concentrations indicates slower thermodiffusion and therefore a higher degree of oligomerization. The values are given as mean ± s.d. (n = 3). Essentially the same results were obtained in another set of measurements (n = 4) which were performed without addition of unlabelled SNAP25 and at room temperature. (**c**) Control experiment showing the normalized fluorescence traces of 500 nM unconjugated cyanine5 (without protein). (**d**) Normalized cyanine5 fluorescence after thermophoresis and temperature jump (F_{norm}, expressed in % of the maximum) plotted versus the calcium concentration (mean ± s.d., n = 3). While the unconjugated dye shows virtually no difference in its thermophoretic mobility at low calcium concentrations, F_{norm} steadily increases at concentrations above 62.5 mM calcium. This behaviour is contrary to the SNAP25-conjugated dye, which shows steadily decreasing F_{norm} values above 62.5 mM calcium (**b**).

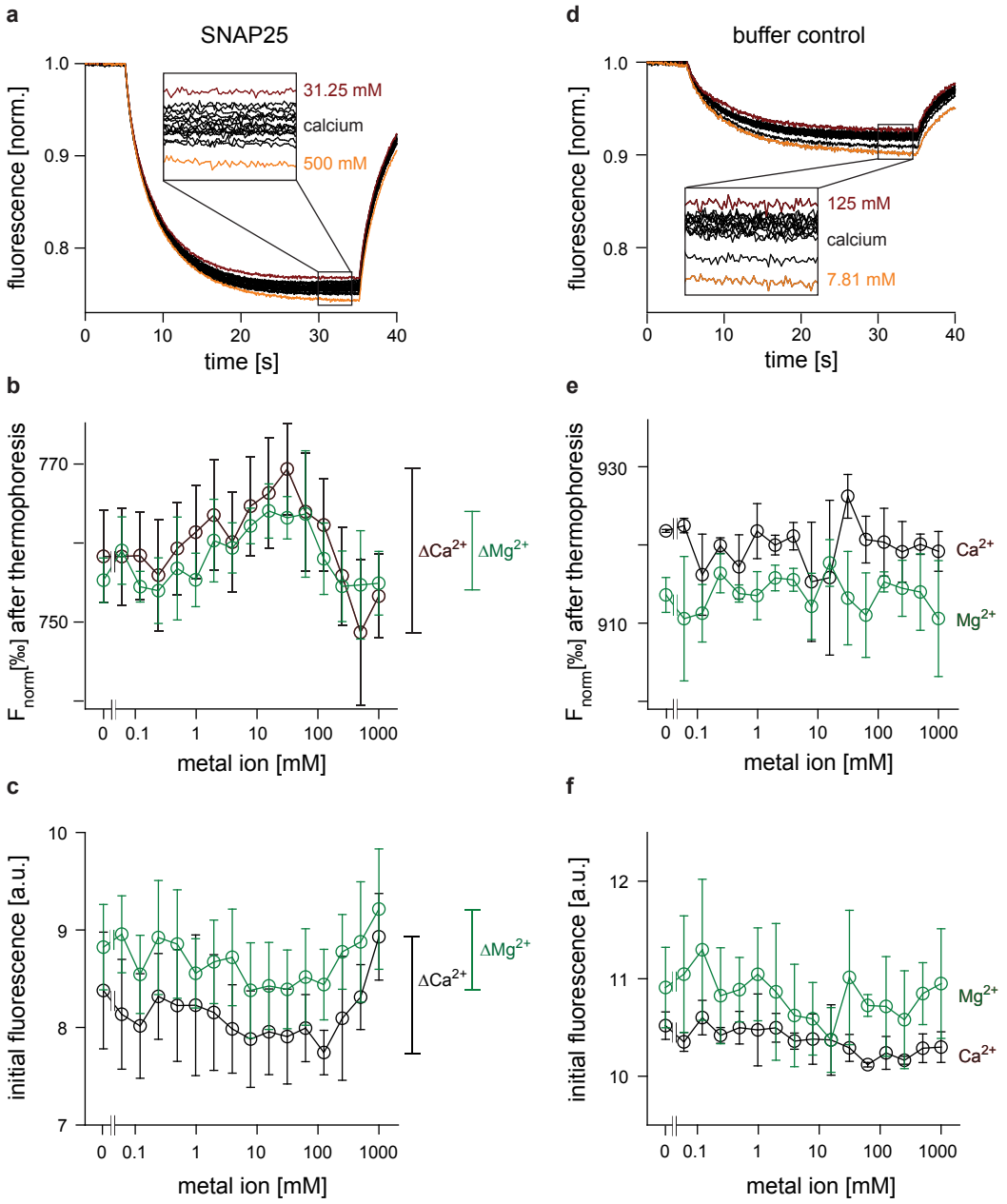

Fig. 14 Biphasic SNAP25 oligomerization in response to Ca^{2+} and Mg^{2+} is verified using label-free thermophoresis. (**a–c**) MST measurements with serial dilutions of $CaCl_2$ or $MgCl_2$ at a fixed concentration of 10 µM unlabelled SNAP25 were performed at 37 °C. (**a**) Normalized SNAP25 tryptophan fluorescence time traces from one MST experiment. Traces yielding the minimum (31.25 mM $CaCl_2$) and maximum (500 mM $CaCl_2$) thermophoretic mobility are shown in purple and orange, respectively. (**b**) Normalized tryptophan fluorescence ratios after thermophoresis and temperature jump (F_{norm}, expressed in per mille) at different divalent ion concentrations (black, Ca^{2+}; green, Mg^{2+}). The development of F_{norm} suggests the presence of low oligomers in the absence of divalent ions, the formation of larger oligomers at intermediate concentrations and dispersal to possibly monomeric SNAP25 at maximal Ca^{2+}. The drop in F_{norm} observed at highest ion concentrations may be underestimated because of the high solution viscosity.

(**c**) Absolute tryptophan fluorescence intensity (blank corrected, see below) measured before thermophoresis and T-jump (t = 0). The dynamic ranges of signal change for Ca^{2+} and Mg^{2+} are indicated by brackets. Values are given as mean ± s.d. (n = 5–9). (**d**) Control experiment showing the normalized background fluorescence traces of the buffer solution (0.1 % Pluronic in TBS, no protein) at increasing Ca^{2+} concentrations. (**e**) Normalized background fluorescence ratios after thermophoresis and temperature jump (F_{norm}) show random variations in the thermophoretic mobility of the buffer solution. (**f**) Absolute background fluorescence intensities which originate from the buffer and the glass capillary containing the fluid measured before thermophoresis and temperature jump (t = 0). Values are given as mean ± s.d. (n = 4). The respective averaged intensities were subtracted as blank values from the averaged SNAP25 tryptophan fluorescence intensities shown in panel **c**. Note that the buffer solution and the glass capillary substantially contribute to the fluorescence signal, but show no ion-concentration dependent changes. Panel **a** and **b** of this figure were previously published in ref. 122.

In order to eliminate any dye artefacts (especially stickiness and the calcium dependent thermophoretic mobility of cyanine5), MST measurements were repeated with unlabelled SNAP25. In this case, thermodiffusion was monitored via the protein's intrinsic tryptophan fluorescence (SNAP25 contains one tryptophan residue). The labelfree MST measurements confirmed the biphasic response to calcium ions (Fig. 14 a, b). Biphasic oligomerization was also observed in response to Mg^{2+} ions, albeit to a lesser extent. Interestingly, SNAP25 thermodiffusion at 500 mM calcium was even faster than without calcium (cf. Fig. 14 b). This suggests that the oligomeric state of SNAP25 at 500 mM calcium is lower than without calcium. In other words, the protein is not monomeric in the absence of calcium. This is in line with the broad size distribution observed in calcium-free SNAP25 samples in the DLS measurements.

In the labelfree MST experiments, the buffer did not show calcium dependent changes in its thermophoretic mobility, but only random fluctuations (Fig. 14 d, e). SNAP25 precipitation (visible through deformed MST traces which were removed from the analyses) was hardly observed in MST measurements, probably for two reasons. First, the measurements required only low (1.25–10 µM) protein concentrations and a low reaction volume of approx. 5 µl. In addition, low amounts of detergent in the buffer further minimized the risk of protein precipitation (and sticking to the reaction vessel).

The biphasic response of both unlabelled and cynaine5-labelled SNAP25 to calcium ions implies biphasic protein oligomerization. However, it should be noted that thermodiffusion is not only dependent on molecule size, but also on charge and solvation entropy of the molecule. Changes in charge and the hydration shell of the protein may thus contribute to the observed effect.

In labelfree MST experiments, the biphasic behaviour of SNAP25 is corroborated by a second, thermodiffusion-independent observation: The initial tryptophan fluorescence (i.e. the fluorescence that is recorded prior to creating a temperature gradient and inducing thermodiffusion) shows a mild decrease at intermediate calcium concentrations (Fig. 14 c). From 100 mM calcium onwards, the initial tryptophan fluorescence increases again. This effect is again more subtle in the case of magnesium ions. A reduction in the tryptophan fluorescence argues for fluorescence self-quenching due to close spatial proximity of the tryptophan residues. Since SNAP25 contains only one tryptophan residue, several proteins need to come into close contact to induce quenching.

5.2 SNAP25 oligomerization in the plasma membrane

To investigate whether ion-induced protein oligomerization can be retraced in the protein's native environment, oligomerization of membrane-bound SNAP25 was analysed. These studies were performed with endogenous SNAP25 which was visualized with antibody stainings to exclude potential artefacts arising from overexpression or fluorescent tags – a GFP molecule, for example, has a size similar to SNAP25 and should influence SNAP25 clustering accordingly.

As a member of the neuronal SNARE protein family that is involved in synaptic vesicle fusion, SNAP25 is predominantly expressed in neuronal tissues[123]. Therefore, neuroendocrine PC12 cells were used as a model neuronal environment for SNAP25 clustering.

5.2.1 Establishment of a membrane sheet based assay to evaluate SNAP25 clustering in its physiological environment

SNAP25 is anchored to the cytosolic leaflet of the plasma membrane (cf. Fig. 8 c). In order to target SNAP25 with ions or antibodies, access to the inner membrane leaflet needs to be provided. This is typically achieved with detergents which create small holes in membranes. The drawback of this approach is that the architecture of the entire membrane is destroyed, and protein clustering is severely altered. In this study, so-called membrane sheets were created instead. Application of a short ultrasonic pulse removes the apical cell membrane and washes away cytosolic components. The intact basal plasma membrane with the inner membrane leaflet facing up is left behind (see Methods and Fig. 7 a for details). Protein diffusion dynamics and the assembly of SNARE complexes remain intact in these preparations[25,124,125].

In a first set of experiments, thus generated membrane sheets were incubated for ten minutes in 140 mM KCl at pH 7.2 supplemented with logarithmically increasing calcium concentrations. Control sheets were incubated with 10 mM EGTA, which chelates trace divalent (and trivalent) ions. Afterwards, proteins were fixed and immunostained using two different antibodies targetting SNAP25: either a monoclonal antibody directed against the N-terminus, or a polyclonal antibody directed against the C-terminus of the protein. The membrane was counterstained with the lipophilic dye TMA-DPH to evaluate membrane integrity, and the samples were then imaged with an epifluorescence microscope. Sheets were selected in the TMA-DPH channel on the basis of intact membrane appearance.

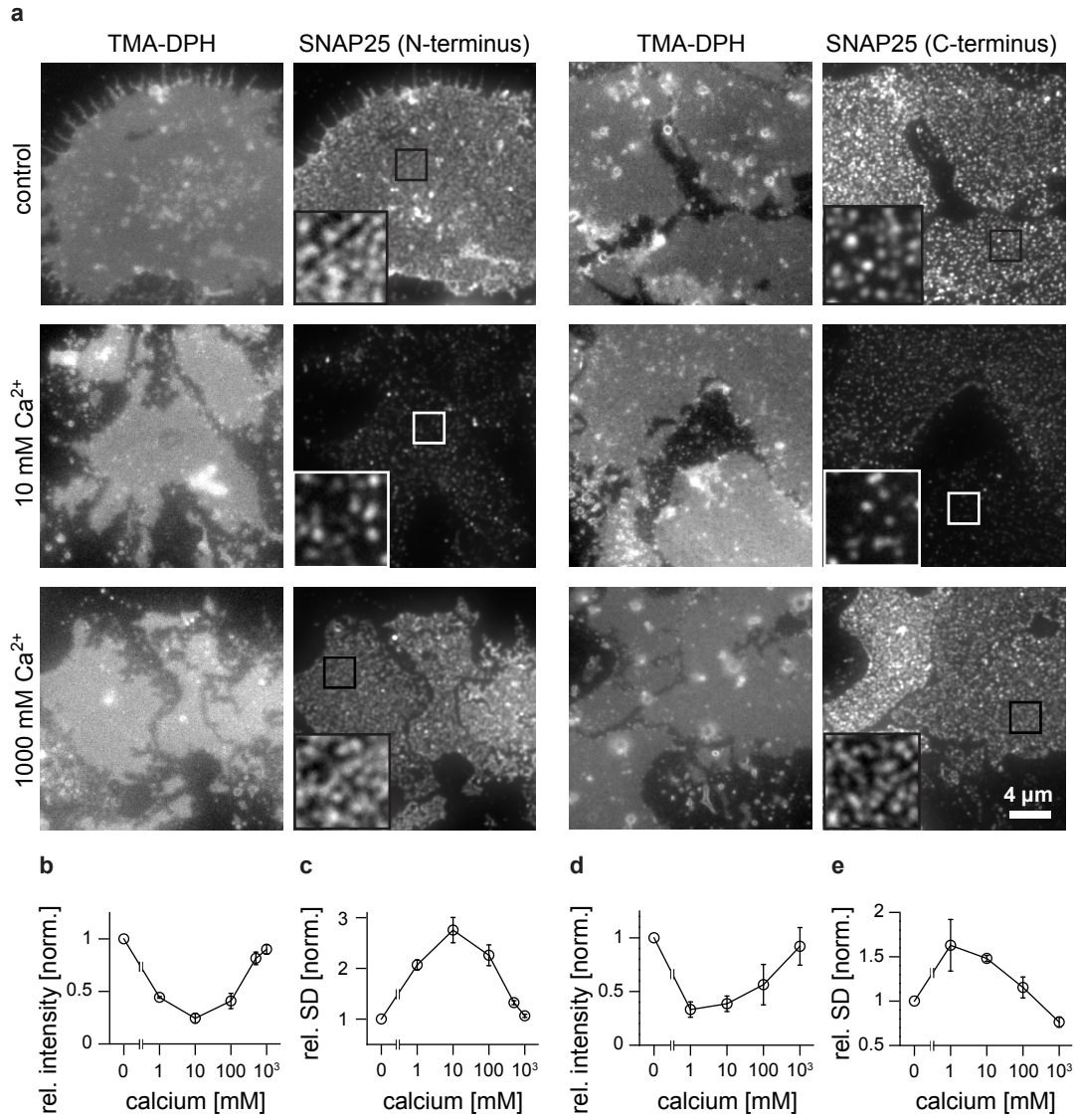

Fig. 15 Biphasic oligomerization of SNAP25 in response to calcium ions in its native plasma membrane environment. PC12 plasma membrane sheets were incubated with 0–1000 mM calcium chloride in Hepes/KCl buffer for 10 min at 37 °C. Sheets were fixed, immunostained for SNAP25, counterstained with TMA-DPH, and analysed with epifluorescence microscopy. (**a**) Images of the membrane dye TMA-DPH (documenting membrane integrity) and the corresponding immunostaining using either a monoclonal mouse antibody directed against the N-terminus of SNAP25 (left) or a polyclonal rabbit antibody directed against the SNAP25 C-terminus (right) in membrane sheets incubated with 0, 10, or 1000 mM $CaCl_2$. Overview images (from one antibody staining) are shown at the same scaling while magnified insets are arbitrarily scaled. (**b**) Average SNAP25 fluorescence intensity, relative to the control condition which contained no calcium ions, in sheets stained with the N-terminal antibody. The decrease in fluorescence intensity at intermediate calcium concentrations indicates epitope masking due to a higher SNAP25 packing density and/or a conformational change, as previously described[29]. (**c**) Relative standard deviation (rel. SD) of the immunostaining pattern in sheets stained with the antibody targetting the N-terminus. (**d**) Normalized SNAP25 fluorescence intensity and (**e**) rel SD. in sheets stained with the antibody directed against the SNAP25 C-terminus. Values are given as mean ± s.e.m. (n = 2–4). Panel **b** and **c** of this figure are modified from ref. 122.

In the control condition, membrane sheets showed a bright and dispersed SNAP25 distribution (Fig. 15 a, upper row). In the presence of 10 mM calcium, the pattern became more punctuate (and dimmer), indicating SNAP25 clustering. This trend then reversed at higher calcium concentrations, at which the appearance of sheets was comparable to the control condition. This argues for biphasic clustering in response to increasing calcium concentrations not only of soluble but also of membrane bound SNAP25.

Based on this observation, it was evaluated how to best quantify the effect to further explore the mechanisms underlying clustering, also testing influences of pH, ionic strength, or depletion forces.

Segmentation-free analyses for clustering

In a first step, the degree of SNAP25 clustering was quantified using two parameters, (1) the average fluorescence and (2) the standard deviation of the fluorescence in a region of interest (ROI).

(1) The average SNAP25 fluorescence intensity was used to address changes in SNAP25 accessibility. A decrease in staining intensity likely reflects epitope masking due to molecular crowding: The more tightly the proteins are packed, the harder it is for the antibodies to access their epitope which in turn produces a darker staining[29]. Crowding may be inter- or intra-molecular; either a SNAP25 cluster comprising several SNAP25 molecules becomes more tightly packed, or individual molecules experience a conformational change.

(2) The standard deviation of the fluorescence intensity was used to evaluate changes in SNAP25 distribution. If the fluorescent particles are accumulated in clusters, the standard deviation from the mean ROI fluorescence increases. Conversely, more equally dispersed fluorescent particles produce a low standard deviation of the mean fluorescence in a ROI.

Both analyses revealed a clearly biphasic development for SNAP25 distribution and accessibility (Fig. 15 b–e). Since this effect is observed with both the N-terminal and the C-terminal antibody, clustering apparently affects wide parts of the protein and is not limited to one of its SNARE domains. However, the increase in the relative standard deviation is more pronounced in sheets stained with the antibody targeting the N-terminus (Fig. 15 c–e). It seems unlikely that this is due to different clustering effects in the SNAP25 N- and C-terminus, since the changes in staining intensities are similar in both of the termini. Instead, already in the control condition, the staining pattern with the polyclonal antibody appears to be more punctuate than with the monoclonal antibody (Fig. 15 a, upper row). It appears that the latter generally recognizes more SNAP25 proteins and therefore offers a greater dynamic range than the polyclonal antibody. Because of its greater sensitivity, the monoclonal antibody was used in subsequent experiments.

Segmentation-based analyses for SNAP25 clustering

The standard deviation of the fluorescence intensity is an appealing analysis since it does not require any form of image segmentation. However, it cannot discriminate between underlying clustering scenarios such as changes in cluster size, density or sorting of more non-clustered molecules into clusters. To address these issues and to complement the rel. SD, an additional analysis was performed for which the fluorescence signal was segmented into clustered and uniformly distributed pools (Fig. 16) (see methods for details). The average signal intensity of both fractions decreases at intermediate calcium concentrations, and then increases again at high calcium. This shows that molecular crowding occurs in both signal pools (Fig. 16 d). When looking at the amount of fluorescence (the integral of the intensity), a peak is observed for the punctuate signal, while the

amount of fluorescence from the uniform signal pool drops at intermediate calcium concentrations (Fig. 16 e). This may indicate recruitment of molecules from the uniform pool into clusters at intermediate calcium concentrations.

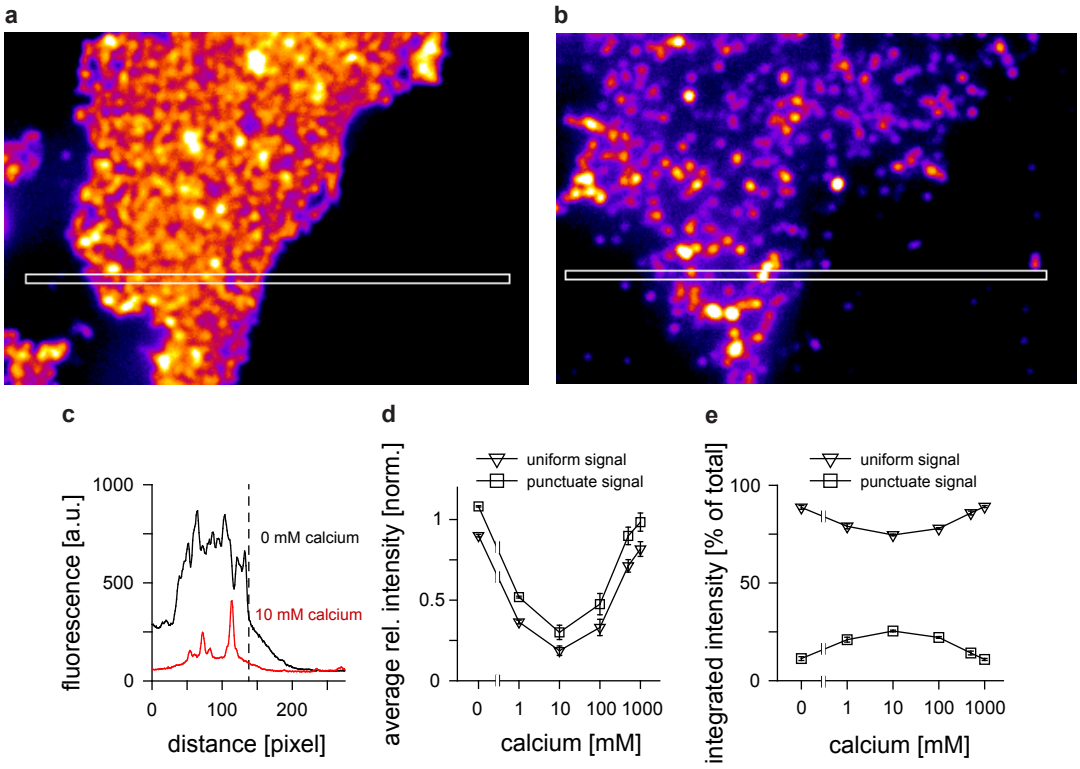

Fig. 16 Immunofluorescence intensity originating from both clustered and non-clustered SNAP25 in the membrane biphasically varies with the calcium concentration. Detailed illustration of the immunofluorescence intensity distribution in the control condition (**a**) and at 10 mM calcium (**b**) with an arbitrarily scaled "fire" lookup table (increasingly brighter pixels are displayed from blue, to red to yellow to white). (**c**) Fluorescence intensity measured with the line scans indicated in white in **a** and **b**. The dotted line marks the edges of the membrane sheets. (**d**) The SNAP25 staining pattern was segmented into punctuate areas (squares) and uniform areas next to them (triangles) as described in the methods section. The fluorescence intensities are given as mean ± s.e.m. (n = 3–4), normalized to total average fluorescence in the control condition (shown in Fig. 15 b). (**e**) Amount of fluorescence originating from uniformly distributed and clustered signal pools expressed as a percentage of the total integrated membrane fluorescence (integrated uniform signal = total area × average uniform signal intensity; integrated punctuate signal = punctuate area × (average punctuate intensity - average uniform intensity)). Note that the fraction of the clustered signal most likely underestimates the fraction of clustered molecules (see text). This figure is modified from ref. 122.

It was speculated that there is an early stage of SNAP25 clustering, at which the potential recruitment of additional molecules into clusters does not yet lead to tighter cluster packing and epitope masking. If clusters were populated by a higher number of molecules and still loosely packed, the average fluorescence of the clustered pool should become brighter. To investigate a mild clustering response, membrane sheets were incubated with 10- and 100-fold lower calcium concentrations than in the previous experiment (Fig. 17 a). This resulted only in a slight increase in the fluorescence intensity of the punctuate signal pool (Fig. 17 c). A transition state with brighter, loosely packed clusters does either not exist or is only short-lived. If clusters accumulate molecules, they apparently do so by increasing molecule packing density instead of growing larger in diameter.

The quantitative figures on the amounts of fluorescence from uniformly and clustered signal pools (Fig. 16 e, 17 c, d) should be treated with caution. The amount of recorded signal that the analysis algorithm categorizes as "clustered" may severely underestimate the actual amount of clustered molecules for the following reasons. First, epifluorescence is diffraction limited and cannot differentiate between an unresolved cluster and random non-clustered molecules. The imaging technique creates a Gaussian intensity distribution (or blur) around each molecule, and accordingly also around the crowded molecules in a cluster. If clusters are dense, the blurred signals from several clusters may overlap and be mistaken for uniform, non-clustered molecules. Finally, the non-clustered molecules may be preferentially recognized by the antibodies, since there is less steric hindrance than with clustered molecules. For these reasons, clustering in subsequent epifluorescence experiments was evaluated using the segmentation-free rel. SD analysis.

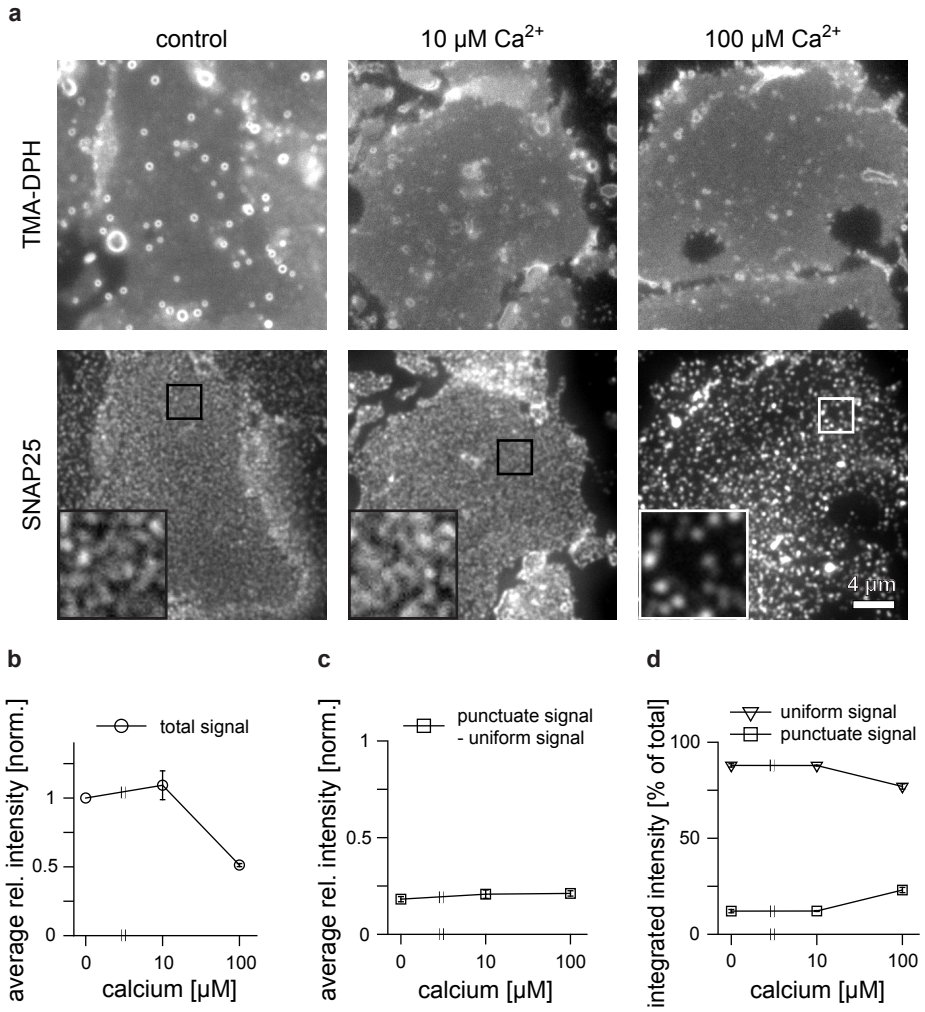

Fig. 17 SNAP25 immunofluorescence intensities at low calcium concentrations. PC12 plasma membrane sheets were incubated with 10 µM, 100 µM or without calcium for 10 min at 37 °C. (**a**) Epifluorescence images of the membrane counterstain (upper row), and the corresponding SNAP25 immunostaining (lower row, overviews are similarly and magnified views arbitrarily scaled). (**b**) Average immunofluorescence intensity of the total SNAP25 signal plotted against the calcium concentration and normalized to the control condition (without calcium). (**c** and **d**) The staining pattern was segmented into uniform and punctuate signal areas as described in the methods section. (**c**) To estimate the average immunofluorescence signal originating from SNAP25 clusters, the average fluorescence intensity in uniform areas was subtracted from the average fluorescence intensity in punctuate areas. These values were normalized to the control (0 mM calcium) in **b**. (**d**) Amount of fluorescence originating from uniformly distributed and clustered signal expressed as a percentage of the total integrated membrane fluorescence (integrated uniform signal = total area × average uniform signal intensity; integrated punctuate signal = punctuate area × (average punctuate intensity - average uniform intensity)). Values are given as mean ± s.e.m. (n = 3).

5.2.2 SNAP25 clustering is insensitive to changes in the pH, ionic strength, osmolarity, and additional depletion forces

Having developed an assay and analysis methods for exploring clustering of membrane-anchored SNAP25, it was then analysed whether biphasic clustering is a specific response to calcium, or whether clustering may also be induced by other forces. To this end, SNAP25 clustering was first analysed at different pH values (pH 6, 7 and 8) and compared to the control buffer used throughout the other experiments (pH 7.2) (Fig. 18). The analysis revealed virtually no difference in SNAP25 clustering between pH 6 and pH 8.

Assuming that electrostatics are involved in clustering, this was to be expected, since the protein should retain its net negative charge in all these conditions. The differences in pH hardly affect the protonation states of glutamate, aspartate, arginine and lysine, since their pK_a values are either much lower (~4 in the case of glutamate and aspartate) or much higher (~10–12 in the case of arginine and lysine) than pH 6–8. However, increasing the pH to 8 results in deprotonation of histidine residues (pK_a ~6), and a half of the cysteine residues should convert to thiol anions. Taking into account the size and the structure of the protein, these deprotonation events have only minor effects, though, since SNAP25 contains only one histidine residue (0.5 % of all residues), and of the four cysteine residues at least one (if not all four, this is a subject of research[126]) are palmitoylated and in close proximity to the plasma membrane. Additionally, the thiol anion is very reactive, and therefore does not substantially contribute to protein charge.

The buffer solution used throughout all experiments so far contained 140 mM KCl to yield an osmolarity and ionic strength close to physiological conditions. In the next experiment, KCl was omitted from the solution to investigate whether the ionic strength in general and K^+ and Cl^- ions in particular contribute to SNAP25 clustering.

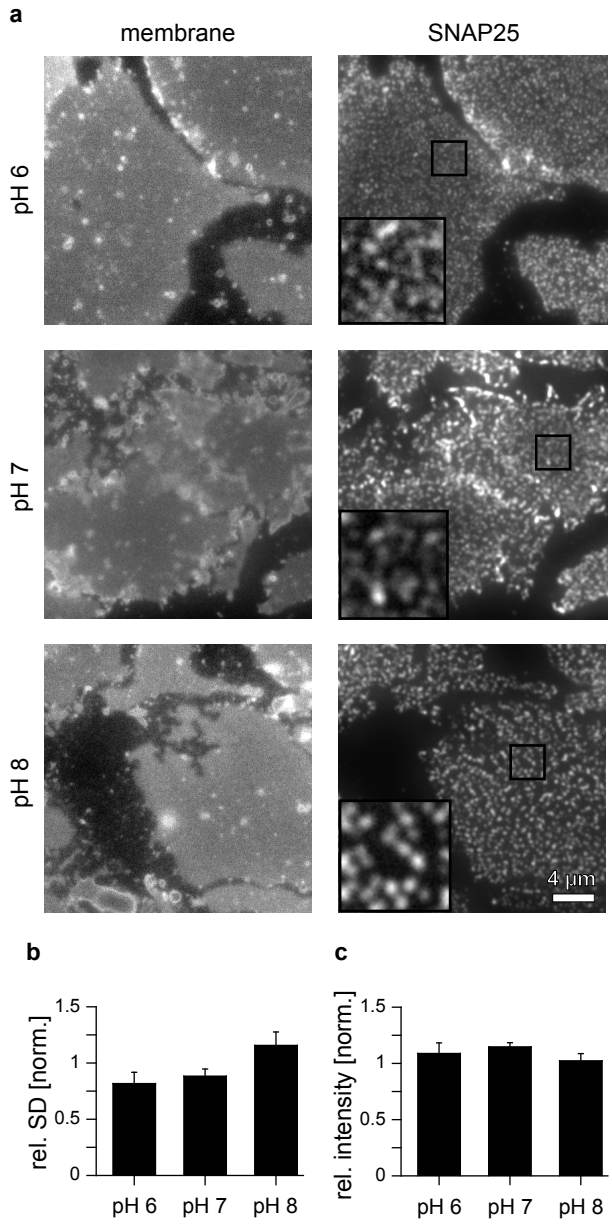

Fig. 18 SNAP25 clustering is hardly affected by changes in the pH. Membrane sheets were incubated with Hepes/KCl buffer solutions at pH 6–8, or a buffer solution at pH 7.2 which additionally contained EGTA for 10 min at 37 °C. (**a**) Images of membranes counterstained with TMA-DPH and the corresponding SNAP25 immunostaining of sheets incubated at pH 6, 7 or 8. Overview images are shown at the same scaling while magnified insets are arbitrarily scaled. SNAP25 clustering was evaluated using (**b**) the relative standard deviation or (**c**) the relative intensity of the immunofluorescence signal (both normalized to the control solution). Values are given as mean ± s.e.m. (n = 3).

This is especially important in the case of chloride, since in all previous experiments calcium was applied in form of a chloride salt, albeit an increase of the chloride concentration by 14 % (from 140 to 160 mM) when applying 10 mM

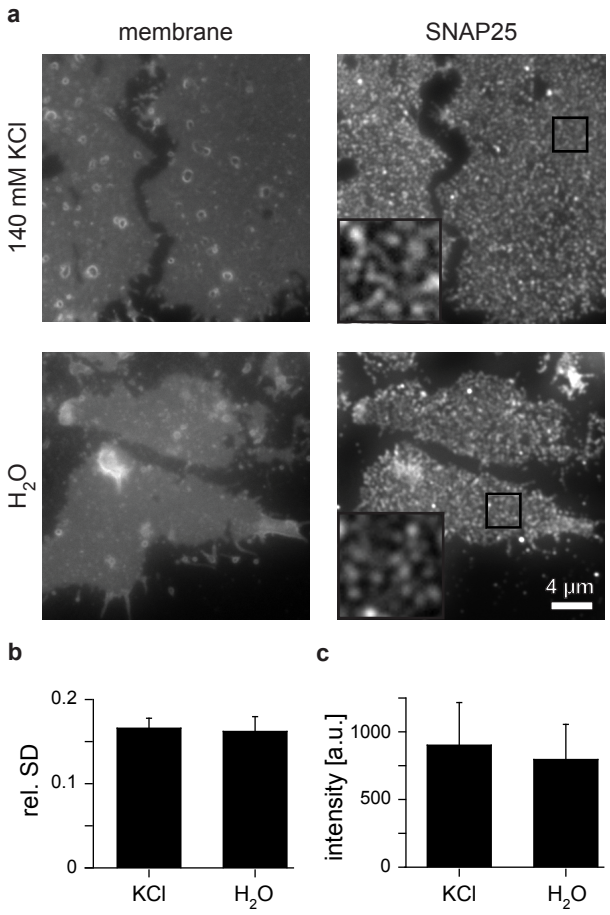

Fig. 19 SNAP25 clustering is not affected by changes in the ionic strength and osmolarity. Membrane sheets were incubated with buffer solutions containing 20 mM Hepes (pH 7.2), 10 mM EGTA (to chelate trace divalent ions) and either 140 mM KCl (yielding a solution with a physiological osmolarity) or no KCl (yielding a hypoosmolar solution) for 10 min at 37 °C. (**a**) Epifluorescence images of the membrane counterstain TMA-DPH (left) and the corresponding SNAP25 immunostaining (right). Overview images are shown at the same, magnified insets at arbitrary scaling. SNAP25 clustering was evaluated using (**b**) the relative standard deviation and (**c**) the relative intensity of the immunofluorescence signal. Values are given as mean ± s.e.m. (n = 3).

$CaCl_2$ is unlikely to have a major effect. The ionic strength determines the electrostatic screening length, and thus the distance at which negatively charged SNAP25 molecules experience electrostatic repulsions. Following the hypothesis that surface charge repulsion diminishes clustering, a reduction in the ionic

strength could possibly lead to a higher degree of protein dispersion, because electrostatic repulsions prevail over larger distances. Membrane sheets incubated in buffer solutions with or without 140 mM KCl showed no difference in SNAP25 clustering (Fig. 19). This confirms that the effects observed in previous experiments with $CaCl_2$ are governed by the Ca^{2+} ions, not the Cl^- ions. Additionally, this experiment proves that the ionic strength of the solution does not influence SNAP25 clustering in membrane sheets. This was verified in experiments in which sheets were incubated with exceedingly high ionic strengths produced by 1 M NaCl or KCl solutions (data not shown).

Next, the effect of trehalose in the buffer solution was analysed. The disaccharide trehalose is a non-reducing sugar which can be used to prevent precipitation of highly concentrated protein solutions (such as therapeutic antibody formulations). Trehalose acts as an extrinsic crowder that induces a depletion attraction between proteins thus stabilizing their compact folded states[32]. According to the Asakura-Oosawa model[127] depletion attraction is entropically driven: close association of the proteins maximizes the volume accessible to the small crowders (see Fig. 20 a). High crowder concentrations are necessary to create a significantly strong depletion attraction. In this experiment, membrane sheets were therefore incubated with 250 mg/ml (731 mM) trehalose (Fig 20 b). This had no effect on SNAP25 clustering in membrane sheets (Fig. 20 c, d).

There are several explanations for the absence of a noticeable depletion attraction in this case. First, the depletion attraction between SNAP25 molecules may be overruled by electrostatic effects. Second, since SNAP25 is confined to the membrane plane and already clustered, the entropic gain due to crowding in larger clusters is low (compared to crowding of spaced proteins in a 3D system). Third, on the level of the 2D plane, the plasma membrane is an environment which is already crowded with a multitude of small particles as lipid headgroups with a comparable size to the trehalose crowder.

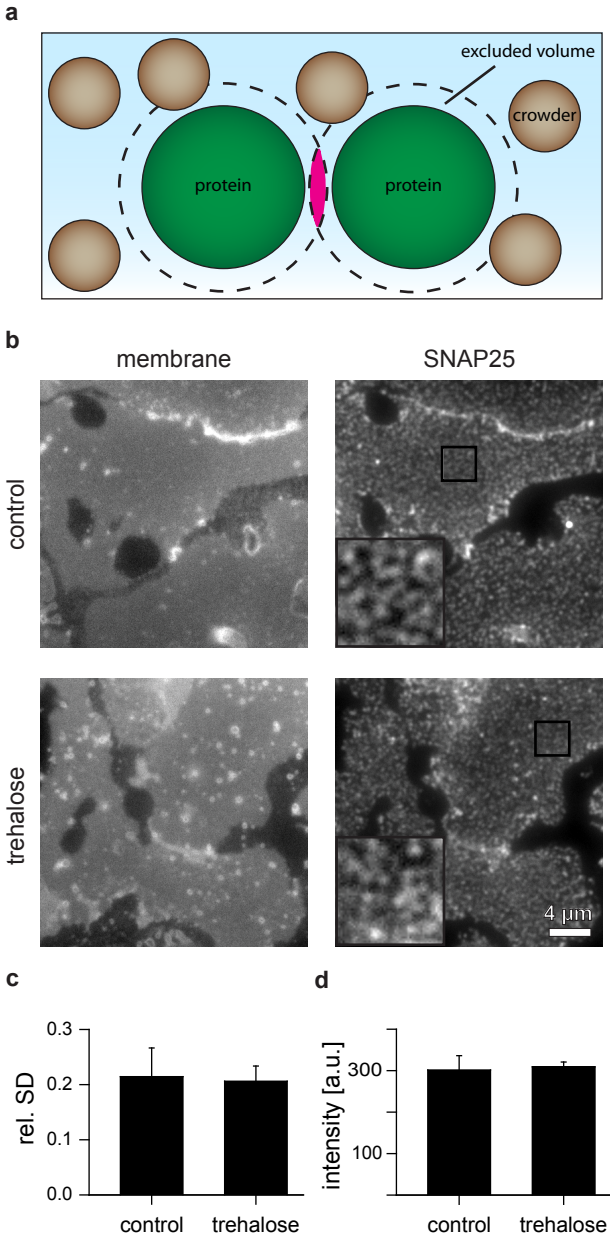

Fig. 20 High concentrations of trehalose cause no noticeable depletion attraction of SNAP25 in membrane sheets. (**a**) Schematic for the depletion attraction between two protein particles (adapted from ref. 32). The volume in the immediate vicinity of the proteins (indicated by the dashed line) cannot be accessed by the centres of crowding molecules. If these individual excluded volumes of the macromolecules overlap (pink), the total excluded volume is reduced. This increases the entropy of the small crowder molecules. (**b**) Epifluorescence images of membrane sheets incubated in Hepes/KCl with or without 250 mg/ml (731 mM) trehalose for 10 min at 37 °C, immunostained for SNAP25 (right) and counterstained with TMA-DPH (left, documenting membrane integrity). SNAP25 overview images are shown at the same, magnified insets at arbitrary scaling. SNAP25 clustering was evaluated using (**c**) the relative standard deviation and (**d**) the relative intensity of the immunofluorescence signal. Values are given as mean ± s.e.m. (n = 3).

In fact, depletion attraction exerted by membrane lipids was suggested to be one factor promoting the general organization of membrane proteins in clusters[128]. Thus, addition of a second crowding agent may not induce any further depletion attraction. Apart from showing the minor importance of additional depletion forces in this system, this experiment underlines that an increase in osmolarity (which is in case of 731 mM trehalose higher than at 100 mM $CaCl_2$) does not affect SNAP25 clustering.

5.2.3 STED superresolution microscopy indicates tighter cluster packing

To further characterize the process of SNAP25 clustering, calcium-induced changes in cluster size and cluster number density were analysed. Membrane protein cluster sizes are typically between 50–200 nm. These size scales cannot be analysed with conventional fluorescence microscopy since these are limited by diffraction to a resolution of ~250 nm. For this reason, STED microscopy was employed to analyse cluster size. The STED set-up consists of a confocal microscope which uses an additional circular STED beam to selectively de-excite fluorophores at the periphery of the excitation spot and thus decrease the spot size from which fluorescence is collected. With the set-up used in this study, in theory a resolution in the range of 30 nm can be achieved. STED images were acquired from membrane sheets incubated with 0, 10 or 1000 mM calcium and immunostained for SNAP25 (Fig. 21).

The analysis of the STED images revealed that clusters do neither grow larger nor become smaller as a result of increased clustering (Fig. 21 b). Instead, the number of clusters per μm^2 is reduced to approx. 50 % at 10 mM calcium. At 1000 mM calcium, the number of clusters increases again to almost its original value. These observations suggest an at least twofold tighter packing of SNAP25 clusters at 10 mM Ca^{2+}, because the SNAP25 molecules are now confined to half as many but equally sized clusters. Taking into account that these fewer clusters may additionally recruit previously uniformly distributed SNAP25 molecules

(the amount of the clustered signal is 2.5-fold increased, see Fig. 16 e), the packing density may even be increased by a factor of five. A uniformly distributed signal pool was, however, under no conditions observed in STED images. This is possibly due to a lower sensitivity of this technique, or because a uniform pool is hardly existent (see section 5.2.1 and 6.2 for details and discussion).

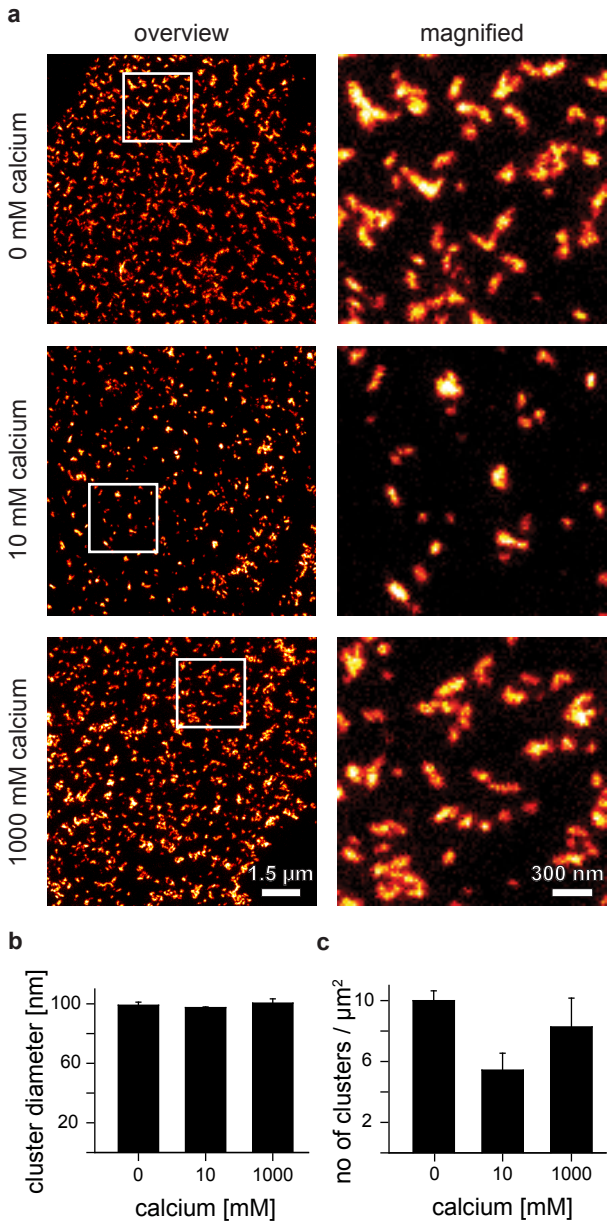

Fig. 21 SNAP25 cluster density varies with calcium concentration while cluster size remains stable. Plasma membrane sheets were incubated with 0, 10 or 1000 mM calcium for 10 min at 37 °C. (**a**) Overview (left) and magnified (right) STED micrographs of SNAP25 immunofluorescence to which the "red hot" look up table was applied (displaying increasingly brighter pixel intensities using a colour code from black to red to yellow to white). (**b**) SNAP25 cluster sizes and (**c**) cluster density per µm² (means ± s.e.m., n = 4) (modified from ref. 122).

5.3 Delineating ion properties that determine protein clustering

The previous experiments indicated that the pathway of SNAP25 clustering involves tighter cluster packing, and possibly the recruitment of previously uniformly distributed molecules into clusters.

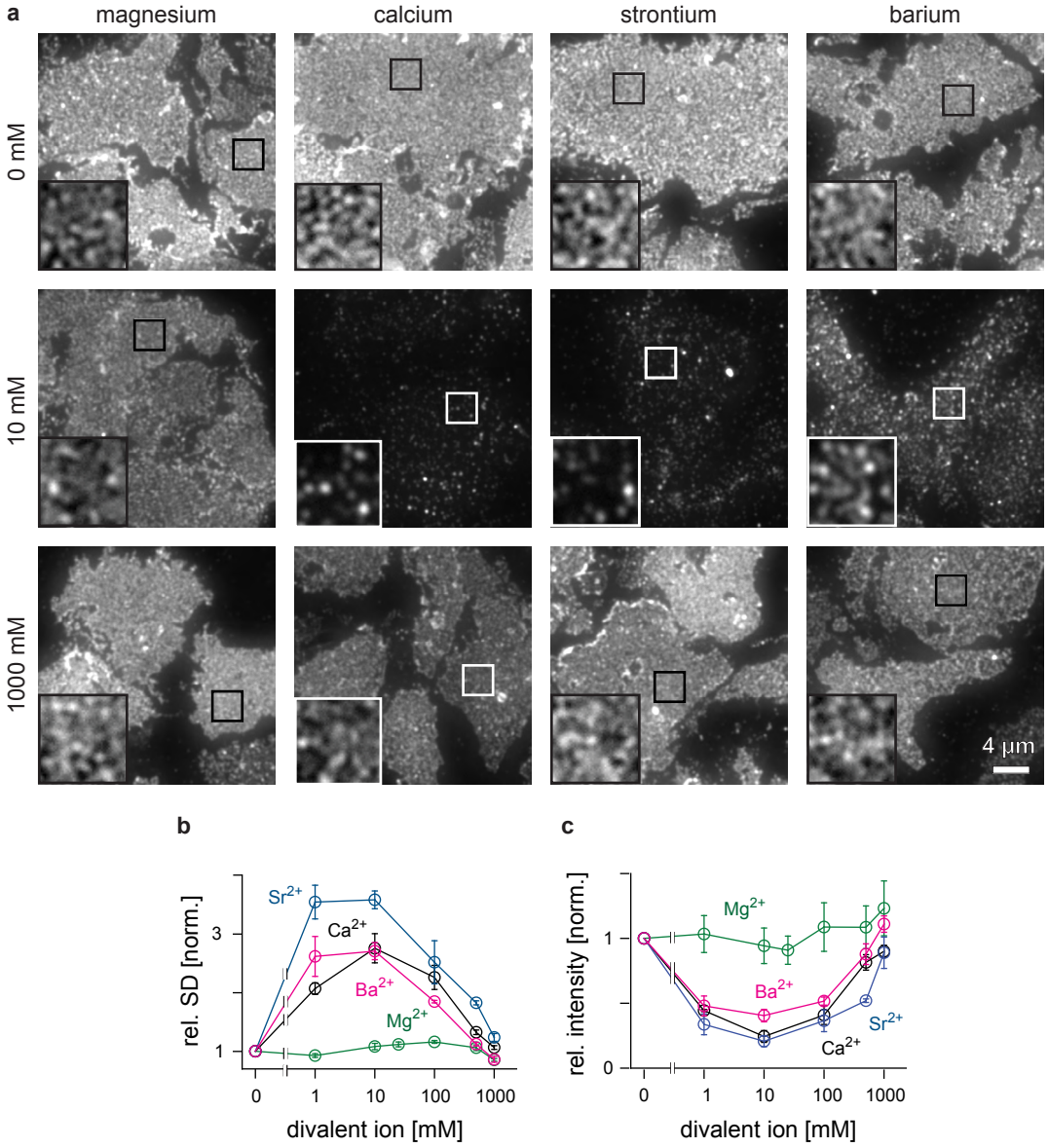

Fig. 22 SNAP25 in plasma membrane sheets shows biphasic clustering in response to several earth alkaline ions. PC12 plasma membrane sheets were incubated with the indicated concentrations of calcium, strontium, barium or magnesium chloride for 10 min at 37 °C. (**a**) Epifluorescence recordings of the SNAP25 immunostaining in membrane sheets incubated with 0, 10, or 1000 mM $CaCl_2$ (overviews are shown at the same, magnified insets at arbitrary scaling). SNAP25 clustering was quantified by calculating (**b**) the relative standard deviation (rel. SD) of the immunostaining pattern and (**c**) the relative fluorescence intensity, both normalized to the baseline condition which contained no divalent cations. Values are means ± s.e.m. (n = 3–4). (Figure modified from ref. 122).

To shed light on the underlying molecular interactions of this process, the effect of calcium ions was compared to other earth alkaline ions. Membrane sheets were hence incubated with logarithmically increasing concentrations of magnesium, calcium, strontium and barium chloride and compared to control sheets incubated with a chelator for divalent ions (Fig. 22 a). Increased SNAP25 clustering at intermediate and re-dispersion at high ion concentrations was observed not only in response to calcium, but also for barium and to an even greater extent for strontium, and in a subtle fashion for magnesium (Fig. 22 b, c).

To understand why some ions provoke more clustering than others, the effects of different cations were comparatively studied and linked to their physico-chemical properties. SNAP25 clustering was evaluated in sheets incubated in buffer solutions containing 1 mM chloride salts of sodium, magnesium, calcium, zinc, strontium, yttrium, barium and lanthanum (Fig. 23 a). These ions were selected in order to cover a wide range of ion properties (see Table 17 and 18). The degree of clustering – based on the rel. SD of SNAP25 fluorescence – which is induced by these ions decreases from:

$$Sr^{2+} > Ba^{2+} > Ca^{2+} > Na^{+} > Mg^{2+} > Zn^{2+} > La^{3+} \sim Y^{3+}$$

In this sequence, Mg^{2+} and Na^{+} mark a turning point: ions to their left increase the degree of SNAP25 clustering, while ions to their right reduce SNAP25 clustering; Mg^{2+} and Na^{+} themselves show hardly any effect (Fig. 23 b).

Plotting the chemical properties of the ions as a function of their clustering efficacy does not reveal any simple linear correlation. Instead, the graphs for the charge-to-radius ratio (Fig. 23 c), the water viscosity, as well as the Gibb's free energy of hydration per coordinating water molecule (Fig. 24) resemble volcano plots in which Sr^{2+} marks the maximum. There was no dependency of clustering efficacy on ion charge, radius, volume, polarizability or softness (Fig. 24).

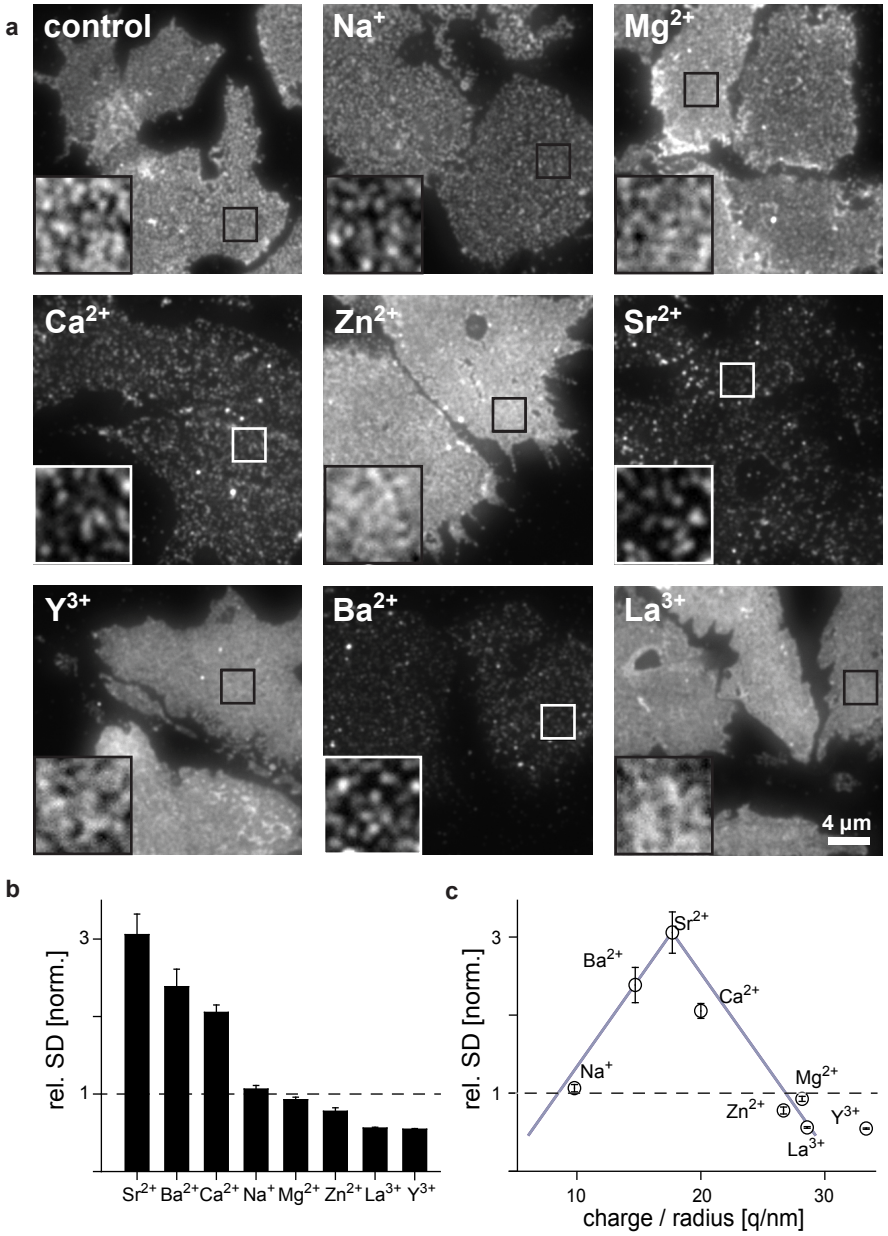

Fig. 23 The efficacy of mono-, di- and trivalent ions on SNAP25 clustering in the cell membrane depends on the ion charge-to-radius ratio. (**a**) Membrane sheets were incubated with 1 mM chloride salts of Na^{+}, Mg^{2+}, Ca^{2+}, Zn^{2+}, Sr^{2+}, Y^{3+}, Ba^{2+} and La^{3+} (sorted by atomic number) for 10 min at 37 °C. Overviews are shown at the same, magnified views at arbitrary intensity scaling. (**b**) The degree of SNAP25 clustering was quantified using the rel. SD of the immunostaining intensity normalized to the control condition. Ions are shown in decreasing order of their clustering efficacy. (**c**) Plotting clustering effectiveness (in terms of the rel. SD) versus the ion charge-to-radius ratio yields a distribution resembling a volcano plot (grey lines). Values are means ± s.e.m. (n = 3–7). This figure was previously published in ref. 122.

The influence of 1 mM K^+ was not evaluated in this experiment, since the buffer solution used here already contains 140 mM potassium. Regarding the ion properties identified crucial for clustering (charge-to-radius ratio, water viscosity, hydration energy per coordinating water molecule) potassium ions resemble

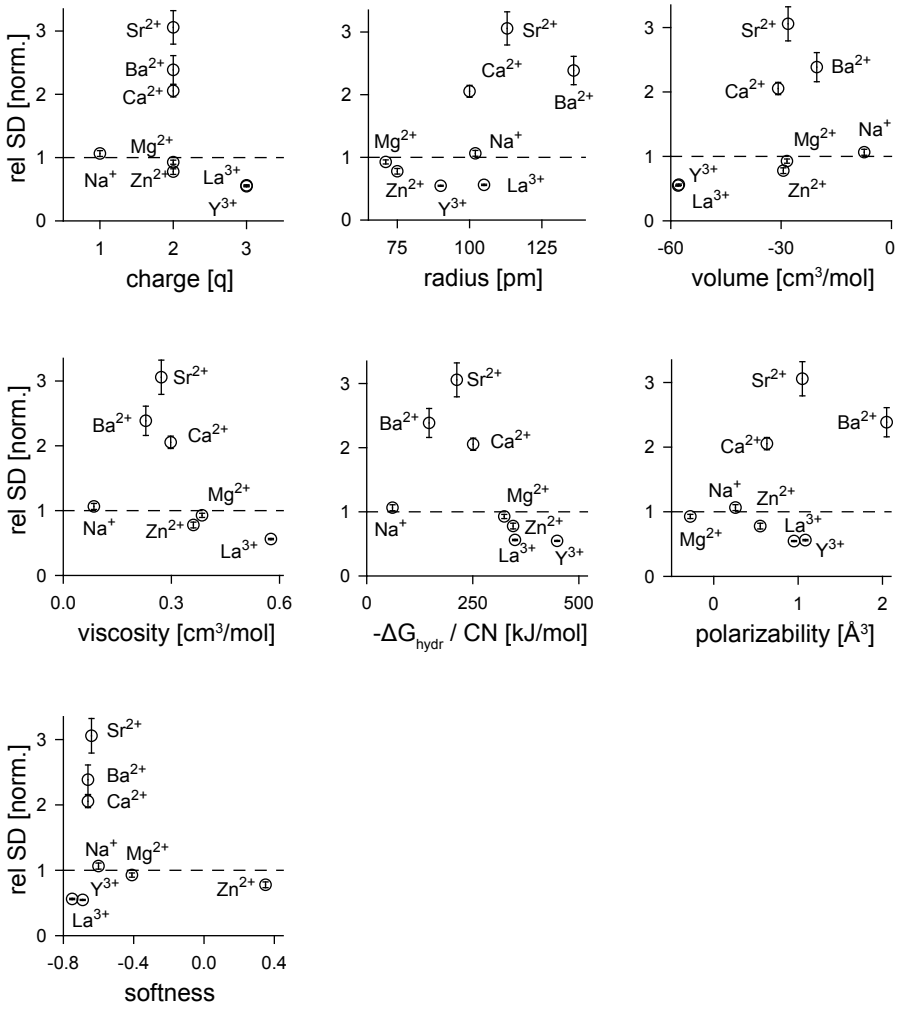

Fig. 24 Ion properties in relation to their effectiveness to cluster SNAP25 in native cell membrane sheets. The relative standard deviation (rel. SD) of the immunofluorescence intensity (normalized to the control condition, indicated by the dashed line; values are taken from Fig. 23 b) is plotted in relation to the following ion properties: charge, crystal radius[154], ionic volume (according to the calculated standard partial molar volumes[167]), the Jones–Dole viscosity B coefficient[154], Gibbs free energy of hydration[168] per coordinating water molecule (for references on the coordination numbers (CN) see ref. 169 (for Mg^{2+}, Ca^{2+}, Sr^{2+}, Ba^{2+}), ref. 170 (for Na^+ and Zn^{2+}), ref. 171 (for La^{3+}) and ref. 172 (for Y^{3+})), ion polarizability[154] and softness[154]. This figure was previously published in ref. 122.

sodium ions (cf. Table 17 and 18). It can thus be speculated that potassium ions have – similarly to sodium ions – no influence on SNAP25 clustering. This was indeed confirmed in previous control experiments (Fig. 19).

Table 17 Ion properties I

ion	charge	radius [pm]	volume [cm³/mol]	charge/radius [q/nm]	polarizability [Å³]	softness
Na^+	1	102	-7.4	9.8	0.26	-0.60
K^+	1	138	1.3	7.25	1.07	-0.58
Mg^{2+}	2	71	-28.4	28.17	-0.28	-0.41
Ca^{2+}	2	100	-30.8	20.00	0.63	-0.66
Sr^{2+}	2	113	-28.1	17.7	1.05	-0.64
Ba^{2+}	2	136	-20.3	14.71	2.05	-0.66
Zn^{2+}	2	75	-29.4	26.67	0.55	0.35
Y^{3+}	3	90	-58	33.33	0.95	-0.69
La^{3+}	3	105	-57.8	28.57	1.09	-0.75

The table presents the charge, radius[154], standard partial molar volume[167], charge-to-radius ratio, polarizability[154] and softness[154] of the metal ions used in this study.

Table 18 Ion properties II

ion	water viscosity [cm³/mol]	coordination number (CN)	ΔG_{hyd} [kJ/mol]	ΔG_{hyd}/CN [kJ/mol]
Na^+	0.09	6	365	61
K^+	-0.01	6	295	49
Mg^{2+}	0.39	6	1945	324
Ca^{2+}	0.30	6	1505	251
Sr^{2+}	0.27	6.5	1380	212
Ba^{2+}	0.23	8.5	1250	147
Zn^{2+}	0.36	6	2070	345
Y^{3+}	n/a	8	3590	449
La^{3+}	0.58	9	3145	349

The table presents the Jones–Dole viscosity B coefficient[154], the coordination number (see ref. 169 for Mg^{2+}, Ca^{2+}, Sr^{2+}, Ba^{2+}; ref. 170 for Na^+ and Zn^{2+}; ref. 171 for La^{3+}; and ref. 172 for Y^{3+}), Gibb's free energy of hydration[168], and Gibb's free energy of hydration per coordinating water molecule of the metal ions used in this study.

It is a curious observation that with Y^{3+}, La^{3+} and Zn^{2+}, SNAP25 clustering is even reduced compared to the control condition – especially since comparable Y^{3+} concentrations were reported to induce biphasic clustering of BSA in solution[89].

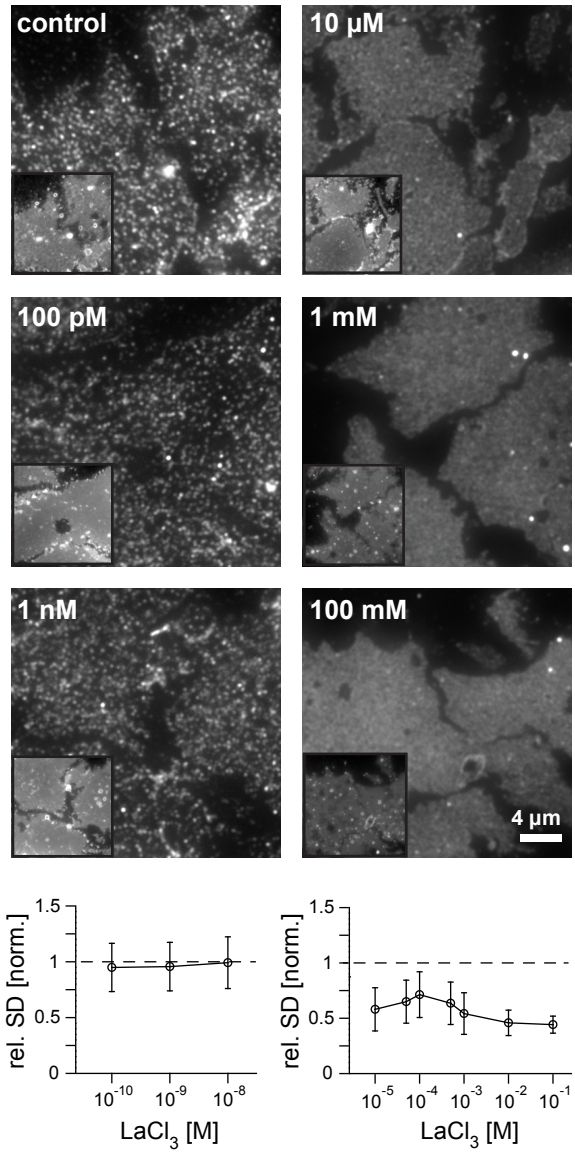

Fig. 25 Biphasic SNAP25 clustering is not observed over a wide range of lanthanum concentrations. The figure presents two single experiments in which membrane sheets were incubated with 0.1–10 nM lanthanum (left column), and 10 µM–100 mM lanthanum (right column), out of a series of experiments in which sheets were incubated with logarithmically increasing lanthanum concentrations between 1 pM (10^{-12} M) and 1 M (10^{0} M). The images illustrate the SNAP25 immunostaining pattern; insets show the corresponding TMA-DPH membrane counterstaining. SNAP25 clustering was evaluated using the relative standard deviation of the immunofluorescence. Values are given as mean ± s.d., normalized to the respective control. A biphasic response to varying lanthanum ion concentration was not observed in any experiment.

It is conceivable that for SNAP25 clustering in membrane sheets, a concentration of 1 mM Y^{3+} or La^{3+} may be either too low or too high and thus outside of the clustering regime (as, e.g. 1000 mM calcium). To test this hypothesis, membrane sheets were incubated with a wide range of logarithmically increasing lanthanum concentrations, ranging from 1 pM (10^{-12} M) to 1 M (10^{0} M). Low La^{3+} concentrations (≤ 10^{-8} µM) had no effect on clustering, while higher concentrations yielded an increasingly dispersed SNAP25 staining pattern (see Fig. 25 for a range from 10^{-10}–10^{-1} M La^{3+}). La^{3+} may be generally unsuitable to induce clustering of SNAP25 in membrane sheets because it lacks the necessary chemical properties (see Fig. 24). Alternatively, the logarithmic steps at which the lanthanum concentration was increased were too big to find a potentially narrow clustering regime.

5.4 Co-clustering of SNAP25 with other charged molecules in the plasma membrane at increased calcium levels

The previous experiments both in solution and in the plasma membrane assume homo-oligomerization of SNAP25. In the plasma membrane, though, there is a multitude of other charged proteins and, especially in the intracellular membrane leaflet, also charged lipids. It is conceivable that calcium ions not only promote homo- but also hetero-oligomerization with other charged species. To test this hypothesis, colocalization of SNAP25 and syntaxin was analysed at different calcium concentrations. Syntaxin-1, like SNAP25, is a plasmalemmal neuronal SNARE protein, and its cytoplasmic domain carries a net amount of twelve negatively charged amino acids (= 4.5 %; for comparison, SNAP25 has a net amount of fourteen negatively charged amino acids which amounts to 6.8 %). Syntaxin and SNAP25 are known binding partners. During neuronal exocytosis, they interact via their SNARE domains and form an acceptor complex for the vesicular SNARE protein synaptobrevin, which ultimately results in membrane fusion[129].

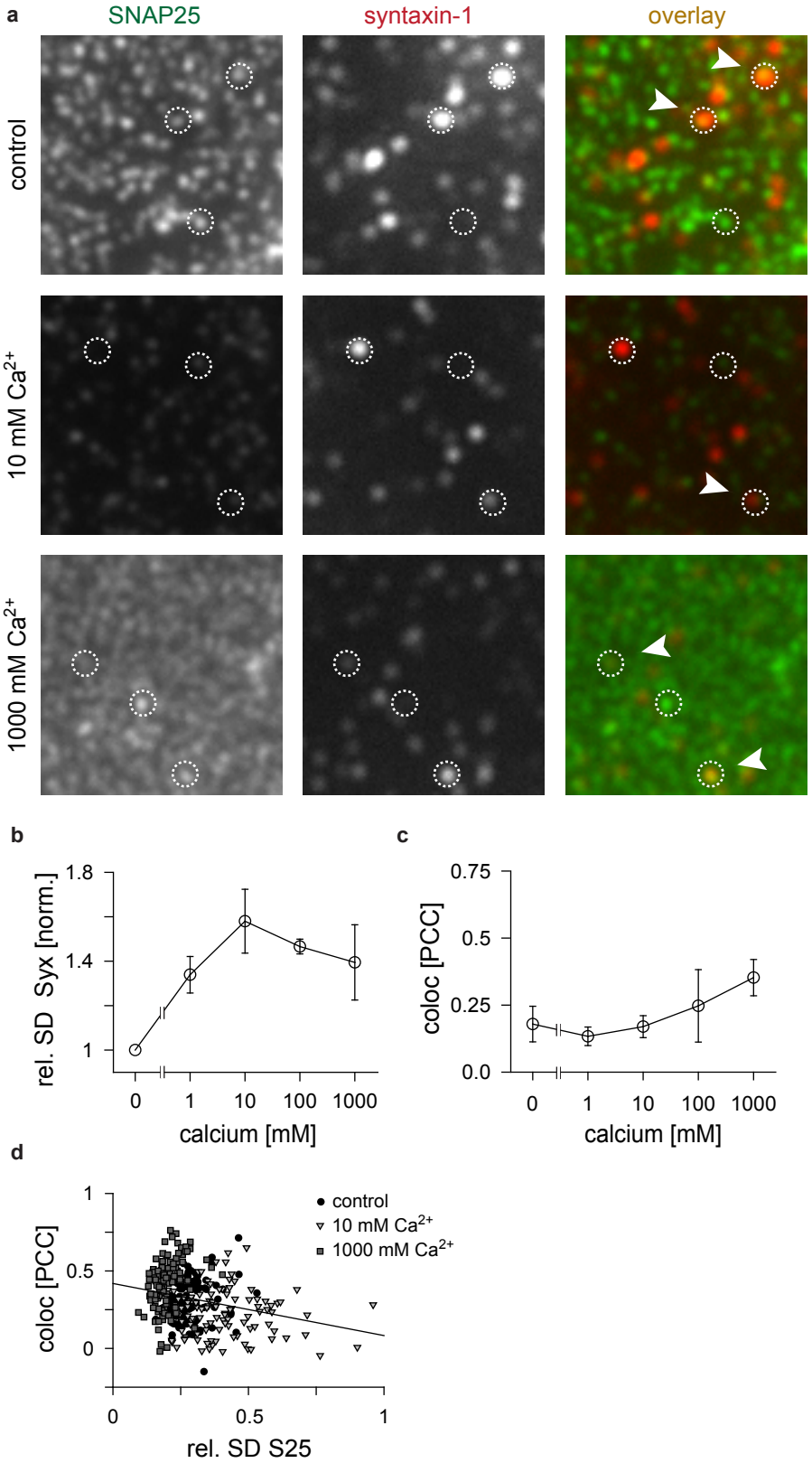

Fig. 26 The colocalization between the two negatively charged proteins SNAP25 and syntaxin does not increase with the degree of SNAP25 clustering. *(Legend continued on next page)*

PC12 membrane sheets were incubated with logarithmically increasing calcium concentrations in Hepes/KCl for 10 min at 37 °C, and immunostained for SNAP25 and syntaxin-1. (**a**) Representative images illustrating the SNAP25 and syntaxin immunostaining pattern separately and as an overlay (green, SNAP25; red, syntaxin-1) at 0, 10 and 1000 mM calcium. The circles indicate the localization of protein clusters, which overlap in cases indicated by the arrows. (**b**) Relative standard deviation (rel. SD) of the syntaxin immunofluorescence intensity (normalized to the control condition) as a function of calcium concentration (mean ± s.e.m., n = 2–3). (**c**) The Pearson correlation coefficient (PCC) between the two channels was calculated for each pixel and plotted against the calcium concentration (mean ± s.e.m., n = 2–3). (**d**) PCC plotted against the relative standard deviation of the SNAP25 immunofluorescence at 0 mM (cirlces), 10 mM (triangles) and 1000 mM (squares) calcium. There is a weak negative correlation (indicated by the black line) between the degree of SNAP25-syntaxin colocalization and the degree of SNAP25 clustering (Spearman's rho = -0.24, $p < 0.0001$; the data points correspond to the individual sheets collected from n = 3 experiments).

Membrane sheets were incubated with increasing calcium concentrations and double stained for SNAP25 and syntaxin-1. While syntaxin – like SNAP25 – clusters at intermediate calcium concentrations, re-dispersion at high calcium is less pronounced (see Fig. 26 a, b). The degree of colocalization between the two proteins was quantified using a pixel-wise Pearson correlation coefficient (Fig. 26 a, c). Without calcium ions, the colocalization between the two proteins is low; the clusters appear to be rather neighbouring than overlapping. At concentrations of 1–10 mM calcium, i.e. in the SNAP25 clustering regime, the colocalization even slightly decreases. An increase in the colocalization between SNAP25 and syntaxin is observed at 1000 mM calcium, at which SNAP25 is again fully dispersed. Thus, while both proteins experience self-clustering at 10 mM calcium, their colocalization does not increase. On the contrary, there is even a weak negative correlation (Spearman's rho = -0.25 ± 0.08, n = 3) between the extent of SNAP25 clustering and the degree of SNAP25–syntaxin colocalization (Fig. 26 d). At least in this case, ion-induced clustering is apparently restricted to protein homo-oligomerization.

In a second experiment, the colocalization between SNAP25 and phosphatidylserine was investigated. Phosphatidylserine is the most abundant

negatively charged membrane lipid, and is especially enriched in the inner leaflet of the plasma membrane[130]. It carries a net amount of one negative charge, which is important for ionic interactions with target proteins that lead to their membrane sequestration and activation[130]. An interaction with SNAP25, however, has not been described so far. Phosphatidylserine can also electrostatically bind calcium ions and may be involved in calcium sensing during vesicle fusion[131].

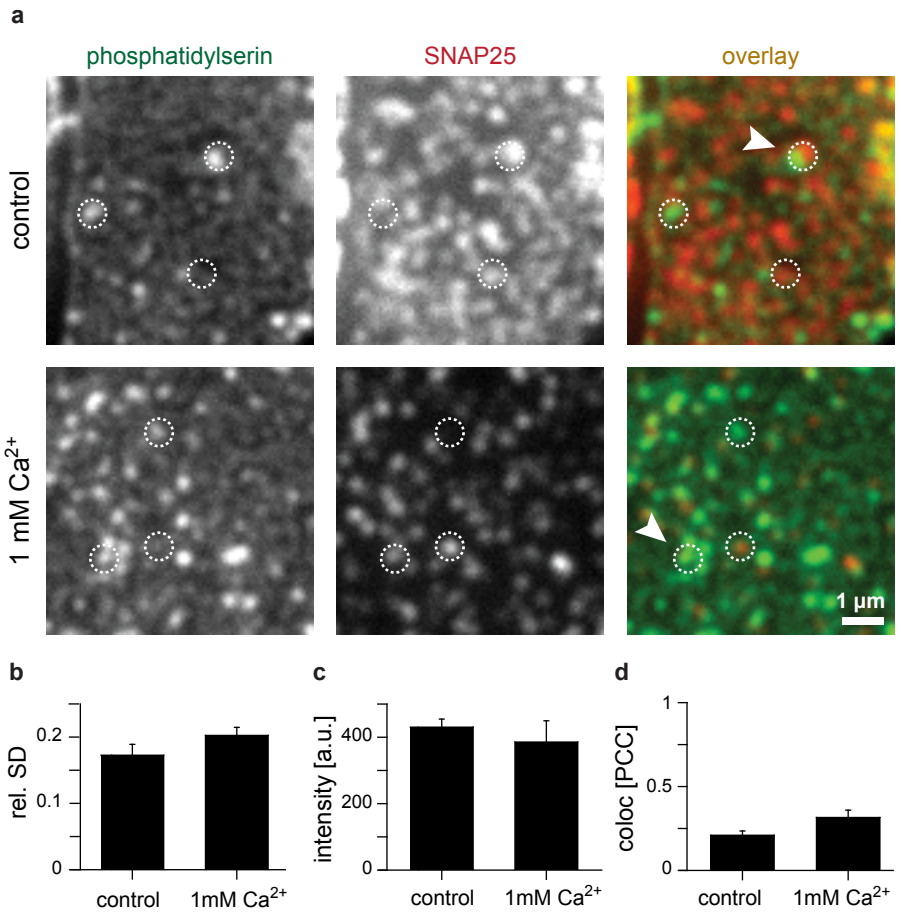

Fig. 27 The colocalization between SNAP25 and the negatively charged membrane lipid phosphatidylserine is not affected by calcium. Membrane sheets were incubated with or without 1 mM calcium in Hepes/KCl for 10 min at 37 °C and immunostained for phosphatidylserine and SNAP25. (**a**) Representative images illustrating the phosphatidylserine and SNAP25 immunostaining pattern separately and as an overlay (green, phosphatidylserine; red, SNAP25). The circles indicate the localization of phosphatidylserine and SNAP25 clusters; overlapping clusters are indicated by the arrows. The degree of phosphatidylserine clustering was evaluated using (**b**) the relative standard deviation and (**c**) the average immunofluorescence intensity. (**d**) The degree of colocalization between phosphatidylserine and SNAP25 was quantified using the pixel-wise Pearson correlation coefficient (PCC) between the two stainings. Values are given as mean ± s.e.m. (n = 3).

Since calcium was found to induce clustering of PIP_2 [132], another calcium-binding negatively charged membrane lipid, it was analysed whether calcium likewise influences the membrane distribution of phosphatidylserine, besides analysing SNAP25–phosphatidylserine co-clustering. Staining lipids is generally challenging, since antibodies are often less specific to lipid than to protein targets. Here, FITC-labelled lactadherin was used to stain phosphatidylserine with high specificity and affinity[I]. Binding is mediated via lactadherin's C2 domain in a calcium-independent manner[134].

Membrane sheets were incubated with or without 1 mM calcium, fixed, and stained with lactadherin and an anti-SNAP25 antibody (Fig. 27 a). Calcium appeared to have no influence on phosphatidylserine clustering (Fig. 27 b, c), different from what was published for PIP_2. This could be due to the lower charge density of phosphatidylserine compared to PIP_2 (the latter carries one more negative charge), and an accordingly weaker binding of the ion. The colocalization between phosphatidylserine and SNAP25 was low in control sheets, and increased only slightly with 1 mM calcium (see Fig. 27 d). There was no consistent correlation between the extent of SNAP25 clustering and the degree of SNAP25–phosphatidylserine colocalization (data not shown). Thus, calcium hardly promotes co-clustering between SNAP25 and phosphatidylserine.

I Annexin V, a commonly used probe for phosphatidylserine, has the disadvantage of binding also to other negatively charged lipids[133].

6 Discussion

This study analysed whether the oligomeric state of the negatively charged protein SNAP25 can be modulated by the use of oppositely charged metal ions. Counterion concentration dependent biphasic clustering, i.e. an increase in oligomerization followed by re-dispersion with increasing ion concentrations, was reported for several charged soluble proteins. In this work, it is demonstrated that biphasic ion-induced clustering can not only be recapitulated for soluble SNAP25, but can also be induced in SNAP25 anchored to the native cell membrane. This effect proved to be independent from changes in ionic strength, osmolarity, or pH. Instead, the effect depends on the ion type. By systematically studying ions with different chemical properties, three properties were found to be decisive for the effectiveness of ion-induced clustering: the ion's charge-to-size ratio, the hydration energy per coordinating water molecule, and the water viscosity coefficient of the ion. These observations allow for a prediction regarding the chemical nature of the ion–protein interactions and the binding patterns that govern the biphasic oligomerization behaviour.

6.1 Biphasic oligomerization of soluble SNAP25

As a starting point for this study, the ion-induced oligomerization behaviour of SNAP25 was characterized in solution, to see whether this protein experiences a biphasic oligomerization behaviour similar to what was published for BSA and lysozyme. Finding a technique that reliably reports the oligomeric state of the protein was challenging because high calcium ion concentrations interfered with some experimental procedures, e.g. in partial proteolysis experiments causing precipitation when mixing with Laemmli buffer, or in FCS measurements

producing a high noise level. Also, attached fluorophores gave rise to artefacts in case of FCS (by increasing protein stickiness) and MST (altering the protein diffusion behaviour). Finally, it appeared that SNAP25 (at least at higher concentrations) did not only form relatively small oligomers, but randomly also large or insoluble aggregates that interfered with the experimental set-up of the partial proteolysis experiments and FCS analysis. Nonetheless, collectively the data from the different approaches suggest biphasic oligomerization of soluble SNAP25.

In this regard, the most insightful approaches proved to be OD, DLS and label-free MST measurements, since these were devoid of dye artefacts, and involved a straight forward assay design with a minimum number of experimental steps. DLS and label-free MST measurements indicated that already in the absence of divalent ions SNAP25 oligomers are present. This is different from typically used model proteins like BSA and lysozyme, which are monomeric in solution. SNAP25 obviously has a higher propensity for self-interaction, which has indeed been observed before[135]. (These self-interactions might be driven by SNARE motif zippering, which is actually the key mechanism in heterologous SNARE domain interactions during vesicle fusion.)

Despite the pre-oligomerized state of the protein, further SNAP25 oligomerization by calcium ions was detected in all assay systems. In addition, the OD, DLS and MST data strongly argue in favour of a biphasic oligomerization response which depends on the ion concentration: an increase in oligomerization at intermediate calcium concentrations, and a lower degree of oligomerization at high concentrations. The DLS experiments revealed that the exact oligomer size in both the low and high calcium condition differed within an experimental run and condition as well as between runs. This suggests an oligomerization process which is affected by random precipitation.

6.1.1 Precipitation as a consequence of aggregation

Protein aggregation that entails precipitation was not reported for lysozyme and BSA. It can be speculated that there are stronger protein–protein interactions between SNAP25 proteins than between lysozyme or BSA proteins. This view is supported by the observation of SNAP25 oligomers even in the absence of ions. Tighter protein–protein interactions, probably SNARE domain-mediated, ultimately lead to the formation of larger oligomers, which are more likely to undergo phase separation. Still, the occurrence of SNAP25 precipitation differed between the experimental approaches. Solid phase separation of SNAP25 aggregates was clearly observed in partial proteolysis experiments (which is why trehalose was added as a stabilizing agent). The extent of precipitation in optical density measurements remains somewhat elusive. Depending on the calcium concentration, the solutions appeared turbid, suggesting precipitation. While sedimentation was not directly observed, it may have become apparent after a centrifugation step. In the thermophoresis experiments, in contrast, precipitation occurred only rarely. This may be due to the small amounts of detergent in the buffer, which destabilizes hydrophobic interactions. However, precipitation is probably also an issue of SNAP25 concentration and the amount of available monomers. While the proteolysis experiments were conducted with 200 µM SNAP25, only 70 µM were used for OD measurements, and merely 10 µM in MST.

6.1.2 Reversibility of aggregation

Can pre-formed SNAP25 oligomers be re-dissolved? OD measurements, which are probably dominated by protein precipitation as a follow-up reaction to oligomerization, suggest at least partial reversibility: While large aggregates still form at high calcium concentrations, they partially dissociate again after several hours (Fig. 10). Since re-dissolution occurred without applying high temperature or pressure[59], it can be speculated that the proteins within these aggregates

were probably not completely denatured and associated to each other via strong hydrophobic forces, or connected via stable β-sheet fibrils. The reversibility rather argues for a relatively loose association. However, the conformation of SNAP25 within the oligomers remains speculative and would need to be elucidated e.g. with circular dichroism (CD) spectroscopy. If a structural alteration does occur during oligomerization, its reversibility into the native conformation after oligomer re-dissolution could be investigated with CD spectroscopy and by testing the protein's biological functionality.

Part of the aggregates was not re-dissolved during the time course of the OD experiments. This may be interpreted either in terms of irreversible aggregation of this fraction, or in terms of insufficient time for re-dissolution. The latter view is supported by the lack of a plateau in turbidity and thus stagnation of re-dissolution with 500 and 100 mM calcium. The maximum extent of reversibility could be investigated by removing calcium from the solution, e.g. by dialysis. In MST measurements, aggregates that form are probably smaller and only rarely undergo phase separation. Along these lines, it should be noted that calcium-induced clustering of membrane-bound SNAP25 was reported to be fully reversible within 3–6 hours after calcium removal[29] (albeit it is unclear whether a similar type of aggregate forms in membrane sheets).

In summary, homophilic SNAP25 interactions lead to a substantially oligomerized protein structure already in the absence of ions. Addition of intermediate calcium concentrations increases the degree of oligomerization, leading to the formation of large multimers. Depending on protein concentration, these structures may precipitate from solution, and the precipitated SNAP25 will be more difficult to redisperse than large soluble aggregates. Addition of high amounts of calcium results again in smaller entities or re-dissolution of precipitates. In conclusion, soluble SNAP25 reveals biphasic oligomerization behaviour in response to calcium ions (see Fig. 28).

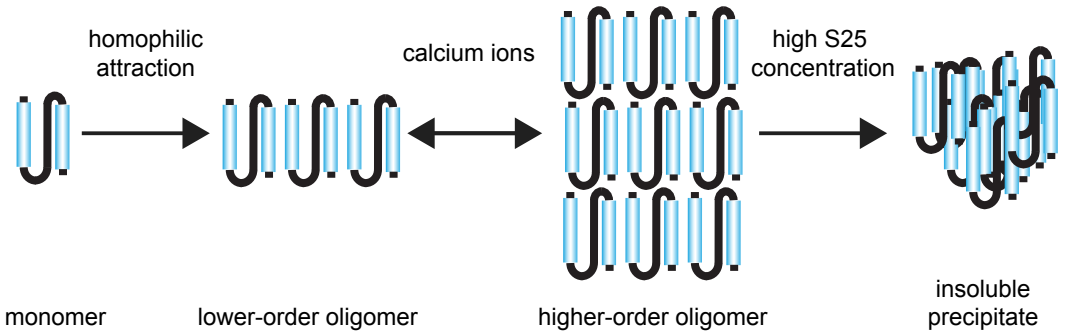

Fig. 28 Biphasic SNAP25 oligomerization in solution. In physiological salt solution, SNAP25 assembles into lower-order oligomeric structures. Addition of calcium ions either favours the formation of higher-order oligomers at low to intermediate calcium concentrations, or the (at least partial) continuance of lower-order oligomers at high calcium concentrations. At high protein concentrations, the aggregates can form insoluble precipitates.

6.2 Extending the principle of ion-induced biphasic oligomerization from solution to the cell membrane

Oligomerization of the membrane-anchored protein was investigated with endogenous SNAP25 in plasma membrane sheets – a plain yet physiological platform for analysing membrane architecture. SNAP25 is substantially (pre)clustered in the membrane even in the absence of ions (cf. e.g. Fig. 19), which is typical of membrane proteins[136,128]. It is interesting to note that this creates a similar pre-oligomerized starting point for both membrane-bound and soluble SNAP25.

Like in solution, addition of increasing concentrations of calcium ions produced a biphasic oligomerization response of membrane-anchored SNAP25. Analysing the relative SD of fluorescence in a ROI shows that at intermediate calcium concentrations, proteins are reorganized from a relatively homogenous distribution to a more clustered one. Judging from the analysis of STED images, this reorganization involves disintegration of approx. 50 % of the clusters and translocation of their molecules to other clusters, or alternatively merging of whole clusters. Whether reorganization also involves incorporation of

previously non-clustered molecules remains unresolved. While this pathway was suggested by a segmentation-based analysis approach of the epifluorescence images (see Fig. 16), a uniformly (i.e.) non-clustered population was not visible in STED images. The segmentation-based analysis most likely overestimates the proportion of uniformly distributed molecules (see page 70 for details), while STED microscopy may be too insensitive to detect it at the high depletion laser powers used here. It can be speculated that if this uniform population does exist, it is rather small.

In addition to molecule redistribution, both epifluorescence and STED images suggest tighter protein crowding as an additional aspect of clustering. The relative fluorescence intensity is reduced at intermediate calcium concentrations, pointing to a reduced accessibility for the antibody to both the N- and the C-terminus of the protein. In addition, the STED images indicate that the same number of molecules is confined in half as many, but equally sized clusters.

In summary, biphasic oligomerization can be induced in both soluble and membrane-bound SNAP25, arguing for a similar underlying physico-chemical mechanism. The following subsections will discuss differences and parallels between these fundamentally different configurations and explore their implications for protein oligomerization.

Both in solution and in the membrane, oligomerization appears to be driven by charge attenuation. In both environments, an increasing amount of monomers is recruited into SNAP25 clusters. However, the reaction that leads to monomer recruitment and incorporation differs between the two systems. In solution, this recruitment leads to massive cluster growth (cf. Fig. 28). The DLS data of soluble SNAP25 provide evidence for a 100–1,000 fold increase in SNAP25 oligomer size upon calcium addition, towards oligomers which are up to 1000 nm in size (this is even more notable on the level of the number of molecules per

oligomer, which – assuming spherical clusters – increases with the third power of oligomer radius). The size of membrane bound SNAP25 clusters, in contrast, was found to be limited to approx. 100 nm irrespective of the calcium concentration. Clusters appeared to increase the amount of their constituents merely by a factor of five in the clustering regime, via tighter cluster packing (see Fig. 29). These different pathways are probably due to four major differences arising from the protein environment. First, the number of available protein monomers is lower, and second, protein movement is restricted in the membrane environment. Third, the membrane contains a multitude of other protein and lipid species, and finally, plasma membrane specific short-range attractive and long-range repulsive forces provide a major contribution to membrane protein clustering.

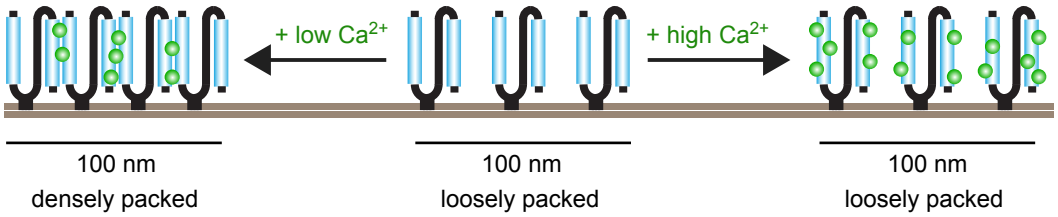

Fig. 29 Biphasic SNAP25 oligomerization in the plasma membrane. In the presence of low calcium concentrations (left), the packing density and the number of molecules in the clusters increase but cluster diameter is unchanged. This is compensated for by a reduced number of clusters per membrane area (not shown; for clarity the figure focusses on a single cluster). In the presence of high calcium concentrations (right), both packing density and cluster diameter resemble the condition without divalent ions (centre).

6.2.1 The number of possibly associating monomers is greater in solution than in membrane sheets

This is a very basic, yet important consideration. Typical PC12 membrane sheets in this study were about 100 μm^2 in size. The PC12 membrane was published to contain 7,500 SNAP25 molecules per μm^2 [137]. Multiplying these numbers, it can be estimated that there are 7.5×10^5 SNAP25 molecules per sheet, and thus the

maximum amount of monomers that could potentially be recruited into a cluster. In the experiments performed with soluble SNAP25, the number of available monomers is several magnitudes higher: The label-free MST experiments for example were conducted with 10 µM SNAP25 in a volume of ~5 µl. This provides ~3×10^{13} SNAP25 molecules per capillary[II]. In the optical density measurements, the monomer number is even higher and amounts to ~4×10^{15} SNAP25 molecules per well[III]. These calculations indicate that already the available amount of SNAP25 monomers limits cluster growth in the membrane environment.

6.2.2 Protein movement is restricted in the plasma membrane

Degrees of freedom

Endogenous SNAP25 is permanently anchored to the membrane bilayer so that it can merely translate along the two-dimensional membrane plane, and it can only rotate around the axis orthogonal to the membrane surface. Therefore, while a soluble protein experiences six degrees of freedom (three translational and three rotational), a membrane protein experiences only three.

Caged diffusion

The Singer and Nicholson model[138] pictured relatively few proteins to be freely diffusing in a sea of inert lipids. Based on this model, one should expect no further restrictions in protein movement apart from the fewer degrees of freedom. However, several aspects of the fluid mosaic model have been challenged by later experimental evidence. Protein diffusion is about a factor twenty slower in plasma membranes compared to artificial membranes or liposomes[139], pointing to constraints arising from membrane structure and composition.

[II] 10 µmol/l × 5 µl × 6.022×10^{23}/mol = 3.011×10^{13}

[III] 70 µmol/l × 100 µl × 6.022×10^{23}/mol = 4.215×10^{15}

Single particle tracking experiments revealed that proteins undergo anomalous diffusion[140] characterized by diffusion within a certain compartment, followed by a hop-movement to an adjacent compartment to which the protein is again temporally confined. The origin of this compartmentalization is the cytoskeleton cortex, which forms sub-plasmalemmal cytoskeleton fences that can only be overcome during their re-assembly or if they happen to be located far enough from the membrane.

During the preparation of membrane sheets, the actin cytoskeleton remains in principle attached to the inner membrane leaflet[6]. The actin cortex then depolarizes within ten minutes[141], i.e. within the time that was spend in this study to incubate the membrane sheets with ions. Thus, at least initially SNAP25 should undergo anomalous diffusion in the membrane sheet experiments. The temporary confinement to the compartments of the cytoskeleton meshwork is even greater for oligomers than for monomers. This appears to be both the result of the increased size and thus greater difficulty to undergo hop diffusion, as well as the higher avidity for binding cytoskeleton fences[142]. This indicates that the more SNAP25 monomers are recruited into a cluster, the less likely it is for two SNAP25 clusters to encounter each other and fuse. The impact of the actin cortex on SNAP25 clustering could be more thoroughly evaluated by analysing sheets of cells incubated with jasplakinolide, a (cell-permeant) inducer of actin polymerization[143].

Apart from passively limiting diffusion, the cytoskeleton specifically tethers some proteins and thus hinders their movement. An active interaction between SNAP25 and the cytoskeleton is not known, and therefore does probably not play a role in this case.

Consequences of movement restriction

Unrestricted mobility is apparently no key issue for ion-induced biphasic clustering. However, the experimental data demonstrate that oligomer growth of membrane-bound SNAP25 is limited, and that formation of giant clusters (or a single giant cluster) – as observed with soluble SNAP25 – is prevented. This can probably be attributed to a combination of passive diffusion restrictions and active interactions with other membrane constituents (see also paragraph 6.2.3 below). It could be speculated that in solution a few very large oligomers are formed, while in the membrane (even though the number of available monomers is lower) many small-to-medium sized oligomers are assembled upon calcium addition.

6.2.3 The plasma membrane contains a multitude of potential interaction partners

Biphasic oligomerization experiments with soluble proteins are typically performed in simple aqueous solutions. Here, the solution contained – besides SNAP25 and $CaCl_2$ – a buffer substance to maintain physiological pH, as well as sodium and chloride ions to mimic physiological osmolarity and salt concentration. These are only few (less than ten) different components. The cell membrane, in contrast, is populated by several thousand different protein species[144,145] and several different classes of lipids[146], which create a complex multi-component environment. The protein of interest likely interacts with several of these other components in addition to interacting with itself.

Influence of membrane components on electrostatics

Interactions between proteins and other proteins or lipids can arise between charged chemical groups or (induced) dipoles, as well as between hydrophobic sections (cf. 2.2.2.3). The number of potential electrostatic interactions is

evidently of major importance in ion-induced protein clustering. In solution, the polybasic region of SNAP25 is free to interact with the overall negatively charged SNARE motifs, leading to partial neutralization of the molecule's negative charge. In case of membrane-bound SNAP25, the polybasic region of the protein is located next to the protein's palmitoyl anchors, and therefore in the immediate vicinity of the inner, negatively charged membrane leaflet. Here, the polybasic region likely interacts with PIP_2 molecules (personal communication from P. Weber and T. Lang, see also[147, 157]), thus precluding intramolecular interactions with negatively charged protein regions. This lipid-mediated neutralization of the polybasic linker increases the net negative charge of the protein and as a consequence intermolecular like-charge repulsions.

On the other hand, charge compensation of negatively charged protein residues by membrane lipids is less likely to occur: there are only few positively charged lipids in general[148] and in the inner plasma membrane leaflet specifically[149]. In fact, the net negative surface charge of the inner membrane leaflet may impart a higher negative charge density to the immediate vicinity of SNAP25 molecules, and thus diminish the capacity of calcium ions to neutralize electrostatic repulsions between the molecules.

Hydrophobic interactions

Hydrophobic interactions likely also play a role in the SNAP25 clustering process, since they are often involved in protein oligomerization in general (see 2.2.2.3), and the formation of coiled coils (such as the SNARE complex) specifically[52]. In solution, hydrophobic patches of SNAP25 presumably show a great degree of interaction due to the lack of other hydrophobic components, and thus favour oligomerization independent from electrostatic mechanisms. In the case of membrane-bound SNAP25, though, the protein's hydrophobic patches can alternatively interact with lipids or hydrophobic patches of other membrane proteins.

Heterologous interactions

This multitude of interaction partners in the membrane creates a different starting point for oligomerization. In addition, the interaction partners or the extent and mode of interaction may change upon addition of ions. This entails a plethora of possible interaction patterns during protein oligomerization which are not available in simple solutions. If the protein of interest interacts with other proteins or lipids, there are fewer functional groups that can engage in homophilic interactions with other SNAP25 molecules. It can be speculated that this leads to a reduced size and to a lower purity of SNAP25 oligomers in the plasma membrane. The differences in oligomer size between soluble and membrane bound SNAP25 have already been discussed in sections 6.2 and 6.2.2. With the exception of examining the SNAP25 interaction partner syntaxin-1, oligomer purity was not experimentally assessed in this study. Therefore, the extent of SNAP25 mixing with other proteins within the membrane SNAP25 cluster remains speculative.

Heterologous interactions with membrane components can also affect protein aggregation by altering the protein secondary structure[150]. From studies with soluble variants of SNAP25 and syntaxin[135,151], we know that the usually unstructured SNAP25 adopts an α-helical conformation upon syntaxin binding. The membrane environment, in which SNAP25 and syntaxin are known to interact[123], thus very likely affects SNAP25 conformation.

However, unlike amyloidogenic proteins, SNAP25 apparently oligomerizes rather randomly, independent from sequential structural changes. It was previously shown with CD spectroscopy that a soluble SNAP25 peptide adopts an α-helical conformation when incubated with calcium ions[135]. The degree of α-helicity was positively (not biphasically) correlated with calcium concentration, and it was even more pronounced for magnesium ions[135] – which were found less potent at inducing clustering in this study. For these reasons, it appears unlikely that the

degree of α-helicity is directly related to the degree of SNAP25 clustering, or that clustering is accompanied by strict sequential changes in the secondary structure. The structural changes imposed by the membrane environment are therefore probably of minor importance in this case.

6.2.4 Network of interactions acting on proteins in solution and in the plasma membrane

Ion–protein vs. protein–protein interactions

What is the difference between ion–protein and protein–protein interactions (cf. also Table 2) in governing protein oligomerization? Both types of interactions are similar in that they involve electrostatic and van-der-Waals forces. Therefore, clustering mechanisms that rely on these forces will predominantly be influenced by the presence of ions. Still, there are several differences between electrostatic fields originating from metal ions compared to proteins. Multivalent ions like Ca^{2+} convey a larger amount of charge than the monovalent amino and carboxylate groups in proteins. This charge is more concentrated (restricted to a single atom) and less polarizable than in the case of amino and carboxylate groups. In addition, ions are smaller and freely moving, unlike the spatially confined charges of a large biomolecule. Ions have thus access to crowded or shielded parts of proteins. Inside a living cell, Ca^{2+} concentrations are subject to large fluctuations making ion–protein interaction shorter lived than protein–protein interactions. Hence, ions exert a strong, dynamic, and locally limited electrostatic force, which may even act at remote protein domains.

The cluster phase model

In the plasma membrane, however, there are additional, lipid-mediated mechanisms that favour protein clustering. These effects are different from the heterologous interactions discussed in 6.2.3, since they are more passive, less direct and less specific.

According to the protein cluster phase model[152,128] lipid-mediated forces in the order of a few k_BT (the thermal energy) are sufficient to induce largely homogenous protein clusters in the membrane, with only few molecules of each protein species remaining in the non-clustered phase. The forces can be categorized in short range (< 1 nm) attractive and long range (> 10 nm) repulsive forces, and will be considered in greater detail in the following two paragraphs.

First, lipids cause a depletion attraction between proteins (cf. Fig. 20 a for a description of this effect). In addition, the hydrophobic mismatch of proteins (i.e. the hydrophobic core being larger or smaller than the membrane diameter) entails alterations in membrane thickness. The energy consumption for these alterations is minimized by clustering of proteins with similar hydrophobic cores. While these two forces may explain clustering of many (trans)membrane proteins[128, 152], they may only partially account for the large extent of "pre"clustering of the palmitoyl-anchored SNAP25.

Repulsive forces are elastic membrane deformations imposed by non-cylindrical (e.g. conical) protein shapes. These deformations are screened in cells beyond distances of a few tens of nanometres because of membrane tension, and membrane coupling to the rigid cytoskeleton[152,128]. In membrane sheets, this screening is probably less efficient due to lower membrane tension and a depolymerizing actin cortex (see 6.2.2). Therefore, these elastic deformations probably contribute to the limitation in cluster growth, in addition to the restricted movement and the limited amount of self-interactions discussed in 6.2.2 and 6.2.3.

Effects of ions on cluster phases

Both in solution and in the membrane, protein clustering is thus driven by electrostatic forces between charged protein residues. In both systems, the densely charged calcium ions likely lead to a charge attenuation of the carboxylate

groups provided by aspartate and glutamate residues at low to intermediate calcium concentrations, and to protein overcharging at high ion concentrations. In solution, electrostatic and van-der-Waals forces are the main determinants of protein clustering. This explains why calcium ions have a major impact on oligomerization of soluble SNAP25 and lead to massive cluster growth. In the membrane environment, protein assembly is governed by various forces. The SNAP25 proteins are already highly pre-clustered, and addition of calcium ions does not increase cluster size but packing density. The effect of calcium ions is thus less pronounced in the membrane, and rather adds an additional level of complexity to the multifactorial membrane protein clustering mechanism.

This is also illustrated by the results on SNAP25–syntaxin co-clustering. In solution, the two SNARE proteins are known to form complexes[135]. Yet, their colocalization was low in the plasma membrane sheets, and was not directly related to the extent of calcium-induced clustering (cf. Fig. 26). As discussed above, the distribution of proteins in the membrane is governed by several factors. Based on the results from this study, the individual protein species within this system such as SNAP25 or syntaxin constitute apparently autonomous sub-groups with little contact between each other. Ion-mediated protein clustering apparently cannot overrule the specific protein–protein and protein–lipid interactions leading to protein homo-clustering discussed above.

6.3 The chemical basis of biphasic ion-induced clustering

Having considered the molecular differences and similarities between protein oligomerization in the membrane and in solution, this section will explore the mutual chemical basis of ion-induced clustering and re-dispersion in these systems.

6.3.1 Calcium ions directly interact with protein carboxylate groups

The membrane sheet experiments revealed that the ability of an ion to induce protein clustering does not depend on its bare charge, but on its charge-to-radius ratio. This indicates that a certain charge density is necessary to attenuate the electrostatic repulsions between two negatively charged protein residues. However, considering only charge density as the driving force for clustering cannot explain why there is an optimum of the charge-to-radius, or in other words, why ions with very high charge densities were incapable of inducing clustering in membrane sheets.

Two other parameters were found to be linked to the extent an ion promotes protein clustering: the ion's water viscosity coefficient and its hydration enthalpy per coordinating water molecule. Both these parameters suggest that water binding energies are important in the clustering process. In aqueous solution, ions are surrounded by a shell of hydrating water molecules. Both the water viscosity coefficient and the hydration enthalpy are parameters which describe the strength of the ion–water interactions. The data thus suggest that in order for the ion to interact with the protein surface, it releases one or several of its hydrating water molecules. Since a former study[29] showed that proteins with a higher content of negatively charged residues experience greater calcium-induced clustering, it appears very likely that the ions engage in a coordinative binding with protein carboxylate groups in exchange for water molecules. This ligand exchange, however, is only energetically favourable if the binding enthalpy between the ion and the carboxylate group is greater than the binding enthalpy between the ion and the water molecule.

Taken together, ion water affinity and charge density can thus account for the observations in this study. Magnesium and the lanthanide ions have energetically unfavourable (or insuperable) hydration energies. This is also

reflected by the water exchange rate, which is about 3,000-fold lower for magnesium than for calcium ions[153]. Therefore, these ions hardly exchange their water molecules for carboxylate groups and do not induce protein clustering. Sodium ions, on the other hand, are easily dehydrated and could readily bind to carboxylate groups. Yet, their charge density may be too low to attenuate the proteins' negative charges, a prerequisite for tighter clustering.

The observation that there is an optimum range for the parameters water viscosity coefficient and hydration enthalpy in which the ions are effective at inducing protein clustering is also consistent with the law of matching water affinities. This law predicts that oppositely charged ions preferentially form contact pairs if they have similar water affinities. Indeed, the water viscosity coefficient[154] of the acetate anion (0.246 cm^3/mol) is similar to that of Sr^{2+} (0.272 cm^3/mol), whereas the water viscosity coefficients for Na^+ (0.085 cm^3/mol) and La^{3+} (0.576 cm^3/mol) are substantially lower and higher, respectively. According to this concept, it could be speculated that lanthanum is most efficient at clustering highly phosphorylated proteins, since it resembles phosphate's water affinity (0.495 cm^3/mol).

Despite these considerable agreements in the water viscosity coefficients observed in this study, it has been shown that so-called Hofmeister (or "ion-specific") effects strongly depend on surface polarity[104], besides polarity and charge of the protein chain[155] and salt concentration[93]. In fact, it has been suggested that there is no universal Hofmeister ranking, but rather a "diverse spectrum of direct, partially altered, and reversed (indirect) series"[155]. Indeed, the series of ions which this study found to be effective at membrane protein clustering is not identical to the Hofmeister series of ions which precipitate proteins in solution. Also lanthanum, while unable to induce SNAP25 clustering in membrane sheets,

was previously shown to influence oligomerization of BSA in solution[89]. There may also be a different effect of magnesium ions on soluble and membrane-bound SNAP25 in this study[IV].

Therefore, the crucial realms of the ion properties (charge-to-size ratio, water viscosity coefficient and hydration energy per coordinating water molecule) identified in this study are most likely not universal, but rather specifically apply to negatively charged proteins anchored to cell membranes. (Even the net amount of the negative charge and the hydrophobicity of the protein of interest could be important). In addition, it could be speculated that the hydrophobic membrane differently affects the distribution of calcium and magnesium ions: Larger cations (in this case calcium) have a higher affinity for hydrophobic surfaces[155]. This is the result of both a larger polarizability and the lower water affinity of these ions[156]. In section 6.2 it was extensively shown that the membrane environment additionally influences protein clustering *per se*. These considerations may explain why the effect of ions depends on the protein properties and on its environment.

Irrespective of the exact realms of water affinities and the charge-to-radius ratio, the data suggest that in case of both membrane-bound and soluble SNAP25, calcium ions directly interact with the protein carboxylate groups. Support for such a direct interaction is also provided by molecular dynamics (MD) simulations (performed by Dr. Thomas H. Schmidt, LIMES Institute, Bonn). All-atom MD simulations were computed with SNAP25 peptides[V], water molecules, sodium and chloride ions,

[IV] Although the readouts cannot be directly compared, magnesium ions appeared to induce approx. 50 % of the calcium clustering effect in solution (compare the dynamic ranges in Fig. 14), while their impact on membrane-bound SNAP25 is much more subtle (see Fig. 22).

[V] The peptides correspond to Leu 35–Met 64 located in the N-terminal SNARE domain. The structure of this peptide was extracted from the crystal structure of the assembled SNARE complex (PDB-ID: 1SFC, chain C).

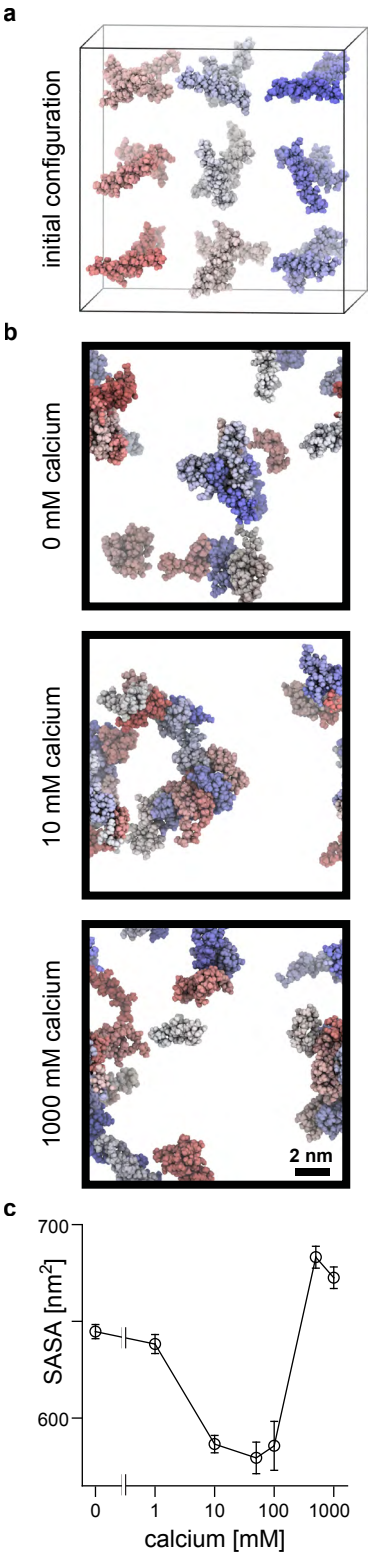

Fig. 30 Biphasic clustering behaviour in response to Ca^{2+} ions is observed for SNAP25 peptides in molecular dynamics (MD) simulations. (**a**) MD initial configuration of 27 SNAP25 peptides solvated in an aqueous environment (for clarity only the peptides are shown, which are coloured according to their position in the simulation box). (**b**) MD system configurations after 100 ns unbiased simulation, illustrating the oligomeric states of the SNAP25 peptides (coloured according to their starting position) at 0, 10 and 1000 mM calcium. Due to periodic boundary conditions, molecules crossing simulation box borders are present at the respective opposite sides. (**c**) The degree of peptide clustering is assessed by the peptides' solvent accessible surface area (SASA) (mean ± s.e.m., n = 4). This figure is modified from ref. 122.

as well as varying calcium concentrations[122]. Similar to soluble and membrane-anchored SNAP25 analysed in the wet lab experiments, the SNAP25 peptides experienced biphasic oligomerization *in silico* (cf. Fig. 30). Analogous to quantifying the proteins' antibody accessibility in the membrane sheet experiments, the solvent accessible protein surface area was quantified for the simulation data. This clearly documents the biphasic trend in clustering (Fig. 30 c). Since the clustering trends *in silico* are remarkably similar to the wet lab experiments, the data were further explored to gain insight into the molecular mechanism on an atomistic level. As already implied by the sheet experiments, it could be shown that calcium ions directly interact with SNAP25 carboxylate groups of glutamate and aspartate side chains and the protein C-terminus. The ions are

located merely ~0.35 nm away from the carboxylate carbon atom. This distance reflects a coordinative oxygen atom binding mode, which requires the calcium ion to release at least one water molecule from its hydration shell.

6.3.2 The stoichiometry of calcium–carboxylate interactions defines the degree of oligomerization

The *in silico* data suggest that clustering is not merely driven by charge attenuation. At concentrations for which the greatest degree of clustering is observed, most bound calcium ions interact with more than one carboxylate group (Fig. 31 a). This means that calcium ions function as bridges or linkers between protein carboxylate groups.

What is the mechanism of protein dispersion at high ion concentrations? One hypothesis states that counterion association beyond charge neutrality is an entropy driven process, since the excluded volume of the solvent molecules is minimized[117,116]. The experiments with membrane sheets incubated with the crowding agent trehalose did not show an effect on SNAP25 clustering (see Fig. 20). This supports the notion that external/additional depletion forces have a rather weak effect on membrane proteins, either because the excluded volume for water (and lipid) molecules in the anyhow crowded membrane is already minimized, or because the depletion forces are overruled by e.g. electrostatic effects.

Alternatively, ion adsorption to the protein surface may be mediated by dispersion forces at high ion concentrations[93]. As a consequence, the surface tension at the protein–water interface would be reduced, which then drives cluster dissolution[93]. In contrast to this concept, I did not find high concentrations of ions with greater polarizability, such as Ba^{2+}, to be more effective at preventing clustering than less polarizable ions such as Ca^{2+}. This would be expected (and was indeed observed by Zhang and Cremer[93]), if non-specific ion-adsorption was

the driving factor for preventing clustering since more polarizable ions adsorb to a surface more easily. This difference may arise from the choice of ions. This study used small monatomic cations which are substantially less polarizable than the polyatomic anions used in the other study[93].

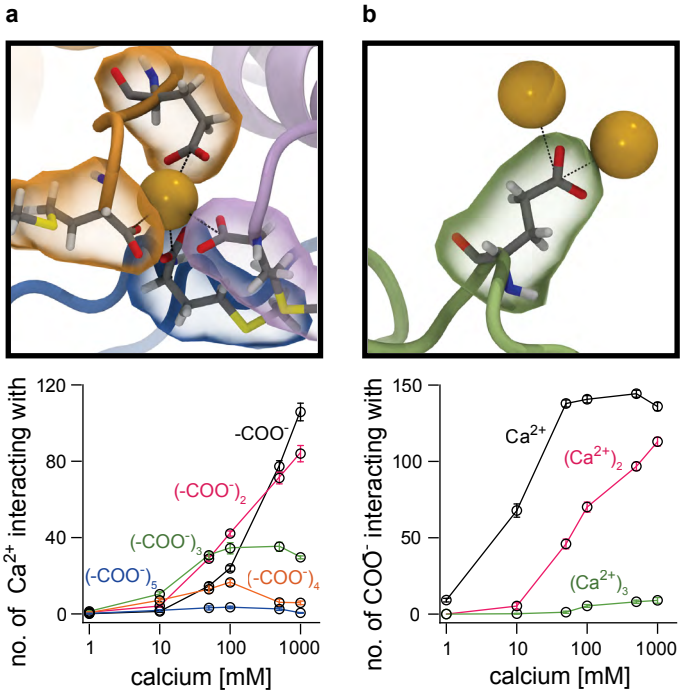

Fig. 31 Ion–protein binding patterns depend on the calcium concentration. (**a**) Snapshot of an interaction between one calcium ion (yellow) and four carboxylate groups (which are provided by three SNAP25 peptides coloured in orange, magenta and blue). The graph shows the number of interactions (mean ± s.e.m., n = 4) between one calcium ion and *i* carboxylate groups (i = 1, 2, … , 5; indicated by different colours) as a function of the Ca^{2+} concentration. (**b**) Snapshot of an interaction between one carboxylate group and two calcium ions. The graph shows the number of interactions between one carboxylate group and *i* calcium ions (i = 1, 2, 3) as a function of the calcium concentration. This figure is modified from a previously published version in ref. 122.

Non-specific calcium adsorption to SNAP25 is not supported by the MD simulations either (although it should be noted that this simulation method does not consider electrons explicitly). Still, SNAP25 dispersal at high calcium concentrations is observed in the simulations which do not include dispersion interactions, indicating that non-specific ion adsorption is at least not crucial to this phenomenon. In the MD simulations, calcium ions continue to bind to

carboxylate groups at high ion concentrations[122]. However, the number of calcium-mediated bridges between three or more carboxylate groups is reduced at high calcium. The majority of calcium ions interact with only one carboxylate group (Fig. 31 a). The ions thus no longer link the SNAP25 molecules to each other.

A concept that considers only interfacial bridges still appears insufficient to explain biphasic protein aggregation. If the number of ion bridges between carboxylate groups were the main (or even sole) factor that determines whether proteins remain separated (few bridges) or aggregate (many bridges), proteins with the highest absolute number or highest percentage of negatively charged residues – and thus maximal number of potential bridges – would be expected to respond strongest. Conversely, a previous study[29] showed that proteins with the highest net charge (i.e. the percentage of negatively minus positively charged residues) are clustered most efficiently by calcium ions. This implies that the global protein charge is also important in the clustering process. Carrying a net amount of fourteen negative charges, the SNAP25 molecule can be considered as heavily charged. Long range electrostatic repulsion have already been suggested by Stradner and colleagues[100] to limit clustering. In addition, short range (< 1 nm) electrostatic repulsion or attraction between charged protein groups certainly contributes to the clustering processes.

Is cluster dissolution at high ion concentrations also influenced by charges? The MD simulations show (at least local) overcharging of SNAP25. With increasing calcium concentration, several COO^- groups simultaneously interact with two or even three Ca^{2+} ions (Fig. 31 b). Since the carboxylate group carries a single negative charge while the calcium ion carries two positive charges, already a 1:1 binding implies a local overcharging with positive charge. The driving force for this association beyond charge neutrality remains unresolved. Ion-ion correlations[114] could be one explanation; dispersion forces or depletion attraction

seem unlikely (see above). The carboxylate groups which are overcharged with positive ions are expected to electrostatically repulse each other, similar to carboxylate groups in the absence of positive ions.

In summary, the stoichiometry of calcium–carboxylate interactions determines whether the proteins aggregate or separate: aggregation is driven by charge attenuation and ion bridging, while separation is characterized by a high (negative or positive) net charge and the absence of ion bridges.

Is biphasic ion-induced aggregation a specific property of SNAP25 or is this inherent to all membrane proteins? Biphasic calcium-induced clustering was also observed for syntaxin in membrane sheets (Fig. 26). Yet, the clustering response at intermediate calcium concentrations is not as strong as for SNAP25, and syntaxin dispersion at high calcium concentrations was not as pronounced. Both these differences are likely due to the overall less negative charge of syntaxin (which has net 4 % negatively charged residues, while SNAP25 has 6.8 %).

Hence, biphasic ion-induced clustering of negatively charged proteins appears to be a general effect. Yet, its characteristics depend on the negative charge of the respective protein, and likely also on the strength of the protein's interactions with other proteins and lipids.

6.4 Biological and technological significance of the study

The intracellular calcium concentration in resting cells is kept to roughly 100 nM. However, during synaptic transmission for example, the local calcium concentrations in the proximity of calcium channels can increase to 100–200 μM[158,159]. The MD simulations unequivocally proved that already a few calcium ions forming ion bridges are sufficient to induce SNAP25 clustering. In line with this observation, depolarization-induced calcium influx is sufficient to

induce SNAP25 clustering in bovine chromaffin cells[29]. Other negatively charged proteins in the channel vicinity are likely to be similarly affected. This membrane reorganization could be an additional way by which calcium ions influence synaptic plasticity (besides the plethora of signalling pathways calcium affects as a second messenger during this process[160]). Interestingly, binding studies with soluble synaptobrevin suggest that calcium-induced clustering appears to be a mechanism that reduces SNARE protein activity[29], and thus possibly also synaptic activity.

In the extracellular milieu the calcium concentration is about 10,000-fold higher than inside the cell, and amounts to about 1.5 mM[161]. This is sufficient to induce salt bridges between membrane proteins on the extracellular leaflet, or between soluble proteins in extracellular fluids such as the blood, lymph or interstitial fluids. In contrast, calcium concentrations that would favour protein cluster dissolution are unlikely to occur *in vivo*.

The apparently conserved physico-chemical principles explored in this study are also interesting in terms of metal ion involvement in amyloidoses. Like many amyloidogenic proteins, SNAP25 is charged and intrinsically disordered. In favour of the applicability of insights from SNAP25, α-synuclein aggregation, a hallmark of Parkinson's disease, was shown to be stimulated by calcium ions[162]. Calcium promoted membrane association of the protein, possibly by bridging the acidic C-terminal tail to the negatively charged plasma membrane components[163]. Binding stabilized the partially folded amyloidogenic conformation, which likely facilitates α-synuclein aggregation in the membrane and seeds aggregation in the cytosolic α-synuclein fraction[164]. Alpha-synuclein carries a similar net percentage of negatively charged residues compared to SNAP25 (6.5 % vs. 6.8 %), is also intrinsically disordered, and may be localized both at the membrane and in the cytosol.

Calcium ions interact with negatively charged residues of both SNAP25 and α-synuclein, but neither one of the proteins presents a canonical calcium binding motif such as the EF hand or the C2 domain[165]. Rather, both proteins feature clusters of negatively charged residues. It is interesting to contemplate that calcium binding does not require a consistent binding motif, but that randomly scattered negatively charged residues are sufficient. It could be speculated that calcium binding to these less well defined sites occurs in a more random, and possibly more loose or transient way compared to classical calcium binding sites. A deeper understanding of this matter would help to more accurately predict calcium binding to proteins.

Finally, a more precise conception of ion-induced protein oligomerization is important for *ex vivo* use of proteins. For pharmaceutical applications it is desirable to create highly concentrated solutions of biologically active proteins. Protein formulations with a certain aggregation state are also important in food technology. These aggregation states could be regulated via addition of ions. In the field of bionanomaterials, aggregation of genetically designed peptides is investigated for diverse applications such as hydrogels, nanotubes and -wires, as inks for microprinting, and as scaffolds to organize metal nanocrystals for use in the electronic industry[166]. For these applications, ions could be one option to control the character of the synthetic protein material.

6.5 Conclusion

Ion concentration dependent protein aggregation is a phenomenon originally described in polymer physics and solution chemistry. Despite the many differences between simple aqueous systems and the crowded multicomponent, two-dimensional environment of the plasma membrane, ion-induced protein clustering and dispersion is observed in both systems, arguing for a fundamental, conserved principle.

The insights of this study provide a conceptual framework at the interface of physics, chemistry and biology for ion–protein interactions that favour or prevent protein aggregation phenomena with implications for biological and industrial processes.

In the case of a cluster – the organizational unit of membrane proteins[136] – the protein monomers are in a dynamic equilibrium with freely diffusing proteins and also with other clusters. In this picture ions can be conceived as modulators of quinary protein structures, since the underlying protein–protein interactions are based on weak surface charges. Ions can link proteins to each other at defined interaction sites, thus creating a protein super structure with a different anatomy and different properties. Ion–protein interactions may thus be an important factor for the creation of cellular supramolecular assemblies.

7 References

1. Messel, S. T. B. and H. Light and Life In The Universe. (Shakespeare head press 1964, 1964).
2. Chaplin, M. Water's Hydrogen Bond Strength. ArXiv07061355 Cond-Mat Physicsphysics (2007).
3. Milo, R. & Phillips, R. Cell Biology by the Numbers. (Taylor & Francis Ltd., 2016).
4. Nelson, D. L. & Cox, M. M. Lehninger Principles of Biochemistry. (W. H. Freeman, 2008).
5. Tanford, C. & Reynolds, J. Nature's Robots: A History of Proteins. (OUP Oxford, 2003).
6. Lillemeier, B. F., Pfeiffer, J. R., Surviladze, Z., Wilson, B. S. & Davis, M. M. Plasma membrane-associated proteins are clustered into islands attached to the cytoskeleton. Proc. Natl. Acad. Sci. 103, 18992–18997 (2006).
7. Markl, J. et al. Markl Biologie. (Klett, 2010).
8. Goodsell, D. S. & Olson, and A. J. Structural Symmetry and Protein Function. Annu. Rev. Biophys. Biomol. Struct. 29, 105–153 (2000).
9. Alemán, J. V. et al. Definitions of terms relating to the structure and processing of sols, gels, networks, and inorganic-organic hybrid materials (IUPAC Recommendations 2007). Pure Appl. Chem. 79, 1801–1829 (2009).
10. Work, W. J., Horie, K., Hess, M. & Stepto, R. F. T. Definition of terms related to polymer blends, composites, and multiphase polymeric materials (IUPAC Recommendations 2004). Pure Appl. Chem. 76, 1985–2007 (2009).
11. Roberts, G. C. K. Encyclopedia of Biophysics. (Springer Berlin Heidelberg, 2013).
12. Mahler, H.-C., Friess, W., Grauschopf, U. & Kiese, S. Protein aggregation: pathways, induction factors and analysis. J. Pharm. Sci. 98, 2909–2934 (2009).
13. Dumetz, A. C., Chockla, A. M., Kaler, E. W. & Lenhoff, A. M. Protein Phase Behavior in Aqueous Solutions: Crystallization, Liquid-Liquid Phase Separation, Gels, and Aggregates. Biophys. J. 94, 570–583 (2008).
14. Wang, W., Nema, S. & Teagarden, D. Protein aggregation – Pathways and influencing factors. Int. J. Pharm. 390, 89–99 (2010).
15. Hayakawa, S. & Nakai, S. Relationships of Hydrophobicity and Net Charge to the Solubility of Milk and Soy Proteins. J. Food Sci. 50, 486–491 (1985).

16. Giegé, R. A historical perspective on protein crystallization from 1840 to the present day. FEBS J. 280, 6456–6497 (2013).

17. Calvert, J. G. Glossary of atmospheric chemistry terms (Recommendations 1990). Pure Appl. Chem. 62, 2167–2219 (2009).

18. Song, L. et al. Structure of Staphylococcal α-Hemolysin, a Heptameric Transmembrane Pore. Science 274, 1859–1865 (1996).

19. Dominguez, R. & Holmes, K. C. Actin Structure and Function. Annu. Rev. Biophys. 40, 169–186 (2011).

20. Ali, M. H. & Imperiali, B. Protein oligomerization: How and why. Bioorg. Med. Chem. 13, 5013–5020 (2005).

21. Choii, G. & Ko, J. Gephyrin: a central GABAergic synapse organizer. Exp. Mol. Med. 47, e158 (2015).

22. Indriati, D. W. et al. Quantitative Localization of Cav2.1 (P/Q-Type) Voltage-Dependent Calcium Channels in Purkinje Cells: Somatodendritic Gradient and Distinct Somatic Coclustering with Calcium-Activated Potassium Channels. J. Neurosci. 33, 3668–3678 (2013).

23. Dutertre, S., Becker, C.-M. & Betz, H. Inhibitory Glycine Receptors: An Update. J. Biol. Chem. 287, 40216–40223 (2012).

24. Abulrob, A. et al. Nanoscale Imaging of Epidermal Growth Factor Receptor Clustering Effects of Inhibitors. J. Biol. Chem. 285, 3145–3156 (2010).

25. Sieber, J. J. et al. Anatomy and Dynamics of a Supramolecular Membrane Protein Cluster. Science 317, 1072–1076 (2007).

26. Kornberg, L. J., Earp, H. S., Turner, C. E., Prockop, C. & Juliano, R. L. Signal transduction by integrins: increased protein tyrosine phosphorylation caused by clustering of beta 1 integrins. Proc. Natl. Acad. Sci. U. S. A. 88, 8392–8396 (1991).

27. Lang, T. & Rizzoli, S. O. Membrane Protein Clusters at Nanoscale Resolution: More Than Pretty Pictures. Physiology 25, 116–124 (2010).

28. Bar-On, D. et al. Evaluation of the Heterogeneous Reactivity of the Syntaxin Molecules on the Inner Leaflet of the Plasma Membrane. J. Neurosci. 29, 12292–12301 (2009).

29. Zilly, F. E. et al. Ca^{2+} induces clustering of membrane proteins in the plasma membrane via electrostatic interactions. EMBO J. 30, 1209–1220 (2011).

30. Chiti, F. & Dobson, C. M. Protein Misfolding, Functional Amyloid, and Human Disease. Annu. Rev. Biochem. 75, 333–366 (2006).

31. Raut, A. S. & Kalonia, D. S. Effect of Excipients on Liquid–Liquid Phase Separation and Aggregation in Dual Variable Domain Immunoglobulin Protein Solutions. Mol. Pharm. 13, 774–783 (2016).

32. Johnston, K. P. et al. Concentrated Dispersions of Equilibrium Protein Nanoclusters That Reversibly Dissociate into Active Monomers. ACS Nano 6, 1357–1369 (2012).

33. Shewan, H. M. & Stokes, J. R. Review of techniques to manufacture micro-hydrogel particles for the food industry and their applications. J. Food Eng. 119, 781–792 (2013).

34. Meredith, S. C. Protein Denaturation and Aggregation. Ann. N. Y. Acad. Sci. 1066, 181–221 (2006).

35. Sharp, K. A., Nicholls, A., Friedman, R. & Honig, B. Extracting hydrophobic free energies from experimental data: relationship to protein folding and theoretical models. Biochemistry (Mosc.) 30, 9686–9697 (1991).

36. Burley, S. K. & Petsko, G. A. Aromatic-aromatic interaction: a mechanism of protein structure stabilization. Science 229, 23–28 (1985).

37. Lanzarotti, E., Biekofsky, R. R., Estrin, D. A., Marti, M. A. & Turjanski, A. G. Aromatic–Aromatic Interactions in Proteins: Beyond the Dimer. J. Chem. Inf. Model. 51, 1623–1633 (2011).

38. Gallivan, J. P. & Dougherty, D. A. Cation-π interactions in structural biology. Proc. Natl. Acad. Sci. 96, 9459–9464 (1999).

39. Crowley, P. B. & Golovin, A. Cation–π interactions in protein–protein interfaces. Proteins Struct. Funct. Bioinforma. 59, 231–239 (2005).

40. Liu, D. et al. Aromatic Side Chain–Porphyrin Interactions in Designed Hemoproteins. J. Am. Chem. Soc. 121, 11798–11812 (1999).

41. Dougherty, D. A. Cation-π Interactions in Chemistry and Biology: A New View of Benzene, Phe, Tyr, and Trp. Science 271, 163–168 (1996).

42. Atkins, P. & Paula, J. de. Physical Chemistry for the Life Sciences. (Oxford University Press, 2015).

43. Ippolito, J. A., Alexander, R. S. & Christianson, D. W. Hydrogen bond stereochemistry in protein structure and function. J. Mol. Biol. 215, 457–471 (1990).

44. Creighton, T. E. Disulphide bonds and protein stability. BioEssays 8, 57–63 (1988).

45. Roth, C. M., Neal, B. L. & Lenhoff, A. M. Van der Waals interactions involving proteins. Biophys. J. 70, 977–987 (1996).

46. Sheinerman, F. B., Norel, R. & Honig, B. Electrostatic aspects of protein–protein interactions. Curr. Opin. Struct. Biol. 10, 153–159 (2000).

47. Sintes, T. & Baumgärtner, A. Protein attraction in membranes induced by lipid fluctuations. Biophys. J. 73, 2251–2259 (1997).

48. Clark, A. H., Kavanagh, G. M. & Ross-Murphy, S. B. Globular protein gelation—theory and experiment. Food Hydrocoll. 15, 383–400 (2001).

49. Chiti, F. & Dobson, C. M. Amyloid formation by globular proteins under native conditions. Nat. Chem. Biol. 5, 15–22 (2009).

50. Konno, T., Morii, T., Shimizu, H., Oiki, S. & Ikura, K. Paradoxical inhibition of protein aggregation and precipitation by transglutaminase-catalyzed intermolecular cross-linking. J. Biol. Chem. 280, 17520–17525 (2005).

51. Wise, S. G. et al. Tropoelastin - a versatile, bioactive assembly module. Acta Biomater. 10, 1532–1541 (2014).

52. Burkhard, P., Stetefeld, J. & Strelkov, S. V. Coiled coils: a highly versatile protein folding motif. Trends Cell Biol. 11, 82–88 (2001).

53. Chiti, F., Stefani, M., Taddei, N., Ramponi, G. & Dobson, C. M. Rationalization of the effects of mutations on peptide andprotein aggregation rates. Nature 424, 805–808 (2003).

54. Pawar, A. P. et al. Prediction of 'Aggregation-prone' and 'Aggregation-susceptible' Regions in Proteins Associated with Neurodegenerative Diseases. J. Mol. Biol. 350, 379–392 (2005).

55. Fang, Y., Gao, S., Tai, D., Middaugh, C. R. & Fang, J. Identification of properties important to protein aggregation using feature selection. BMC Bioinformatics 14, 314 (2013).

56. McConkey, E. H. Molecular evolution, intracellular organization, and the quinary structure of proteins. Proc. Natl. Acad. Sci. 79, 3236–3240 (1982).

57. Monteith, W. B., Cohen, R. D., Smith, A. E., Guzman-Cisneros, E. & Pielak, G. J. Quinary structure modulates protein stability in cells. Proc. Natl. Acad. Sci. 112, 1739–1742 (2015).

58. Rajalingam, D., Loftis, C., Xu, J. J. & Kumar, T. K. S. Trichloroacetic acid-induced protein precipitation involves the reversible association of a stable partially structured intermediate. Protein Sci. 18, 980–993 (2009).

59. Meersman, F. & Heremans, K. Temperature-Induced Dissociation of Protein Aggregates: Accessing the Denatured State. Biochemistry (Mosc.) 42, 14234–14241 (2003).

60. Jones, S. & Thornton, J. M. Principles of protein-protein interactions. Proc. Natl. Acad. Sci. 93, 13–20 (1996).

61. Nooren, I. M. A. & Thornton, J. M. Diversity of protein–protein interactions. EMBO J. 22, 3486–3492 (2003).

62. Payandeh, J., Scheuer, T., Zheng, N. & Catterall, W. A. The crystal structure of a voltage-gated sodium channel. Nature 475, 353–358 (2011).

63. Jahn, R. & Scheller, R. H. SNAREs — engines for membrane fusion. Nat. Rev. Mol. Cell Biol. 7, 631–643 (2006).

64. Striegel, A. R. et al. Calcium Binding by Synaptotagmin's C2A Domain is an Essential Element of the Electrostatic Switch That Triggers Synchronous Synaptic Transmission. J. Neurosci. 32, 1253–1260 (2012).

65. Zhivotovsky, B. & Orrenius, S. Calcium and cell death mechanisms: A perspective from the cell death community. Cell Calcium 50, 211–221 (2011).

66. Perry, J. J. P., Shin, D. S., Getzoff, E. D. & Tainer, J. A. The structural biochemistry of the superoxide dismutases. Biochim. Biophys. Acta 1804, 245–262 (2010).

67. Alies, B., Hureau, C. & Faller, P. The role of metal ions in amyloid formation: general principles from model peptides. Metallomics 5, 183 (2013).

68. Markov, D., Naryshkina, T., Mustaev, A. & Severinov, K. A zinc-binding site in the largest subunit of DNA-dependent RNA polymerase is involved in enzyme assembly. Genes Dev. 13, 2439–2448 (1999).

69. Brayer, K. J. & Segal, D. J. Keep Your Fingers Off My DNA: Protein–Protein Interactions Mediated by C2H2 Zinc Finger Domains. Cell Biochem. Biophys. 50, 111–131 (2008).

70. Tang, J. X., Wong, S., Tran, P. T. & Janmey, P. A. Counterion induced bundle formation of rodlike polyelectrolytes. Berichte Bunsenges. Für Phys. Chem. 100, 796–806 (1996).

71. Carraway, K. L., Triplett, R. B. & Anderson, D. R. Calcium-promoted aggregation of erythrocyte membrane proteins. Biochim. Biophys. Acta BBA - Protein Struct. 379, 571–581 (1975).

72. Breydo, L. & Uversky, V. N. Role of metal ions in aggregation of intrinsically disordered proteins in neurodegenerative diseases. Metallomics 3, 1163–1180 (2011).

73. Leal, S. S., Cardoso, I., Valentine, J. S. & Gomes, C. M. Calcium Ions Promote Superoxide Dismutase 1 (SOD1) Aggregation into Non-fibrillar Amyloid. A link to toxic effects of calcium overload in amyotrophic lateral sclerosis (ALS)? J. Biol. Chem. 288, 25219–25228 (2013).

74. Durer, Z. A. O. et al. Loss of Metal Ions, Disulfide Reduction and Mutations Related to Familial ALS Promote Formation of Amyloid-Like Aggregates from Superoxide Dismutase. PLOS ONE 4, e5004 (2009).

75. Quintanar, L. et al. Copper and Zinc Ions Specifically Promote Nonamyloid Aggregation of the Highly Stable Human γ-D Crystallin. ACS Chem. Biol. 11, 263–272 (2016).

76. C. Lee, E. et al. Copper(ii)–human amylin complex protects pancreatic cells from amylin toxicity. Phys. Chem. Chem. Phys. 15, 12558–12571 (2013).

77. Salamekh, S. et al. A Two-Site Mechanism for the Inhibition of IAPP Amyloidogenesis by Zinc. J. Mol. Biol. 410, 294–306 (2011).

78. Noormägi, A., Gavrilova, J., Smirnova, J., Tõugu, V. & Palumaa, P. Zn(II) ions co-secreted with insulin suppress inherent amyloidogenic properties of monomeric insulin. Biochem. J. 430, 511–518 (2010).

79. Hoernke, M., Falenski, J. A., Schwieger, C., Koksch, B. & Brezesinski, G. Triggers for β-Sheet Formation at the Hydrophobic–Hydrophilic Interface: High Concentration, In-Plane Orientational Order, and Metal Ion Complexation. Langmuir 27, 14218–14231 (2011).

80. Chen, W.-T., Liao, Y.-H., Yu, H.-M., Cheng, I. H. & Chen, Y.-R. Distinct Effects of Zn^{2+}, Cu^{2+}, Fe^{3+}, and Al^{3+} on Amyloid- Stability, Oligomerization, and Aggregation: Amyloid Destabilization Promotes Annular Protofibril Formation. J. Biol. Chem. 286, 9646–9656 (2011).

81. Isaacson, T. et al. Sample extraction techniques for enhanced proteomic analysis of plant tissues. Nat. Protoc. 1, 769–774 (2006).

82. Dessau, M. A. & Modis, Y. Protein Crystallization for X-ray Crystallography. J. Vis. Exp. JoVE (2011). doi:10.3791/2285

83. Broide, M. L., Tominc, T. M. & Saxowsky, M. D. Using phase transitions to investigate the effect of salts on protein interactions. Phys. Rev. E 53, 6325 (1996).

84. Sauter, A. et al. Nonclassical Pathways of Protein Crystallization in the Presence of Multivalent Metal Ions. Cryst. Growth Des. 14, 6357–6366 (2014).

85. Ghadiri, M. R., Soares, C. & Choi, C. A convergent approach to protein design. Metal ion-assisted spontaneous self-assembly of a polypeptide into a triple-helix bundle protein. J. Am. Chem. Soc. 114, 825–831 (1992).

86. Dannhauser, P. N., Platen, M., Böning, H. & Schaap, I. a. T. Durable protein lattices of clathrin that can be functionalized with nanoparticles and active biomolecules. Nat. Nanotechnol. 10, 954–957 (2015).

87. Besteman, K., Van Eijk, K. & Lemay, S. G. Charge inversion accompanies DNA condensation by multivalent ions. Nat. Phys. 3, 641–644 (2007).

88. Pelta, J., Livolant, F. & Sikorav, J.-L. DNA Aggregation Induced by Polyamines and Cobalthexamine. J. Biol. Chem. 271, 5656–5662 (1996).

89. Zhang, F. et al. Reentrant Condensation of Proteins in Solution Induced by Multivalent Counterions. Phys. Rev. Lett. 101, (2008).

90. Zhang, F. et al. Universality of protein reentrant condensation in solution induced by multivalent metal ions. Proteins Struct. Funct. Bioinforma. 78, 3450–3457 (2010).

91. Roosen-Runge, F., Heck, B. S., Zhang, F., Kohlbacher, O. & Schreiber, F. Interplay of pH and Binding of Multivalent Metal Ions: Charge Inversion and Reentrant Condensation in Protein Solutions. J. Phys. Chem. B 117, 5777–5787 (2013).

92. Kubíčková, A. et al. Overcharging in Biological Systems: Reversal of Electrophoretic Mobility of Aqueous Polyaspartate by Multivalent Cations. Phys. Rev. Lett. 108, (2012).

93. Zhang, Y. & Cremer, P. S. The inverse and direct Hofmeister series for lysozyme. Proc. Natl. Acad. Sci. 106, 15249–15253 (2009).

94. Wen, Q. & Tang, J. X. Absence of charge inversion on rodlike polyelectrolytes with excess divalent counterions. J. Chem. Phys. 121, 12666–12670 (2004).

95. Messina, R. Electrostatics in soft matter. J. Phys. Condens. Matter 21, 199801–199801 (2008).

96. Derjaguin, B. & Landau, L. Theory of the stability of strongly charged lyophobic sols and of the adhesion of strongly charged particles in solutions of electrolytes. Prog. Surf. Sci. 43, 30–59 (1993).

97. Verwey, E. J. W. Theory of the Stability of Lyophobic Colloids. J. Phys. Colloid Chem. 51, 631–636 (1947).

98. Liang, Y., Hilal, N., Langston, P. & Starov, V. Interaction forces between colloidal particles in liquid: theory and experiment. Adv. Colloid Interface Sci. 134–135, 151–166 (2007).

99. Lin, M. Y. et al. Universality in colloid aggregation. Nature 339, 360–362 (1989).

100. Stradner, A. et al. Equilibrium cluster formation in concentrated protein solutions and colloids. Nature 432, 492–495 (2004).

101. Stradner, A., Cardinaux, F. & Schurtenberger, P. A Small-Angle Scattering Study on Equilibrium Clusters in Lysozyme Solutions. J. Phys. Chem. B 110, 21222–21231 (2006).

102. Salis, A. & Ninham, B. W. Models and mechanisms of Hofmeister effects in electrolyte solutions, and colloid and protein systems revisited. Chem. Soc. Rev. 43, 7358–7377 (2014).

103. Hofmeister, F. Zur Lehre von der Wirkung der Salze. Arch. Für Exp. Pathol. Pharmakol. 24, 247–260 (1888).

104. Schwierz, N., Horinek, D. & Netz, R. R. Reversed Anionic Hofmeister Series: The Interplay of Surface Charge and Surface Polarity. Langmuir 26, 7370–7379 (2010).

105. Lo Nostro, P. & Ninham, B. W. Hofmeister Phenomena: An Update on Ion Specificity in Biology. Chem. Rev. 112, 2286–2322 (2012).

106. Fesinmeyer, R. M. et al. Effect of Ions on Agitation- and Temperature-Induced Aggregation Reactions of Antibodies. Pharm. Res. 26, 903–913 (2008).

107. Jain, S. & Udgaonkar, J. B. Salt-Induced Modulation of the Pathway of Amyloid Fibril Formation by the Mouse Prion Protein. Biochemistry (Mosc.) 49, 7615–7624 (2010).

108. Madhavan, N., Robert, E. C. & Gin, M. S. A Highly Active Anion-Selective Aminocyclodextrin Ion Channel. Angew. Chem. Int. Ed. 44, 7584–7587 (2005).

109. Zhao, H. Effect of ions and other compatible solutes on enzyme activity, and its implication for biocatalysis using ionic liquids. J. Mol. Catal. B Enzym. 37, 16–25 (2005).

110. Collins, K. D. Why continuum electrostatics theories cannot explain biological structure, polyelectrolytes or ionic strength effects in ion–protein interactions. Biophys. Chem. 167, 43–59 (2012).

111. Omta, A. W., Kropman, M. F., Woutersen, S. & Bakker, H. J. Negligible Effect of Ions on the Hydrogen-Bond Structure in Liquid Water. Science 301, 347–349 (2003).

112. Collins, K. D. Charge density-dependent strength of hydration and biological structure. Biophys. J. 72, 65–76 (1997).

113. Washabaugh, M. W. & Collins, K. D. The systematic characterization by aqueous column chromatography of solutes which affect protein stability. J. Biol. Chem. 261, 12477–12485 (1986).

114. Grosberg, A. Y., Nguyen, T. T. & Shklovskii, B. I. Colloquium: the physics of charge inversion in chemical and biological systems. Rev. Mod. Phys. 74, 329 (2002).

115. Nguyen, T. T., Grosberg, A. Y. & Shklovskii, B. I. Macroions in salty water with multivalent ions: giant inversion of charge. Phys. Rev. Lett. 85, 1568 (2000).

116. Lozada-Cassou, M. & Jimenez-Angeles, F. Overcharging by macroions: above all, an entropy effect. arXiv:physics/0105043 (2001).

117. Ovanesyan, Z. et al. Excluded volume and ion-ion correlation effects on the ionic atmosphere around B-DNA: Theory, simulations, and experiments. J. Chem. Phys. 141, 225103 (2014).

118. Kim, H.-K., Tuite, E., Nordén, B. & Ninham, B. W. Co-ion dependence of DNA nuclease activity suggests hydrophobic cavitation as a potential source of activation energy. Eur. Phys. J. E 4, 411–417 (2001).

119. Homsi, Y. et al. The Extracellular δ-Domain is Essential for the Formation of CD81 Tetraspanin Webs. Biophys. J. 107, 100–113 (2014).

120. Halemani, N. D., Bethani, I., Rizzoli, S. O. & Lang, T. Structure and Dynamics of a Two-Helix SNARE Complex in Live Cells. Traffic 11, 394–404 (2010).

121. Sipos, T. & Merkel, J. R. Effect of calcium ions on the activity, heat stability, and structure of trypsin. Biochemistry (Mosc.) 9, 2766–2775 (1970).

122. Batoulis, H. et al. Concentration Dependent Ion-Protein Interaction Patterns Underlying Protein Oligomerization Behaviours. Sci. Rep. 6, 24131 (2016).

123. Bajohrs, M., Darios, F., Peak-Chew, S.-Y. & Davletov, B. Promiscuous interaction of SNAP-25 with all plasma membrane syntaxins in a neuroendocrine cell. Biochem. J. 392, 283–289 (2005).

124. Bar-On, D. et al. Imaging the assembly and disassembly kinetics of cis-SNARE complexes on native plasma membranes. FEBS Lett. 582, 3563–3568 (2008).

125. Frick, M., Schmidt, K. & Nichols, B. J. Modulation of lateral diffusion in the plasma membrane by protein density. Curr. Biol. CB 17, 462–467 (2007).

126. Greaves, J. & Chamberlain, L. H. Differential palmitoylation regulates intracellular patterning of SNAP25. J. Cell Sci. 124, 1351–1360 (2011).

127. Asakura, S. & Oosawa, F. Interaction between particles suspended in solutions of macromolecules. J. Polym. Sci. 33, 183–192 (1958).

128. Destainville, N. Cluster phases of membrane proteins. Phys. Rev. E 77, (2008).

129. de Wit, H. et al. Synaptotagmin-1 docks secretory vesicles to syntaxin-1/SNAP-25 acceptor complexes. Cell 138, 935–946 (2009).

130. Vance, J. E. & Tasseva, G. Formation and function of phosphatidylserine and phosphatidylethanolamine in mammalian cells. Biochim. Biophys. Acta 1831, 543–554 (2013).

131. Rogasevskaia, T. P., Churchward, M. A. & Coorssen, J. R. Anionic lipids in Ca^{2+}-triggered fusion. Cell Calcium 52, 259–269 (2012).

132. Christian, D. A. et al. Spotted vesicles, striped micelles and Janus assemblies induced by ligand binding. Nat. Mater. 8, 843–849 (2009).

133. Kay, J. G. & Grinstein, S. Sensing Phosphatidylserine in Cellular Membranes. Sensors 11, 1744–1755 (2011).

134. Shi, J., Heegaard, C. W., Rasmussen, J. T. & Gilbert, G. E. Lactadherin binds selectively to membranes containing phosphatidyl-L-serine and increased curvature. Biochim. Biophys. Acta 1667, 82–90 (2004).

135. Fasshauer, D., Bruns, D., Shen, B., Jahn, R. & Brunger, A. T. A Structural Change Occurs upon Binding of Syntaxin to SNAP-25. J. Biol. Chem. 272, 4582–4590 (1997).

136. Saka, S. K. et al. Multi-protein assemblies underlie the mesoscale organization of the plasma membrane. Nat. Commun. 5, (2014).

137. Knowles, M. K. et al. Single secretory granules of live cells recruit syntaxin-1 and synaptosomal associated protein 25 (SNAP-25) in large copy numbers. Proc. Natl. Acad. Sci. 107, 20810–20815 (2010).

138. Singer, S. J. & Nicolson, G. L. The fluid mosaic model of the structure of cell membranes. Science 175, 720–731 (1972).

139. Kusumi, A. et al. Dynamic organizing principles of the plasma membrane that regulate signal transduction: commemorating the fortieth anniversary of Singer and Nicolson's fluid-mosaic model. Annu. Rev. Cell Dev. Biol. 28, 215–250 (2012).

140. Sako, Y. & Kusumi, A. Compartmentalized structure of the plasma membrane for receptor movements as revealed by a nanometer-level motion analysis. J. Cell Biol. 125, 1251–1264 (1994).

141. Heuser, J. The production of 'cell cortices' for light and electron microscopy. Traffic 1, 545–552 (2000).

142. Iino, R., Koyama, I. & Kusumi, A. Single molecule imaging of green fluorescent proteins in living cells: E-cadherin forms oligomers on the free cell surface. Biophys. J. 80, 2667–2677 (2001).

143. Holzinger, A. Jasplakinolide: an actin-specific reagent that promotes actin polymerization. Methods Mol. Biol. Clifton NJ 586, 71–87 (2009).

144. Beck, M. et al. The quantitative proteome of a human cell line. Mol. Syst. Biol. 7, 549 (2011).

145. Wiśniewski, J. R., Zougman, A. & Mann, M. Combination of FASP and StageTip-based fractionation allows in-depth analysis of the hippocampal membrane proteome. J. Proteome Res. 8, 5674–5678 (2009).

146. van Meer, G. Cellular lipidomics. EMBO J. 24, 3159–3165 (2005).

147. Aikawa, Y., Xia, X. & Martin, T. F. J. SNAP25, but not syntaxin 1A, recycles via an ARF6-regulated pathway in neuroendocrine cells. Mol. Biol. Cell 17, 711–722 (2006).

148. McLaughlin, S. in Current Topics in Membranes and Transport (ed. Kleinzeller, F. B. and A.) 9, 71–144 (Academic Press, 1977).

149. Higgins, J. A. & Evans, W. H. Transverse organization of phospholipids across the bilayer of plasma-membrane subfractions of rat hepatocytes. Biochem. J. 174, 563–567 (1978).

150. Morillas, M., Swietnicki, W., Gambetti, P. & Surewicz, W. K. Membrane Environment Alters the Conformational Structure of the Recombinant Human Prion Protein. J. Biol. Chem. 274, 36859–36865 (1999).

151. Fasshauer, D., Otto, H., Eliason, W. K., Jahn, R. & Brunger, A. T. Structural Changes Are Associated with Soluble N-Ethylmaleimide-sensitive Fusion Protein Attachment Protein Receptor Complex Formation. J. Biol. Chem. 272, 28036–28041 (1997).

152. Meilhac, N. & Destainville, N. Clusters of Proteins in Biomembranes: Insights into the Roles of Interaction Potential Shapes and of Protein Diversity. J. Phys. Chem. B 115, 7190–7199 (2011).

153. Maguire, M. E. & Cowan, J. A. Magnesium chemistry and biochemistry. Biometals 15, 203–210 (2002).

154. Marcus, Y. Ion properties. (Marcel Dekker, 1997).

155. Schwierz, N., Horinek, D. & Netz, R. R. Anionic and Cationic Hofmeister Effects on Hydrophobic and Hydrophilic Surfaces. Langmuir 29, 2602–2614 (2013).

156. dos Santos, A. P. & Levin, Y. Surface and interfacial tensions of Hofmeister electrolytes. Faraday Discuss 160, 75–87 (2013).

157. van den Bogaart, G. et al. Membrane protein sequestering by ionic protein–lipid interactions. Nature 479, 552–555 (2011).

158. Rizzuto, R. & Pozzan, T. Microdomains of Intracellular Ca^{2+}: Molecular Determinants and Functional Consequences. Physiol. Rev. 86, 369–408 (2006).

159. Naraghi, M. & Neher, E. Linearized Buffered Ca^{2+} Diffusion in Microdomains and Its Implications for Calculation of $[Ca^{2+}]$ at the Mouth of a Calcium Channel. J. Neurosci. 17, 6961–6973 (1997).

160. Voglis, G. & Tavernarakis, N. The role of synaptic ion channels in synaptic plasticity. EMBO Rep. 7, 1104–1110 (2006).

161. Carafoli, E. Intracellular Calcium Homeostasis. Annu. Rev. Biochem. 56, 395–433 (1987).

162. Nielsen, M. S., Vorum, H., Lindersson, E. & Jensen, P. H. Ca^{2+} Binding to α-Synuclein Regulates Ligand Binding and Oligomerization. J. Biol. Chem. 276, 22680–22684 (2001).

163. Tamamizu-Kato, S. et al. Calcium-triggered membrane interaction of the alpha-synuclein acidic tail. Biochemistry (Mosc.) 45, 10947–10956 (2006).

164. Uversky, V. N., Li, J. & Fink, A. L. Metal-triggered Structural Transformations, Aggregation, and Fibrillation of Human α-Synuclein. A Possible Molecular Link between Parkinson's Disease and Heavy Metal Exposure. J. Biol. Chem. 276, 44284–44296 (2001).

165. Yáñez, M., Gil-Longo, J. & Campos-Toimil, M. in Calcium Signaling (ed. Islam, M. S.) 461–482 (Springer Netherlands, 2012). doi:10.1007/978-94-007-2888-2_19

166. Zhang, S. Fabrication of novel biomaterials through molecular self-assembly. Nat. Biotechnol. 21, 1171–1178 (2003).

167. Marcus, Y. Thermodynamics of solvation of ions. Part 6.—The standard partial molar volumes of aqueous ions at 298.15 K. J Chem Soc Faraday Trans 89, 713–718 (1993).

168. Marcus, Y. A simple empirical model describing the thermodynamics of hydration of ions of widely varying charges, sizes, and shapes. Biophys. Chem. 51, 111–127 (1994).

169. Peschke, M., Blades, A. T. & Kebarle, P. Hydration Energies and Entropies for Mg 2+ , Ca 2+ , Sr 2+ , and Ba 2+ from Gas-Phase Ion−Water Molecule Equilibria Determinations. J. Phys. Chem. A 102, 9978–9985 (1998).

170. Persson, I. Hydrated metal ions in aqueous solution: How regular are their structures? Pure Appl. Chem. 82, (2010).

171. Habenschuss, A. & Spedding, F. H. The coordination (hydration) of rare earth ions in aqueous chloride solutions from x-ray diffraction. III. SmCl3, EuCl3, and series behavior. J. Chem. Phys. 73, 442 (1980).

172. Buz'ko, V. Y., Sukhno, I. V., Buz'ko, M. B., Polushin, A. A. & Panyushkin, V. T. Study of the structure and stability of aqua complexes Y(H2O) n 3+ (n = 1–10) by Ab initio methods. Russ. J. Inorg. Chem. 51, 1276–1282 (2006).

8 Acknowledgements

I would like thank Prof. Thorsten Lang for giving me the opportunity to work on this interesting and diverse topic. I am grateful for his constant support and advice, and the lively and fruitful discussions we have had.

I am also very thankful for the interesting collaboration with Dr. Thomas H. Schmidt, who did the MD simulations on the SNAP25 peptide. It was intriguing and instructive to discuss the matters of this study with you and to get an insight into a very different experimental approach. Special thanks also to Dr. Gero Schlötel for help with image analyses and STED microscopy, and to Pascal Weber for contributing FRAP measurements and for his general support during the review process of the publication accompanying this thesis.

I would also like to thank all other current and former members of the Lang group, especially Elisa Merklinger, Dennis de Coninck, Yahya Homsi and Nora Karnowski, for helpful discussions and suggestions, teaching me useful tips and tricks to master technical difficulties, and the great team-oriented work atmosphere.

I am obliged to Dr. Thomas Sorkalla and Prof. Hanns Häberlein from the Institute of Biochemistry and Molecular Biology, for supervising me during FCS measurements, and discussing the results and experimental strategies. I am also thankful to the Famulok group, especially Dr. Anton Schmitz and Christian Sieg, for giving me the opportunity to use the MST apparatus and your helpful instructions.

I would especially like to thank Dr. Laurence Salomé and Dr. Catherine Tardin of the Institute of Pharmacology and Structural Biology (IPSB) in Toulouse for the enjoyable collaboration. It was a pleasure to stay at your laboratory and I am grateful for your supervision and help with the DLS measurements. Thanks also to Prof. Nicolas Destainville from the Laboratoire de Physique Théorique in Toulouse for fruitful discussions.

I would further like to thank Prof. Ulrich Kubitscheck, Prof. Christoph Thiele, and Prof. Martin Hofmann-Apitius for taking the time to evaluate the thesis and being part of the dissertation committee.

Thanks also to the members of the Thiele, Burgdorf, Tavosanis and Brömer groups for the pleasant atmosphere and your willingness to exchange reagents and know-how at any time. I am also grateful for the SFB 647 of the DFG that provided the necessary research funding.

Finally I would like to thank my family for their continuous support and advice. Last but not least I want to thank my fiancé Lars Hoffmann – for your help with typesetting the thesis, for encouraging me and making me happy, and for your love and patience.